Skolkovo Institute of Science and Technology

MOLECULAR SIGNATURES AND MECHANISMS BEHIND LIFESPAN EXTENSION

Doctoral Thesis

by

ALEXANDER TYSHKOVSKIY

DOCTORAL PROGRAM IN LIFE SCIENCES

Supervisors
Professor Vadim Gladyshev
Professor Philipp Khaitovich

Moscow - 2018

Abstract

Lifespan of an organism is a variable demonstrating significant variation both across- and within the species. Indeed, maximum lifespan of mammals ranges between 3.2 years in Etruscan shrew to more than 200 years in bowhead whale. Within the species, lifespan can also be shortened and most importantly extended by some environmental and genetical interventions, resulting in up to 10-fold increase in longevity in certain animal models. However, molecular signatures and mechanisms responsible for such lifespan variation remain unclear.

Here, we examined this problem by performing high-throughput analysis of both across- and within-species models. We performed RNA sequencing of fibroblasts of exceptionally long-lived naked mole rat (NMR) and mouse in response to DNA damage, induced by γ-irradiation. We then identified and experimentally validated gene expression signatures associated with high resistance of the NMR to DNA damage.

We further extensively characterized DNA methylation changes occurring during aging in mice, using 141 individuals representing 16 age groups. We identified general trends and pathways associated with these changes along with the effect of lifespan-extending intervention (caloric restriction) on them.

Finally, we performed RNA sequencing of 8 lifespan-extending interventions in mouse and aggregated this data with publicly available gene expression data, resulting in the coverage of 17 different healthspan- and lifespan-extending interventions. We characterized similarity of gene expression profiles across interventions and examined their feminizing effect in males. We then identified common signatures of longevity

interventions along with the signatures associated with the degree of lifespan extension. We further applied these signatures for the identification of new lifespan-extending conditions and estimation of differences in lifespan across mouse strains.

We observed common and distinct signatures associated with lifespan extension across- and within-species models. We note the importance of NRF2-regulated acute stress response and antioxidative defense along with apoptosis as a mechanism of NMR resistance to DNA damage and lifespan extension by interventions. Other processes, such as oxidative phosphorylation, glucose metabolism and immune response seem to be uniquely associated with interventions while autophagy appears to be distinctive for response in NMR. Notably, gene expression signatures obtained from the analysis of lifespan-extending interventions were shown to properly predict the effect of other conditions on longevity based on gene expression profile, pointing to a possibility of their application for the identification of new lifespan-extending interventions, facilitating the development of novel antiaging therapies.

Publications

1. Zhao Y.*, **Tyshkovskiy A.***, Muñoz-Espín D., Tian X., Serrano M., de Magalhaes J.P., Nevo E., Gladyshev V.N., Seluanov A., and Gorbunova V. (2018). Naked mole rats can undergo developmental, oncogene-induced and DNA damage-induced cellular senescence. Proc. Natl. Acad. Sci. *115*, 1801–1806.

*** Authors contributed equally to this work**

2. Sziráki A., **Tyshkovskiy A.**, and Gladyshev V.N. (2018). Global remodeling of the mouse DNA methylome during aging and in response to calorie restriction. Aging Cell e12738.
3. **Tyshkovskiy A.**, Borodinova A.A., Khaitovich P., Miller R.A., Gladyshev V.N. (2018). Identification and application of gene expression signatures of lifespan-extending interventions. ***Submitted to Cell Metabolism.***

Acknowledgments

I would like to thank my supervisor in Harvard Medical School Dr. Vadim Gladyshev for the opportunity to conduct this research in his lab and his priceless support during all steps of the work. I would also like to thank my Skoltech supervisor Dr. Philipp Khaitovich for contacting me with Vadim and supporting me in Skoltech during my stay in Boston.

Big thanks to all members of the lab, in particular, to Maxim Gerashchenko and Margarita Meer, for their help, collaborations and parties. Thanks to all collaborators, especially to Richard Miller and Vera Gorbunova, for their incredible expertise and valuable insights. Special thanks to my partner in crime Aleksei Mikhalchenko, with whom we went to Vadim's lab and spent these 3 years in Boston keeping each other from nervous breakdowns.

Huge heartful thanks to my parents Eduard Tyshkovskiy and Nataliya Romashkina, all members of my big family and all my friends, especially Aleksei Mikhalchenko, Ilia Kurochkin, Ivan Rusinov, Anastasia Borodinova and Yaroslava Pavlova, for moral support and psychological therapy during all steps of the work. Unlimited thanks to my passed away grandmother Lyudmila Romashkina, who, as a physician, helped me to make my first steps in biology and medicine during my childhood, and my grandfather Petr Romashkin, who advised me to apply for Department of Bioengineering and Bioinformatics in MSU. I am happy and grateful that their dream has become true.

My infinite and sincere gratitude to my school teacher Vera Zaitseva, who implanted me the love of biology and science, despite my unskillful resistance in the earlier

school years. Thanks to all professors and mentors in Moscow State University and Massachusetts Institute of Technology, who filled me with knowledge, skills and interest to natural sciences and study of aging, in particular. Special thanks to Alexander Kondratenko, Sergey Spirin, Andrei Alexeevski, Aleksandra Rakhmaninova, Andrey Mironov and Mikhail Gelfand for their instructions and guidance in mathematics and bioinformatics during my education in MSU, which provided me with toolkit and background necessary for this work.

Finally, I would like to thank all mice, naked mole rats and neurons in my brain, who sacrificed their lives to let this work happen. Without you, this work would never be completed.

Table of Contents

List of Symbols, Abbreviations

4E-BP1 – eukaryotic translation initiation factor 4E-Binding Protein 1

AIC – Akaike Information Criterion

AMP – Adenosine MonoPhosphate

AMPK – AMP-activated protein Kinase

ANOVA – ANalysis Of VAriance

ATP – Adenosine TriPhosphate

BH – Benjamini-Hochberg procedure

BMI – Body Mass Index

BMR – Basal Metabolic Rate

BP – Biological Process

BrdU - 5-bromo-2'-deoxyuridine

C. elegans – *Caenorhabditis elegans*

CGI – CpG Island

CR – Caloric Restriction

CS – Cellular Senescence

DAVID – Database for Annotation, Visualization and Integrated Discovery

DGAT – DiGlyceride AcylTransferase

DHS – Dnase Hypersensitive Site

DNA – DeoxyriboNucleic Acid

DNMT – DNA MethylTransferase

ECI – Early Contact Inhibition

Ecr – Evolutionary conserved region

EOD – Every-Other Day feeding

FC – Fold Change

FDR – False Discovery Rate

FGF – Fibroblast Growth Factor

GH – Growth Hormone

GHR – Growth Hormone Receptor

GHRKO – Growth Hormone Receptor Knockout

GSEA – Gene Set Enrichment Analysis

GST – Glutathione S-Transferase

HA – Hyaluronic Acid

IGF1 – Insulin-like Growth Factor 1

IL – Interleukin

INK4 – INhibitors of cyclin dependent Kinase 4

IR – γ-Irradiation

IS – Initial Shift

ITP – Interventions Testing Program

kcal – kilocalories

KEGG – Kyoto Encyclopedia of Genes and Genomes

LOO – Leave-one-out procedure

MAE – Mean Absolute Error

MAPK – Mitogen-Activated Protein Kinase

MAT – Methionine AdenosylTransferase

MDP – Muramyl DiPeptide

MEF – Mouse Embryonic Fibroblasts

MF – Molecular Function

ML – Maximum Lifespan

MR – Methionine Restriction

mRNA – messenger RNA

MSF – Mouse Skin Fibroblasts

mTOR – mammalian Target Of Rapamycin

MUP – Major Urinary Protein

NDGA - NorDihydroGuaiaretic Acid

NEF – Naked mole rat Embryonic Fibroblasts

NES – Normalized Enrichment Score

NIA – National Institute of Aging

NMR – Naked Mole Rat

NSF – Naked mole rat Skin Fibroblasts

OMF – Original Methylation Fraction

PAS – Pathway Activation Score

PCA – Principal Component Analysis

PI3K – PhosphatidylInositol 3 Kinase

PUFA – PolyUnsaturated Fatty Acids

RMS – Residual Methylation Fraction

RNA – RiboNucleic Acid

RNAseq – RNA sequencing

ROS – Reactive Oxygen Species

RRBS – Reduced Representation Bisulfite Sequencing

S6K1 – S6 Kinase 1

SD – Standard Deviation

SE – Standard Error

SIPS – Stress-Induced Premature Senescence

SASP – Senescence-Associated Secretory Phenotype

TAT – Time After Treatment

TCA – TriCarboxylic Acid cycle

TFBS – Transcription Factor Binding Site

TGFβ – Transforming Growth Factor Beta

TNF – Tumor Necrosis Factor

TSS – Transcription Start Site

USA – United States of America

UTR – UnTranslated Region

UV – Ultraviolet

w/w – weight/weight

XME – Xenobiotic Metabolizing Enzyme

List of Figures

List of Tables

Chapter 1. Review of Literature

1.1 Aging and lifespan control

Aging is characterized by the gradual reduction in the ability to cope with physiological challenges, which ultimately leads to death (Johnson et al., 1999). From the mechanistic perspective, it is associated with accumulation of deleterious changes (deleteriome) with age (Gladyshev, 2016). Such changes include mutations, protein aggregation, generation of reactive oxygen species (ROS), mitochondrial dysfunction, telomere shortening, stem cell exhaustion, etc. (Lopez-Otin et al., 2013) These damages seem to lead to aging-associated diseases, such as cancer, atherosclerosis, cardiovascular diseases, cataracts, type 2 diabetes and neurodegenerative disorders (e.g., Alzheimer's, Parkinson's and Huntington's diseases). For example, incidence of different types of cancer was shown to be very well correlated with mutation accumulation over time (Podolskiy et al., 2016). Aging-related diseases, in the end, significantly decrease fitness of an organism, leading to its death.

Therefore, accumulation of deleterious changes seems to be the main driver of aging (Gladyshev, 2016). Such age-related changes effect different levels of biology, ranging from the organs (and systems of organs) to the individual molecules. For example, methylation profile of DNA in cells was shown to demonstrate consistent age-related changes in both human (Horvath et al., 2012; Johansson et al., 2013; Jones et al., 2015; McClay et al., 2014; Rakyan et al., 2010; Sun et al., 2010) and mice (Maegawa et al., 2010). Indeed, DNA methylation is gradually decreased during aging, but certain genomic regions, such as CpG islands (CGIs) and gene promoters, are known to gain methylation

with age (Cole et al., 2017; Stubbs et al., 2017). Such changes formed the basis of methylation clock, developed to predict the biological age of an organism based on methylation profile of it cells. The clock was created for individual tissues, such as blood and liver, in human (Hannum et al., 2013) and mice (Petkovich et al., 2017; Wang et al., 2017) as well as across different tissues (Horvath, 2013; Stubbs et al., 2017) with a good precision (mean absolute error (MAE) equal to ~5% of lifespan). Moreover, in human, only 3 individual methylation sites, measured in blood, allowed to predict biological age with similar quality (Weidner et al., 2014). Importantly, such clocks reflect biological rather than chronological age of individuals. Indeed, in humans, accelerated methylation age was associated with higher all-cause mortality in later life (Marioni et al., 2015). In mice, epigenetic aging was accelerated in response to ovariectomy or high-fat diet, both of which reduce the average lifespan (Stubbs et al., 2017). In humans, no significant effect of specific diet on methylation clock was detected, but body mass index (BMI) was found to be significantly associated with epigenetic age (Quach et al., 2017). Finally, biological age is reset close to zero after reprograming of adult somatic cells into induced pluripotent stem cells (iPSCs) both in human (Horvath, 2013; Weidner et al., 2014) and mice (Petkovich et al., 2017).

From demographical perspective, however, aging may be thought simply as an increase in probability of death with time. Indeed, for the majority of animal species, including human, the dependence of mortality rate of an organism on time follows Gompertz law (Gompertz, 1825). Based on the law, regardless of any extrinsic factors, the mortality rate of the organism increases exponentially with time. In human, it doubles every

8 years. Gompertz law leads to a standardized shape of survival curve (Figure 1). However, although increase in mortality with age is a common feature of different species from different clades, in some species mortality rate does not increase (e.g., *Hydra maginpapillata*) or even decreases (e.g., desert tortoise *Gopherus agassizii*) with age (Jones et al., 2014). Such examples exist in mammals as well. Small rodent, naked mole rat (NMR), doesn't show any change of mortality rate with time (Ruby et al., 2018). At the same time, it seems to be highly resistant against age-related diseases, such as cancer (Buffenstein, 2008). Therefore, the most direct consequence of aging seems to be lifespan, which is highly variable across tree of life as relative species may have strikingly different lifespans as can be demonstrated by mice and naked mole rats with maximum lifespans (ML) equal to approximately 4 and 31 years, respectively (de Magalhães et al., 2005).

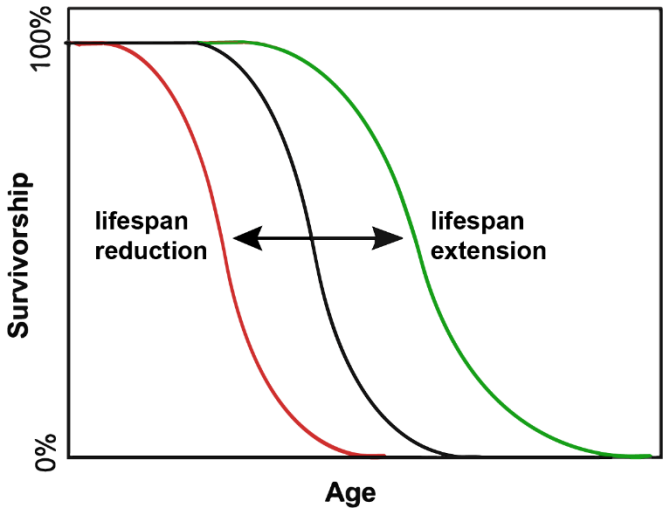

Figure 1. Typical survival curve and its response to lifespan-reducing and -extending interventions

Lifespan seems to be also significantly variable across individuals within the certain species. Not surprisingly, lots of environmental and genetic factors affect survival curve

by increasing mortality rate and, therefore, reducing lifespan (Tyner et al., 2002; Zhang et al., 2015). Other interventions, however, may lead to the decrease of mortality rate and, therefore, to extension of lifespan (Figure 1). Up to date, number of such lifespan-extending interventions has been identified for plenty of model organisms, ranging from yeasts to mice and even primates (Fontana et al., 2010; Mattison et al., 2017). Their effect may be quite significant, reaching 10-fold increase of lifespan in certain animal models (Ayyadevara et al., 2008). From demographical point of view, they effect one or both parameters of Gompertz model, being basal level of mortality (vulnerability) and rate of increase in mortality with age (aging rate). Interestingly, different interventions extend lifespan through downregulation of different parameters of Gompertz model, and same intervention may work through different parameters in different species (Garratt et al., 2016). Meta-analysis on all longevity studies of rapamycin and caloric restriction (CR) effect in different species revealed that in mice rapamycin mainly effects vulnerability while CR effects aging rate. At the same time, in *C. elegans* rapamycin effects aging rate, but not vulnerability (Garratt et al., 2016).

Thus, significant variation of lifespan may be observed both across and within the species. Even within pretty tight in evolutionary sense class of mammals (with the last common ancestor dated approximately 210 million years ago) lifespan of different species varies by more than 100 times (de Magalhães et al., 2005). Lifespan within the specific species is also variable and may be decreased or increased by variety of different environmental and genetic factors. This review will specify certain molecular and physiological mechanisms behind variation of lifespan across and within the species.

1.2 Lifespan variation across species

Mammals exhibit remarkable variety of lifespan ranging from small short-lived Etruscan shrews (*Suncus etruscus*), weighting only 1.8 grams and living up to 3.2 years, to large long-lived bowhead whales (Balaena mysticetus), weighting more than 100 tons and having maximum lifespan of more than 200 years (de Magalhães et al., 2005; Figure 2). Interestingly, the maximum lifespan of bowhead whale was estimated based on harpoon points found in captured whales in 2007. Remarkably, such harpoon points were last time manufactured in 1880s, which provided minimum estimate of maximum lifespan in these creatures (George and Bockstoce, 2008).

Generally, there is a strong positive association between body mass and lifespan across species (Sacher, 1959; Figure 2). Besides longer life, bigger animals also tend to have longer development, fewer offsprings, lower mass-specific metabolic rates and bigger female time to maturity, i.e. the time to reach puberty (Fushan et al., 2015; Sacher, 1959; Western, 1979). Therefore, from evolutionary perspective bigger lifespan in large animals seems to be a byproduct of natural selection acting on other features, such as period of development and female time to maturity. Generally, larger animals need more time for growth and development to adult state, capable of reproduction. Not surprisingly, extension of these periods leads to extension of lifespan in general.

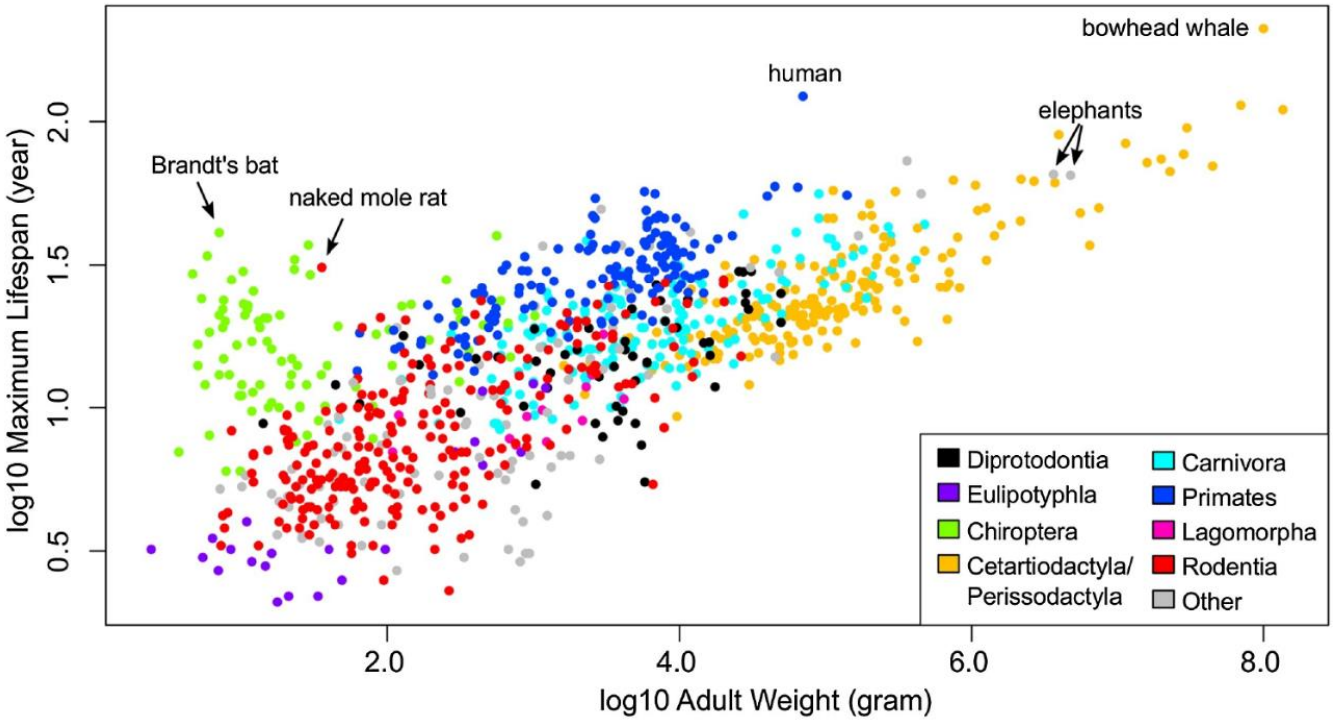

Figure 2. Correlation between adult body mass and maximum lifespan across mammalian species

Individual dots represent specific species colored based on taxonomic orders. Values for 995 mammalian species are taken from AnAge Database (de Magalhães et al., 2005). Figure is taken from (Ma and Gladyshev, 2017) with permission.

However, such dependence couldn't explain long lifespan in so-called exceptionally long-lived species. These species defy the trend defined by correlation between body mass and maximum lifespan and, therefore, are outliers on the corresponding plot. In other words, they live significantly longer than expected based on body mass dependence (Figure 2). These outliers include famous rodent naked mole rat (*Heterocephalus glaber*) (Buffenstein, 2008), some small bats, such as Brandt's bat (*Myotis brandtii*) (Seim et al., 2013), and humans. Indeed, maximum recorded lifespan for human is 122.5 years, while other primates live only up to 60 years in captivity (de Magalhães et

al., 2005). Therefore, although longevity and body mass generally coevolve together, they are, at least partially, defined by different molecular and physiological mechanisms. Analysis of molecular patterns associated with lifespan adjusted for body mass across mammals, along with study of features of exceptionally long-lived animals may point to the mechanisms related to variation of lifespan across species.

1.2.1 Molecular signatures of lifespan across mammals

Several recent studies examined associations of different molecular features, such as gene expression (Fushan et al., 2015; Ma et al., 2016), metabolome (Ma et al., 2015a), ionome (Ma et al., 2015b) and lipidome (Bozek et al., 2017), with maximum lifespan across mammals. For accurate conclusions, results were adjusted for body mass to filter out associations, which can be completely described by this factor.

Gene expression associations with maximum lifespan were identified both at the level of organs, such as liver, brain and kidney (Fushan et al., 2015), and at the level of cultured fibroblasts (Ma et al., 2016) obtained from different mammalian species. DNA repair genes, including base-excision repair and nonhomologous end-joining pathways (e.g., *Xrcc5*, *Xrcc6* and *Prkdc*), were positively associated with longevity in fibroblasts and across the organs, consistent with previous studies (Hart and Setlow, 1974). Interestingly, some genes coding for DNA repair enzymes were also identified to be positively selected in several exceptionally long-lived species, including *Apex1* in naked mole rates (Kim et al., 2011), *Rad40* and *Xrcc5* in Brandt's bat (Seim et al., 2013), and *Ercc1* and *Ercc5* in bowhead whale (Keane et al., 2015), supporting the association between DNA repair system and longevity at genetic level. Fibroblasts obtained from long-lived species also

showed higher resistance to stress-inducing compounds, such as paraquat and cadmium (Ma et al., 2016). Besides, upregulation of immune response was detected in long-lived species across the organs, supported by positive selection of *c-Rel* (Zhang et al., 2013) and expansion of immunoglobulin-coding gene families (Seim et al., 2013) in long-lived microbats. On the other hand, genes negatively associated with longevity across mammals included fatty acid metabolism, TCA and oxidative phosphorylation, and ubiquitin complex across organs (Fushan et al., 2015), and proteolysis and apoptotic genes (e.g., *Tp53*, *Foxo3* and *Bax*) in fibroblasts (Ma et al., 2016). Interestingly, several exceptionally long-lived species demonstrate genomic signatures associated with apoptotic genes. Thus, bowhead whale demonstrates positive selection of pro-apoptotic gene Foxo3 (Keane et al., 2015), while microbats show positive selection of *Atm* and *Mdm2* coding for checkpoint proteins. Finally, African elephant (*Loxodonta africana*), the largest land mammal, has 19 additional copies of *Tp53* gene in the genome, and its cells are approximately 2 times more sensitive to DNA-damage-induced apoptosis than human cells (Abegglen et al., 2015). These features may explain how "Peto's paradox", being that larger animals don't have higher incidence of cancer despite higher number of cells in the body (Peto et al., 1975), is resolved in elephants. Indeed, such big number of p53 copies in the genome increases resistance to tumor by decreasing threshold of DNA damage required for cell cycle arrest and apoptosis of mutant cells. Moreover, if p53 is mutated in a certain cell, there will be still 19 other copies of this gene, preventing cancer transformation. Based on mathematical modeling of cancer incidence, only 2-fold decrease in mutation rate may result in 100-fold

increase in cell mass free from cancer (Caulin et al., 2015). Therefore, mentioned above features may be enough to provide cancer resistance in elephants.

Metabolome analysis across brain, heart, liver and kidney of 26 mammalian species identified positive association with longevity for sphingomyelins (in brain) along with negative association for amino acids (in brain), triglycerides with polyunsaturated fatty acids (PUFA) (in kidney), lysophosphatidyl-cholines (in brain and heart) and -ethanolamines (in brain and kidney) (Ma et al., 2015a). Interestingly, high levels of sphingomyelins and low levels of PUFA triglycerides were also found to be associated with female familial longevity in a study on human plasma lipidome of nonagenarians (i.e., people of 90-99 years old) offsprings (Gonzalez-Covarrubias et al., 2013). Lower level of PUFA triglycerides may be related to higher resistance to oxidative stress, as these molecules are highly sensitive to peroxidation, especially when incorporated to cell membrane (Hulbert, 2008). This hypothesis is confirmed by significant negative correlation between peroxidation index for membrane composition and longevity across mammals, birds and even invertebrates (Hulbert et al., 2014). Role of lipids in determination of lifespan across mammals was further described by high-throughput lipidome study across 6 organs in 35 mammalian species (Bozek et al., 2017). Logistic elastic net regression built in this study was able to predict lifespan of the certain species based on its lipidome composition with higher than 90% accuracy. Most significant positive predictors included triglycerides, while negative predictors included glycerophospholipids and sphingolipids. Interestingly, significant stabilizing selection was detected for genes linked to metabolism of corresponding lipids in human and naked mole

rat (Bozek et al., 2017), pointing to the interaction between genetic and metabolomic patterns of longevity.

Besides, positive association with lifespan was identified for urate-allantoin ratio (Ma et al., 2015a), consistent with the lower level of uricase expression in liver in long-lived species (Fushan et al., 2015). Finally, 2 tryptophan degradation products were negatively associated with longevity. This finding is nicely confirmed by experiments in *C. elegans* (van der Goot et al., 2012) and *Drosophila melanogaster* (Oxenkrug, 2010), where knockdown of *Tdo*, coding for tryptophan catabolism enzyme, was shown to extend lifespan.

Finally, ionome study across 3 organs revealed significant negative association of selenium level with longevity in liver (Ma et al., 2015b). Selenium, in selenocysteine form, is incorporated into 25 mammalian proteins involved in antioxidant response (Kryukov and Castellano, 2003). On the other hand, cadmium, being a toxic element, was found to be positively associated with lifespan in kidney and liver. As there is no known biological function of cadmium, this association may be a consequence of poor excretion of this element and, therefore, its accumulation in the bodies of long-lived animals.

1.2.2 Longevity molecular signatures of naked mole rat

Naked mole rat (NMR) (*Heterocephalus glaber*) seems to be one of the most interesting exceptionally long-lived mammals and even has a title of "Vertebrate of the year" given by *Science* in 2013 (2013). Weighting about 35 grams, comparable to the weight of a house mouse (*Mus musculus*), this creature has a maximum recorded lifespan of 31 years, typical for the animals with the body size of lion (*Panthera leo*;

ML = 27 years) or bison (*Bison bison*; ML = 33.5 years) (de Magalhães et al., 2005). Besides, it doesn't show number of standard ageing-associated physiological declines until very late of their lives (Buffenstein, 2008). Indeed, over age, no significant changes in body mass, percentage body fat, basal metabolic rate (BMR) and bone mineral density are observed (O'Connor et al., 2002). Moreover, NMR females don't exhibit menopause, staying fertile even after 20 years (Buffenstein, 2008). NMRs are also poikilotherms, meaning that their rate of oxygen consumption and body temperature are almost completely dependent on ambient temperature, switching to partially endothermic mode only under high temperature (> 31°C) (Buffenstein and Yahav, 1991). Finally, due to living in subterranean environment, NMR exhibits extraordinary resistance to hypoxia. Indeed, it can live in an atmosphere with 80% CO_2 and only 20% O_2. When placed in 5% O_2 conditions for 5 hours, no deviations from normal activity and side effects are detected, while mice, under the same conditions, die within 5 minutes. Mole rats can even survive in 0% O_2 atmosphere for 18 minutes and return to normal physiological state after reoxygenation (Park et al., 2017). In response to such super-hypoxic conditions, NMR was shown to switch to fructose-fueled anaerobic glycolysis, producing lactic acid. Such physiological features of NMR were associated with higher gene expression of the GLUT5 fructose transporter and ketohexokinases KHK-A and KHK-C, compared to mice (Park et al., 2017). Finally, NMRs show decreased metabolic rates, being about 70% of that in mice, which is a typical signature of subterranean mammals (Buffenstein, 2005).

Besides all physiological features, NMRs are known to be unique in their extreme resistance to cancer. Indeed, only few cases of cancer have been detected in these organisms (Taylor et al., 2017). At the cellular level, NMR fibrobalsts also demonstrated resistance to malignant transformation induced by transfection of activated Ras and SV40 LT (Seluanov et al., 2009). Consistently, NMR induced pluripotent stem cells (iPSCs) are inefficient in forming teratomas (Lee et al., 2017; Miyawaki et al., 2016). Combination of several genetic and cellular mechanisms explaining such phenomenon, has been proposed. Studies of NMR fibroblasts revealed their higher sensitivity to contact inhibition compared to mice, named "early contact inhibition" (ECI) (Seluanov et al., 2009). In other words, cell cycle arrest in NMR occurs at much lower cell density. ECI was shown to be regulated through induction of $p16^{Ink4a}$, contrary to regular contact inhibition, regulated by $p27^{Kip1}$ similar to human and mice. Therefore, NMR cells have two layers of contact inhibition associated cell cycle arrest. Genomic sequencing of NMR revealed two early stop codons in $p16^{Ink4a}$ transcript (Kim et al., 2011), and cloning confirmed shorter length of the corresponding protein compared to mice, although it was still functional (Miyawaki et al., 2015). Furthermore, besides $p15^{Ink4b}$ and $p16^{Ink4a}$ proteins, encoded in INK4a/b (inhibitors of cyclin dependent kinase 4) locus, additional protein isoform is encoded there, which is unique to NMR and is absent in both human and mouse cells (Tian et al., 2015). This, so-called $pALT^{Ink4a/b}$ isoform, being a hybrid of $p15^{Ink4b}$ and $p16^{Ink4a}$, was shown to be activated by ECI and number of stresses (e.g., UV, expression of oncogenes and γ-irradiation), and had higher ability to induce cell cycle arrest than either $p15^{Ink4b}$ or

$p16^{Ink4a}$, as shown both in NMR and human cell models (Tian et al., 2015). Finally, ECI was shown to be mediated through hyaluronic acid (HA), which has higher molecular mass in NMR and is secreted in larger amounts compared to mice and humans (Tian et al., 2013). Such finding is further supported by genomic sequencing, which has revealed unique amino acid changes in NMR hyaluronan synthase 2 (HAS2) (Kim et al., 2011). Increased level of high-molecular-mass HA results in viscous extracellular matrix, providing higher level of contact inhibition. Consistently, knockdown of *Has2* or overexpression of HA degradation enzyme, hyaluronidase HYAL2, makes NMR cells susceptible to malignant transformation and tumor formation (Tian et al., 2013).

Besides, NMR cells have unique 28S ribosomal RNA structure, associated with much higher translation fidelity compared to mouse cells, resulting in up to 10 times fewer amino acid mis-incorporations in the protein sequence (Azpurua et al., 2013). In addition, NMR demonstrates unique amino acid changes in proteins associated with DNA integrity and repair, such as *Apex1*, *Rfc1* and *Top2a* (Kim et al., 2011), together with upregulation of DNA repair genes compared to mouse at the gene expression level, similar to human (MacRae et al., 2015). Altogether, these mechanisms provide low rate of mistake appearance together with their strong control. This may lead to decreased rate of damage accumulation in NMR cells and, consequently, reduced rate of cancer and aging, according to deleteriome theory (Gladyshev, 2016).

Several other molecular and cellular signatures may also contribute to longevity of the NMR. Thus, cytoprotective activity of NRF2 along with its mRNA and protein level is higher in NMR compared to mouse, while the level of its main negative

regulator, KEAP1, is lower in long-lived rodents (Leiser and Miller, 2010). Moreover, the level of *Keap1* expression was shown to be negatively associated with maximum lifespan across rodents, pointing to the importance of acute stress response system for achieving longevity. Gene expression analyses also revealed lower expression of genes involved in insulin and IGF1 signaling pathway (IIS) in the NMR liver compared to mouse (Kim et al., 2011). IIS is known to be negatively associated with lifespan within the species, as confirmed by many lifespan-extending interventions, acting through this pathway (Figure 3). Proteasome activity seems to be higher in NMR compared to mouse, while accumulation of ubiquitinated proteins and irreversibly oxidized cysteines is significantly lower (Perez et al., 2009). At the same time, less urea-induced protein unfolding is observed. Altogether, this points to higher level of protein stability and better mechanism for protein removal and replacement in NMR, consistent with previous findings of lower damage accumulation in NMR.

If cellular senescence (CS), being a state of permanent cell-cycle arrest that cells adopt in response to stress, occurs in NMR is, however, still unknown. CS is usually induced by many stresses, including telomere shortening (replicative senescence), expression of oncogenes (oncogene-induced senescence) and DNA damage, such as γ-irradiation (stress-induced premature senescence, SIPS). CS is believed to be an important mechanism to prevent cancer (Collado et al., 2005; Xue et al., 2007). However, CS also has its deleterious effects. Accumulation of senescent cells impairs tissue function and promotes aging. Persistent senescent cells also display senescence-associated secretory phenotype (SASP), which may result in aging-related diseases,

including cancer (Coppé et al., 2010a, 2008, 2010b). Remarkably, elimination of senescent cells extends the health and life span of mice (Baar et al., 2017; Baker et al., 2016), indicating that CS contributes to aging and age-related diseases (Tacutu et al., 2011; Yanai and Fraifeld, 2018). It is known that similarly to other small rodents, NMR do not display replicative senescence and express telomerase in somatic tissues (Kim et al., 2011; Seluanov et al., 2007, 2008). However, other types of senescence have not been investigated in this exceptionally long-lived species.

1.3 Lifespan variation within species

Variation of lifespan across individuals of the same species seems to be also quite broad. Lifespan can be both reduced or extended by number of different genetic and environmental factors. Indeed, simple change of temperature by 5°C effects lifespan of *C. elegans* by about 25% (Zhang et al., 2015). Importantly, different species generally demonstrate consistent effect of different interventions on their lifespan, although there are some differences in size of an effect and particular physiological features (Fontana et al., 2010). Up to date, the best example of such consistency is caloric restriction (CR), which was shown to extend lifespan, at least under one experimental design, in all tested species, including yeasts (Lin et al., 2000), worms (Lakowski and Hekimi, 1998), flies (Mair et al., 2003), mice (Mitchell et al., 2016), domestic dogs (Kealy et al., 2002), grey mouse lemurs (Pifferi et al., 2018) and rhesus monkeys (Mattison et al., 2017). On the other hand, some interventions may significantly extend lifespan in a certain organism but not provide such substantial effect in the other. For example, resveratrol provides significant lifespan-extending effect in *C. elegans* (Wood et al., 2004) but not in mouse

(Miller et al., 2011), although it still improves some healthspan age-related disorders in the latter, such as cardiovascular and locomotor function (Pearson et al., 2008a).

Another general feature of lifespan-effecting interventions appears to be their reversibility. If certain intervention extends or shortens lifespan or healthspan, the opposite intervention compared to control conditions typically has an opposite effect. For example, while increase in temperature from 20° to 25° in *C. elegans* shortens its lifespan by about 23%, decrease of temperature from 20° to 15° extends it by comparable 27% (Zhang et al., 2015). Similarly, high-fat diet reduces lifespan of mouse (Baur et al., 2006), while CR (Mitchell et al., 2016) and low-fat ketogenic diets (Newman et al., 2017) typically extend it. However, extreme version of lifespan-extending intervention may have an opposite effect. Thus, not surprisingly, too extreme restriction of calories would result in starvation and decrease of fitness and longevity of the individual (Fontana et al., 2010).

The effect of intervention on lifespan is tested through longevity studies (Figure 1), where a cohort of organisms is observed till the death of all its individuals. Then survival curve is built based on distribution of deaths with time. Afterwards, the distribution is compared to the survival curve of control individuals, and statistical significance of the difference is estimated (e.g., log-rank test for comparison of median lifespans). Apparently, the power of this test is highly dependent on the sample size. Therefore, although in simple short-lived animals, such as *C. elegans* with a lifespan of several weeks, lots of individuals can be used for longevity study, and the length of study seems to be pretty short, for other animals and, most importantly, for mammals

such study would be significantly longer (about 3-4 years for mouse) and more expensive. Therefore, longevity studies for mammals are rare and less reliable because of the typically low sample size.

To overcome this problem, a multi-institutional study called Interventions Testing Program (ITP) was designed by National Institute of Aging (NIA). Every year, ITP tests 4-7 pharmacological interventions for the longevity effect in genetically heterogenous mouse strain (UM-HET3) (Miller et al., 2007). Independent study of every intervention in 3 laboratories across the USA together with high sampling within each site (80 and 170 in treatment and control group, respectively) ensures high reliability of the results. To date, this program has identified significant median lifespan-extending effect, at least in one sex, for aspirin (Strong et al., 2008), acarbose (Harrison et al., 2014; Strong et al., 2016), 17-α-estradiol (Harrison et al., 2014; Strong et al., 2016), Protandim™ (Strong et al., 2016), rapamycin (Harrison et al., 2009; Miller et al., 2011, 2014) and nordihydroguaiaretic acid (NDGA), whereas other treatments such as oxaloacetic acid, green tea extract, simvastatin, fish oil, resveratrol and metformin showed no statistically significant effect on lifespan (Miller et al., 2011; Strong et al., 2013, 2016).

Interestingly, longevity interventions unequally affect different sexes. Thus, introduction of rapamycin (14 ppm) in mice leads to 21% increase of median lifespan in females, but only to 13% in males (Miller et al., 2014), whereas NDGA only increases male median lifespan (by 9-12%) and does not affect female lifespan (Harrison et al., 2014; Strong et al., 2008). The male-only effects were also observed for 17-α-estradiol (Harrison

et al., 2014; Strong et al., 2016) and Protandim™ (Strong et al., 2016). Generally, except for rapamycin, interventions have larger effect on the longevity of males than females. At the same time, UM-HET3 control females live about 13% longer than males, on average (Strong et al., 2013). Several theories tried to connect these observations by focusing on the role of sex hormones in determination of lifespan (Viña et al., 2005). Indeed, estrogen seems to provide some properties beneficial for healthspan, such as increased antioxidative defense (Mann et al., 2007) and, consequently, lower rate of oxidative DNA damage in females compared to males as shown in human leukocytes (Proteggente et al., 2002), along with anti-inflammatory effect (Benedusi et al., 2012). Moreover, castration of male rats leads to lifespan extension (Drori and Folman, 1976), whereas ovariectomy of females decreases average lifespan (Asdell et al., 1967). For some lifespan-extending interventions, such as CR and growth hormone mutants, feminizing effect was observed in males at the level of gene expression (Buckley and Klaassen, 2009; Estep et al., 2009; Fu and Klaassen, 2014). Altogether, the effect of lifespan-extending interventions may be associated with recapitulation of estrogen feminizing effect, which would explain the consistent difference in size of effect between males and females along with the exclusive beneficial effect of 17-α-estradiol in males. However, interestingly, lifespan of males subjected to this drug outperforms lifespan of female controls (Strong et al., 2016). Therefore, it seems that feminizing effect of sex hormones couldn't completely explain the effect of interventions, although there are certainly some shared mechanisms and features between them on systemic level. In general, molecular signatures associated with many individual lifespan-

extending interventions have been identified but universal necessary and sufficient mechanisms of the lifespan extension effect remain unclear.

1.3.1 Molecular and physiological signatures of lifespan-extending interventions

Despite wide range of individual lifespan-extending interventions, they can be generally divided into several categories based on their types, such as environmental, dietary, pharmacological and genetic. Environmental interventions do not require any direct manipulations with an organism and include temperature decrease (Zhang et al., 2015) and hypoxia (Honda and Honda, 2002) in *C. elegans*. Dietary interventions differ in amount, composition and regime of food consumption. Most popular of them are caloric restriction, a decrease in amount of food (typically by 20-40% in mouse) without any change in food composition (Mitchell et al., 2016); every-other-day feeding (EOD), a repeated regime of one day of full starvation following by one day of full *ad libitum* access to the food (Xie et al., 2017); methionine restriction (MR), a normal diet with the restriction in only one amino acid (methionine) (Richie et al., 1994), and ketogenic diet, which is a change in food composition so that 89% kcal are obtained from fat (compared to 17% kcal in the control diet) and less than 1% is represented by carbohydrates (compared to 65% in the control diet) (Roberts et al., 2017). Genetic lifespan-extending interventions are represented by knockout and overexpression models. Major group of such interventions includes different mutants associated with growth hormone production and signaling deficiency, such as growth hormone receptor (*Ghr*) knockout (GHRKO) (Zhou et al., 1997); Little mice, knockouts of growth hormone-releasing hormone receptor (*Ghrhr*) (Sun et al., 2013), and Ames (Brown-Borg et al., 1996) and Snell (Flurkey et al., 2001)

dwarf mice, knockouts of *Prop1* and *Pit1* genes, respectively, involved in the development of pituitary gland and production of growth hormone (GH). Other genetic interventions include overexpression of fibroblast growth factor 21 (*Fgf21*) (Zhang et al., 2012), deletion of S6K1 (Selman et al., 2009) and haploinsufficiency of MYC (Hofmann et al., 2015). Finally, pharmacological interventions are individual chemical compounds or combinations of them including rapamycin (Miller et al., 2011), acarbose (Harrison et al., 2014) and others tested by ITP.

Although wide range of interventions of different kind is currently identified, many of them seem to share common molecular and physiological signatures and even act through the same signaling pathways. One of the most conserved pathways linked to longevity is insulin and IGF1 signaling (IIS) pathway (Figure 3). Activated by growth hormone (GH), insulin-like growth factor (IGF1) and insulin through corresponding receptors, this pathway is significantly negatively associated with longevity across yeasts, worms, flies and mammals (Fontana et al., 2010). Important downstream targets of this pathway include mTOR complexes and the FOXO family of transcription factors, also involved in aging and lifespan extension. Downregulation of all members of the IIS pathway, including GH receptor (Zhou et al., 1997), IGF1 receptor (van Heemst, 2010), insulin receptor (Bartke, 2011), PI3K (Foukas et al., 2013) and AKT (Nojima et al., 2013), was shown to increase lifespan across model organisms. Thus, homozygous nonsense mutation in *age-1*, PI3K ortholog in *C. elegans*, resulted in the most significant extension of lifespan in this organism, being 10-fold increase (Ayyadevara et al., 2008). Interestingly, number of studies supports the role of the IIS pathway in determination of longevity in

humans. Thus, mutations in the IGF1 receptor gene are overrepresented among Ashkenazi Jewish centenarians (Suh et al., 2008), and genotype associated with reduced level of IGF1 in plasma was overrepresented among long-lived people (Bonafè et al., 2003). Moreover, gene variants of AKT and FOXO3A were found to be consistently associated with human lifespan in number of cohorts (Pawlikowska et al., 2009).

Interestingly, GH and IGF1 levels seem to decrease during natural aging as well as in models of accelerated aging (Schumacher et al., 2008). This is a nice counterargument to hypothesis that lifespan-extending interventions act simply by reversing all age-related changes. In fact, it seems that some of the changes, like this, are defensive response of an organism to accumulation of damage, and increase its fitness (Garinis et al., 2008). It's important to distinguish such compensatory mechanisms from harmful drivers of aging.

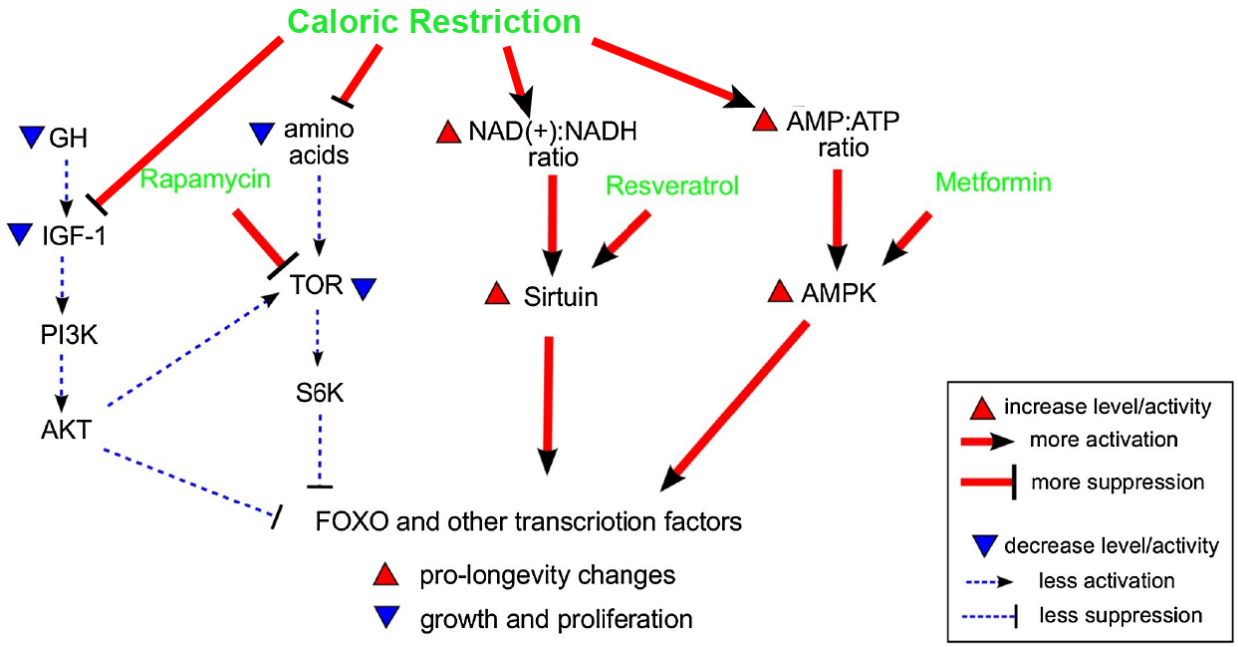

Figure 3. Nutrient sensing pathways associated with longevity

The majority of known lifespan-extending interventions act through certain components of these pathways. Some of the most famous and well-studied interventions are shown in green along with

their targets. The picture is taken from (Ma and Gladyshev, 2017) with permission and modified by the author.

Important downstream target of IIS pathway is mammalian target of rapamycin (mTOR) (Figure 3). mTOR is a major amino-acid and nutrient sensor presented in two protein complexes, mTORC1 and mTORC2. Much more is known about regulation and function of mTORC1 complex. mTORC1 is activated by the IIS and amino acids, and repressed by AMP-activated protein kinase (AMPK), main sensor of energy status in the cell. mTORC1 is responsible for plenty of functions including cell growth and proliferation, translation, lipid biosynthesis, mitochondrial function and autophagy (Johnson et al., 2013). In particular, it upregulates protein synthesis by activating ribosomal protein S6 kinase 1 (S6K1) and inhibiting eukaryotic translation initiation factor 4E-binding protein 1 (4E-BP1). mTOR inhibition by genetic manipulations (mutations and knockdown) or compounds, such as rapamycin, consistently extends lifespan across different model organisms, such as yeasts (Kaeberlein, 2012), worms (Robida-Stubbs et al., 2012), flies (Bjedov et al., 2010) and mice (Miller et al., 2014), making it one of the most conservative longevity-associated targets. Moreover, inhibition and activation of its downstream targets S6K1 (Selman et al., 2009) and 4E-BP1 (Zid et al., 2009), respectively, alone are enough for lifespan extension. Interestingly, lifespan-extending effect of S6K1 deletion in mice was sex-specific, with only females receiving longevity benefit.

AMP-activated protein kinase (AMPK) is a main sensor of energy status in cell activated in response to low ATP levels (Figure 3). By inhibiting mTOR, it switches off growth and synthesis program in the absence of nutrients (Alers et al., 2012). Overexpression of AMPK (Apfeld et al., 2004) along with its activation by metformin (De

Haes et al., 2014) were found to extend lifespan in *C. elegans*. Interestingly, AMPK is required for longevity effect of *daf-2* (IGF1 ortholog) mutation in *C. elegans* (De Haes et al., 2014).

Sirtuins, NAD^+-dependent protein deacetylases, seem to be positively associated with longevity. Their overexpression or activation by resveratrol have been shown to extend lifespan in yeasts (Kaeberlein et al., 1999), worms (Wood et al., 2004) and mice (Kanfi et al., 2012). In yeasts, their activity is associated with inhibition of formation of toxic extrachromosomal ribosomal DNA circles. In *C. elegans*, *sir-2.1* was shown to activate FOXO ortholog, DAF-16 (Berdichevsky et al., 2006). Interestingly, SIR-2.1 was shown to directly deacetylate FOXO protein and was not required for the lifespan-extending effect of IIS pathway, pointing to independent regulation of FOXO factors by sirtuins and IGF1. In mammals, SIRT6 was shown to regulate genomic stability, NF-κB signaling and glucose homeostasis through histone H3K9 deacetylation. Its overexpression significantly extended longevity of male, but not female, mice, once again demonstrating sex-specific differences common for lifespan-extending interventions (Kanfi et al., 2012).

Therefore, generally nutrient sensing pathways seem to be related to growth and proliferation program, which is associated with accumulation of damage and low control over it, whereas inhibition of these pathways leads to the switch to survival mode, characterized by significant defense response and removal of accumulated damage. Such defense mechanisms include upregulation of acute stress and antioxidative response regulated by NRF2, associated with the lower level of damage accumulation (Steinbaugh et al., 2012), autophagy, important for removal of dysfunctional components of the cell

(Madeo et al., 2015), and stem cell function, required for regenerative potential of the tissues (Yilmaz et al., 2012), along with downregulation of mRNA translation, which may be beneficial for protein homeostasis and preference for protein repair over synthesis of new molecules (Kaeberlein and Kennedy, 2008), and cellular senescence and associated secretory phenotype, leading to the lower level of inflammation (Laberge et al., 2015). Interestingly, long-lived rodent naked mole rat demonstrates some similarities at the level of longevity-associated mechanisms. Thus, it also shows increased level of autophagy (Zhao et al., 2014), higher level of NRF2 activity (Leiser and Miller, 2010), and decreased expression level of genes involved in IIS pathway (Kim et al., 2011).

Consistently, direct regulation of some of these processes may extend organism lifespan. Thus, overexpression of *Atg5*, involved in autophagosome formation, in mice significantly increases its median lifespan by 17% (Pyo et al., 2013). Overexpression of regulator of acute stress SKN-1, ortholog of NRF2, in *C. elegans* extends their lifespan (Tullet et al., 2008), similar to heterozygous deletion of NRF2 inhibitor, *Keap1*, in flies (Sykiotis and Bohmann, 2008). Inhibition of translation through overexpression of 4E-BP1 extends longevity of *Drosophila melanogaster* (Zid et al., 2009). Finally, mouse lifespan may be significantly increased by the elimination of naturally occurring senescent cells (Baker et al., 2016).

Caloric restriction seems to work through the different nodes of nutrient sensing pathways (Figure 3). Thus, ketone bodies, such as β-hydroxybutyrate, generated in response to CR, activate FOXO3A (Shirakawa et al., 2013), linking it to the mechanism of ketogenic diet (Roberts et al., 2017). CR also leads to increase of IGF binding protein 1

(IGFBP1) in plasma, decreasing the concentration of bioavailable IGF1 (Fontana et al., 2016). In addition, diet inhibits mTOR and activates AMPK and SIRT1 through inhibition of the IIS pathway and deprivation of absorbed amino acids, decrease in level of ATP as a consequence of fewer sources of energy received with the food, and increase in NAD^+ availability, respectively. Through these cellular sensors, CR seems to activate survival modes of an organism, including upregulation of autophagy (Galluzzi et al., 2014), and acute stress response and antioxidative defense system regulated by NRF2 (Pearson et al., 2008b; Steinbaugh et al., 2012).

However, although CR and many other lifespan-extending interventions act through common nutrient sensing pathways and linked molecular targets, their effect is not completely reproduced by each other. Indeed, CR applied to growth hormone deficient mice is able to further extend their lifespan, and vice versa (Bartke et al., 2001). In addition, combination of rapamycin and metformin has more effect on lifespan extension than rapamycin alone, although metformin doesn't have any statistically significant effect on lifespan by itself (Strong et al., 2016). On the other hand, manipulation of some nutrient-sensing hubs does not necessarily lead to lifespan extension. Besides metformin, good example of this phenomenon is resveratrol, a sirtuin activator (Gertz et al., 2012), which could only increase the lifespan of mice subjected to a high calorie diet, apparently by alleviation of hepatosteatosis consequences caused by such diet (Baur et al., 2006; Pearson et al., 2008a), but was ineffective in mice on a regular diet (Miller et al., 2011; Pearson et al., 2008a; Strong et al., 2013). Therefore, it is still unclear what aspects of the drug, diet, or mutant effect is either necessary or sufficient for lifespan extension.

1.4 Project objectives

Main goal of the project was to identify specific molecular patterns associated with lifespan extension both across and within the species. For that, we specified 2 main studies related to the goal, being (i) response to DNA damage in exceptionally long-lived rodent naked mole rat, and (ii) response to lifespan-extending interventions in mouse at the level of DNA methylation and gene expression.

In Chapter 2, we identify molecular mechanisms responsible for high resistance to DNA damage and cancer in naked mole rat compared to other rodents, such as mouse. To do that, we perform RNA sequencing of NMR and mouse embryonic and skin fibroblasts subjected to γ-irradiation, one of the standard DNA-damage inducers. We analyze common and distinct gene expression responses of the species to DNA damage and validate our findings with experimental data.

In Chapter 3, we identify age-associated changes in DNA methylation profile in mouse blood samples, together with the effect of caloric restriction on these changes. We perform detailed analysis of methylation profile change with age in mice using 141 samples from 16 different age groups and characterize main patterns associated with it, including role of specific functions, genomic regions and entropy effect. Then we characterize how lifespan-extending intervention (CR) effects age-related molecular changes with time and prove our findings using another mouse strain.

In Chapter 4, we perform high-throughput analysis of hepatic gene expression response to 17 different interventions, associated with lifespan- and healthspan extension in mouse. We characterize common genes and pathways regulated by lifespan-extending

interventions and characterize similarity of interventions based on their effect on mouse transcriptome. Finally, we identify new candidates for lifespan-extending interventions based on obtained longevity signatures and validate this approach, using two mouse strains with significantly different lifespans.

In Chapter 5, we conclude our findings and specify molecular patterns and mechanisms associated with different perspectives of lifespan extension. We discuss signatures of lifespan on both across- and within-species levels.

Chapter 2. Molecular Mechanisms of Cellular Resistance to DNA Damage in Naked Mole Rats

2.1 Materials and Methods

2.1.1 Cell Culture

Mouse embryonic fibroblasts (MEFs) and skin fibroblasts (MSFs) were grown at 37 °C in an atmosphere of 5% CO2 and 3% O2. Naked mole rat (NMR) embryonic fibroblasts (NEFs) and skin fibroblasts (NSFs) were grown at 32 °C (in vivo body temperature of naked mole rat) with 5% CO2 and 3% O2. All cells were cultured in EMEM medium (ATCC) with 15% (vol/vol) FBS, 100 μg/mL penicillin, and 100 U/mL streptomycin (Gibco).

2.1.2 γ-Irradiation-Induced Cellular Senescence

Growing mouse and naked mole rat fibroblasts were subjected to 10 Gy or 20 Gy γ-irradiation, and allowed to grow for 12 days for SA-β-gal assay and RNA extraction for RNA sequencing (RNAseq), or 2 days for BrdU assay and western blot.

2.1.3 SA-β-Gal Assay

For SA-β-gal staining, cells were fixed and stained using a commercial senescence β-galactosidase staining kit (Cell Signaling). Images were captured for 5 replicates and counted at least 100 cells for each replicate.

2.1.4 RNAseq Data Processing and Analysis

Raw reads generated from the Illumina HiSeq2500 sequencer were demultiplexed using configurebcl2fastq.pl, version 1.8.4. Quality filtering and adapter removal were

performed using Trimmomatic version 0.32. Processed/cleaned reads were then mapped with STAR (version 2.5.2b) (Dobin et al., 2013) to the set of orthologs common to naked mole rats and mice (Ma et al., 2016) to ensure consistent annotation between the species and, therefore, to make them appropriate for subsequent cross-species analyses. Read counting was performed by featureCounts (Liao et al., 2014). To filter out genes with low number of reads and expressed only in one species, only genes with at least 1 count per million (cpm) in at least 3 samples (25%) in each species were included, which resulted in the expression set of 11,178 genes across 24 samples. Filtered data was then passed through RLE normalization (Anders and Huber, 2010). Principal component analysis (PCA) was performed on the standardized expression values and the first 2 principal components were extracted with the corresponding percentage of explained variance. Differential expression analysis was performed with the R package edgeR (Robinson et al., 2009). We declared gene expression to be significantly changed, if p-value, adjusted by the Benjamini-Hochberg procedure, was smaller than 0.05 and fold change was larger than 2 in any direction. When identifying commonly changed genes across NMRs and mice, we included factors responsible for each of the 4 phenotype groups (MEF, MSF, NEF and NSF) to the model but specified an IR effect 19 as a single factor common to all groups, and tested its difference from 0. When identifying genes with the differential response to IR between NMR and mice, we added a factor responsible for the NMR-specific IR effect to the previous model and tested its difference from 0. Unpaired Mann-Whitney test against two-sided alternative hypothesis was used to examine statistical significance of difference between standard deviations of mice and NMR genes logFC before and after γ-irradiation.

The Z-score proportion test against two-sided alternative hypothesis was used when examining if differences in the number of enriched functions between NMR and mice in each of functional groups could be explained by difference in the number of enriched functions. The total number of enriched functions was considered as the number of trials, and the number of enriched functions corresponding to a particular functional group were considered as the number of successes. The Benjamini-Hochberg method was used to adjust for multiple comparisons. FDR threshold of 0.05 was used to select statistically significant functional groups. GSEA (Subramanian et al., 2005) was performed on a pre-ranked list of genes based on z-scores, calculated as:

$$z\text{-}score = -\ln(pv) \times sgn(lfc),$$

where *pv* and *lfc* are p-value and logFC of certain gene, respectively, based on edgeR output and *sgn* is signum function (is equal to 1 if value is positive, -1 if negative and 0 if equal to 0). REACTOME, KEGG and GO biological process and molecular function from Molecular Signature Database (MSigDB) have been used as gene sets for GSEA (Subramanian et al., 2005). q-value cutoff of 0.05 was used to select statistically significant functions.

2.1.5 Western Blotting

Two days after γ-irradiation (IR), cells were harvested and lysed in Laemmli Sample Buffer (Bio-Rad) with 1 mM PMSF. Extracts were boiled and centrifuged at 14,000 × g for 15 min at 4 °C. Protein samples were resolved by SDS-polyacrylamide gel electrophoresis and transferred to PVDF membranes (Bio-Rad). Membranes were incubated with a rabbit monoclonal anti-p21 primary antibody (ab109199; Abcam). A

horseradish peroxidase (HRP)-conjugated antirabbit IgG (Abcam) secondary antibody was used. Proteins were visualized using an ECL kit (BioRad).

2.1.6 BrdU-Incorporation Assay

Two days after IR, cells were cultured in the presence of 5-bromo-2'-deoxyuridine (BrdU) (3 μg/ml) for 48 h, and fixed using 4% paraformaldehyde for 60 min, washed with PBS for 5 times, followed by treatment with 2N HCl for 30 min. After washed with PBS for 3 times, cells were blocked with 5% FBS in PBS with 0.2% Triton X-100 for 2 h. A FITC-conjugated anti-BrdU antibody (Sigma; 1:200) was used to incubate the cells at 4 °C overnight. Cells were then incubated 18 with Hoechst for 10 min at room temperature, and observed under a fluorescence microscope. Images were acquired for five replicates and counted for at least 100 cells for each replicate.

2.1.7 Comet Assay

Cells were kept on ice and subjected to 10 or 20 Gy IR, and were then harvested immediately. DNA damage was detected by using a commercial comet assay kit (Trevigen) following the manufacture. Images were acquired and the percentage of tail DNA was analyzed from 100 cells per sample using CaspLab software.

2.1.8 Apoptosis Assay

Mouse and NMR fibroblasts were subjected to 10 or 20 Gy γ-irradiation. Three days after irradiation, cells were harvested and stained using an Annexin V-Fluo staining kit (Roche). Cell death was measured using FACS on a BD LSR II Flow Cytometer.

2.2 Results

2.2.1 Comparison of Gene Expression Changes in Response to γ-Irradiation in NMR and Mouse Fibroblasts

γ-Irradiation induces stress-induced premature senescence (SIPS) in human and mouse fibroblasts by activating a DNA damage response (D'Adda Di Fagagna, 2008). To perform an unbiased characterization of the differences in response to DNA damage, between NMR and the mouse at the gene expression level, we subjected embryonic and skin fibroblasts derived from three animals of each species (MEF, MSF, NEF, and NSF cells) to 20 Gy of γ-irradiation and performed RNA sequencing (RNAseq). Total RNA was collected from both treated and untreated cells 12 d later, a time point when irradiated cells displayed positive SA-β-gal staining (Figure 9A), and sequenced. Three biological replicates (primary cells isolated from three different animals) were sequenced for each condition.

To achieve uniform annotation of sequenced genes between the species, we mapped the reads to the set of mouse and NMR orthologs, which, after filtering and normalization, resulted in the coverage of 10,959 genes. Following this procedure, samples across species and cell types showed similar gene expression profile distribution, making them appropriate for subsequent analysis. To assess the gene expression patterns across cell types and species, we performed principal component analysis (Figure 4). The samples segregated more predominantly by species (first component; 51.5% variance explained) than by the type of fibroblasts (mainly second component; 24.7% variance explained).

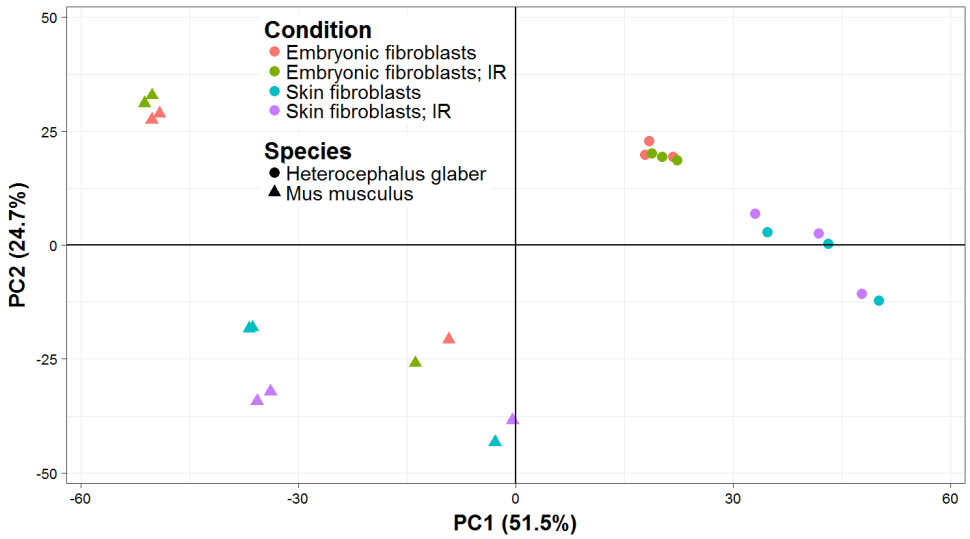

Figure 4. Principal component analysis of mouse and NMR individual samples
Samples generally segregated by species (first principal component explaining 51.5% of variance). Irradiation samples tend to group together with their paired controls. PC: Principal Component; IR: After γ-irradiation.

As expected, irradiated samples also tended to cluster with their paired controls, confirmed by Pearson correlation matrix of gene expression profiles (Figure 5). Interestingly, gene expression across different NMR samples was more tight than across mouse samples (Figure 5), possibly reflecting chromosomal instability typical of cultured mouse cells (Gaztelumendi and Nogués, 2014). To compare within-species and within-cell-type variation of gene expression changes in response to γ-irradiation, we calculated gene fold changes averaged across replicates for each species and cell type and built a Pearson correlation matrix of the four analyzed groups. The correlation matrix showed clear separation by species, confirming that within-species variation is lower than variation in the within-cell types.

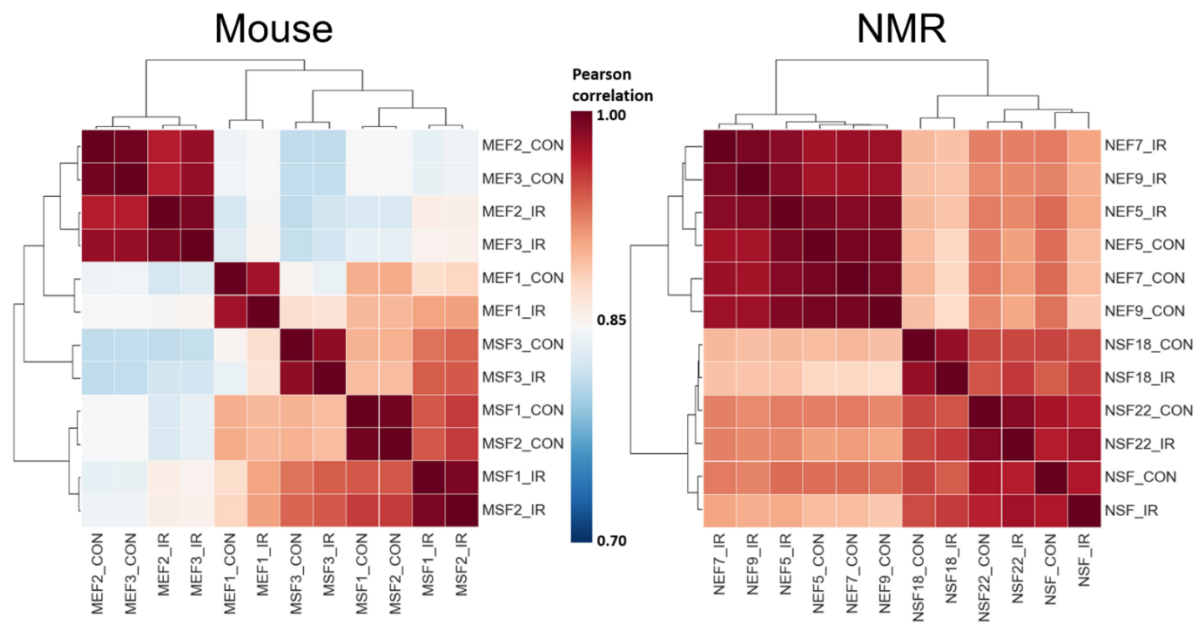

Figure 5. Pearson correlation matrix for mouse and NMR individual samples
Within species, samples generally cluster based on types of fibroblasts. NMR samples show higher similarity across samples compared to mouse samples. NEF: NMR Embryonic Fibroblasts; NSF: NMR Skin Fibroblasts; MEF: Mouse Embryonic Fibroblasts; MSF: Mouse Skin Fibroblasts; CON: Control; IR: After γ-irradiation.

To identify changes induced by γ-irradiation in the NMR and mouse transcriptomes, we examined differentially expressed genes for each species and cell type using edgeR (Robinson et al., 2009). We used a Benjamini–Hochberg procedure to adjust for multiple comparisons and qualified as significantly changed the genes with the adjusted $P < 0.05$ and fold change of >2 in any direction. Approximately two times more differentially expressed genes were detected in mouse fibroblasts (651 for MEF and 751 for MSF) compared with NMR fibroblasts (323 for NEF and 220 for NSF) (Figure 7A). Notably, the number of statistically significant upregulated genes exceeded the number of downregulated genes for all analyzed groups (Figure 7A). In addition, many upregulated genes were shared across cell types and species (Figure 6). Although we observed within-

species clustering of gene fold changes, we also observed statistically significant positive Pearson correlation of genes logFC between any two analyzed groups (Pearson correlation test $P < 2 \cdot 2 \cdot 10^{-16}$ for all comparisons), even when comparing different cell types of NMR and mice ($\rho = 0.17$ for mice EF vs. NMR SF and $\rho = 0.2$ for mice SF vs. NMR EF), pointing to the existence of a general gene expression response of fibroblasts to γ-irradiation across species and types of fibroblasts.

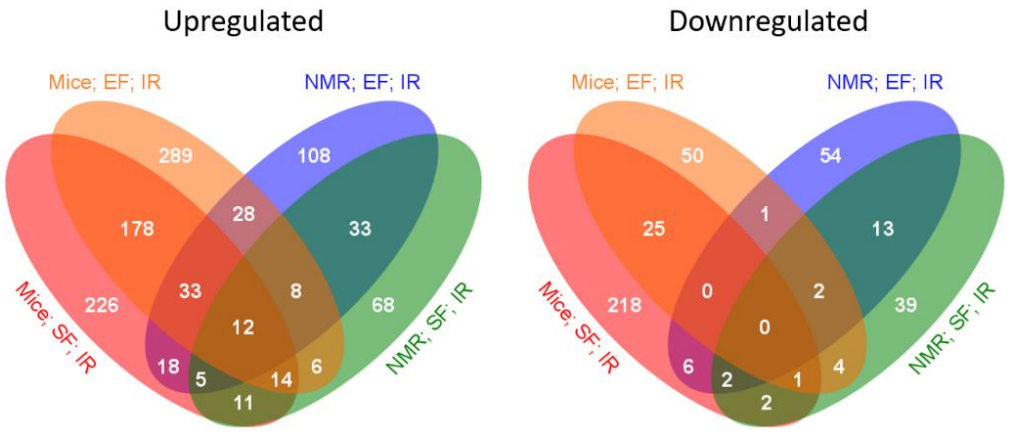

Figure 6. Numbers of differentially expressed in mouse and NMR
Many differentially expressed genes (adjusted p-value < 0.05; FC > 2) overlap between different analyzed groups, especially between different types of fibroblasts within the same species. EF: Embryonic Fibroblasts; SF: Skin Fibroblasts; IR: After γ-irradiation.

To further investigate the transcriptome response of NMR and mice fibroblasts to γ-irradiation, we performed Gene Set Enrichment Analysis (GSEA) for each of the four analyzed groups using the GO Biological Process (GO BP) and Molecular Function (GO MF), Kyoto Encyclopedia of Genes and Genomes (KEGG) and REACTOME database gene sets as a reference. Interestingly, although more genes were identified as differentially expressed in mouse fibroblasts, more pathways were detected as enriched in NMRs (1,151 for NEF and 551 for NSF) than in mice (140 for MEF and 262 for MSF) (Figure 7B),

indicating that gene expression changes in the NMR are less drastic, but more systematic and nonstochastic. Indeed, SDs of logFC induced by γ-irradiation in mouse samples are statistically significantly higher than those in NMR samples (P = 0.015), as determined by Mann–Whitney U test, pointing to higher stochasticity and scale of transcriptome changes in mice.

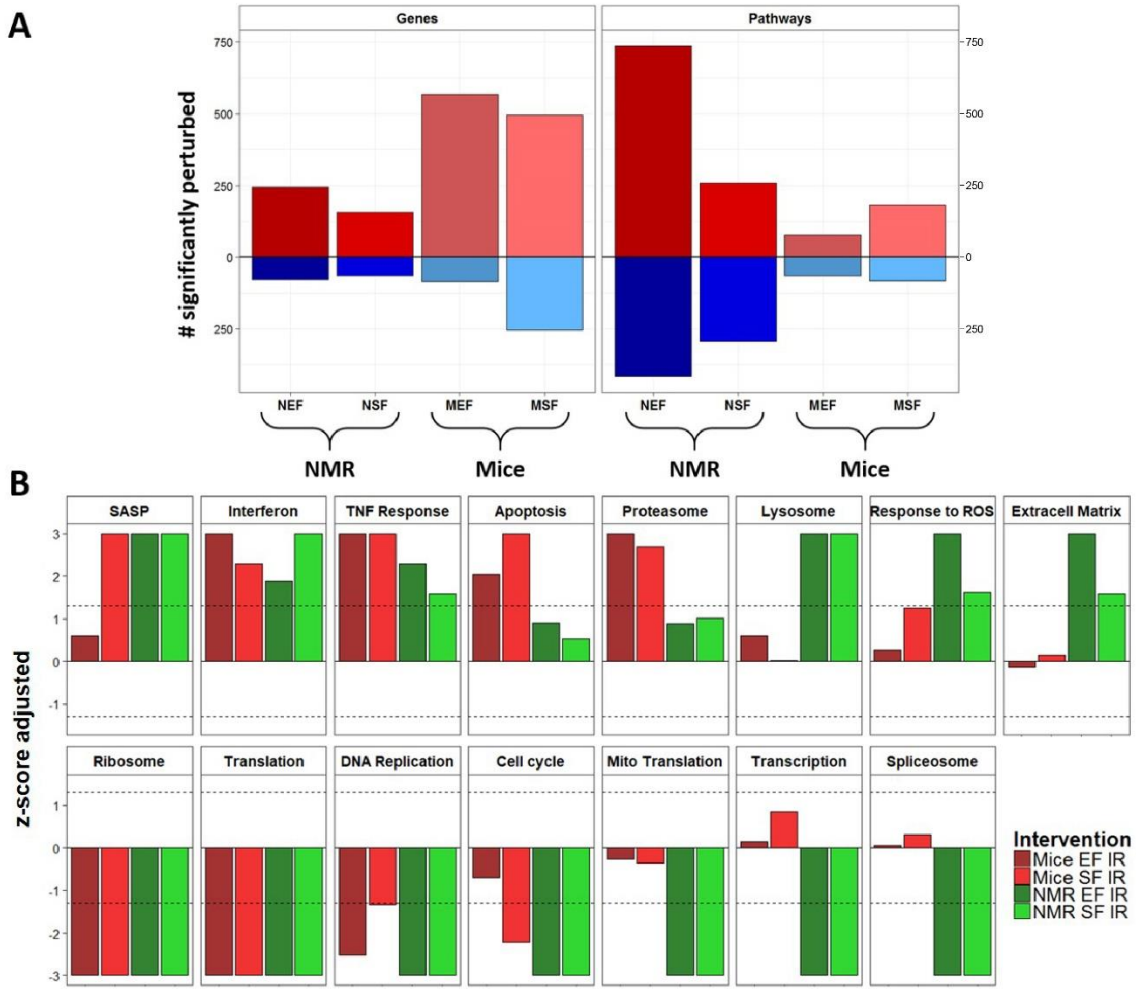

Figure 7. Changes induced by γ-irradiation in NMR and mouse fibroblasts
(A) Numbers of identified statistically significant differentially expressed genes (Benjamini-Hochberg adjusted p-value < 0.05; fold change (FC) > 2 in any direction) and enriched functions (q-value < 0.05) in NMR and mouse fibroblasts in response to γ-irradiation. Up- and downregulated entities are shown in red and blue, respectively. **(B) Pathways enrichment of genes**

differentially induced by γ-irradiation based on GSEA. Z-scores (in logarithmic scale) corresponding to presented functions are shown for each analyzed group. Z-scores of mouse and NMR fibroblasts are colored in red and green, respectively. Dotted line corresponds to q-value = 0.05. SASP: senescence-associated secretory phenotype genes; Interferon: Interferon alpha/beta signaling (REACTOME); TNF response: Response to Tumor Necrosis Factor (GO BP); Apoptosis: Apoptosis (REACTOME); Proteasome: Proteasome (KEGG); Lysosome: Lysosome (KEGG); Response to ROS: Response to Reactive Oxygen Species (GO); Extracell Matrix: Extracellular Matrix Binding (GO); Ribosome: Ribosome (KEGG); Translation: Translation (REACTOME); DNA Replication: DNA Replication (KEGG); Cell cycle: Cell cycle (KEGG); Mito Translation: Mitochondrial translation (GO BP); Transcription: Transcription (REACTOME); Spliceosome: Spliceosome (KEGG).

Many enriched functions and pathways were shared across cell types and species. They include upregulation of genes involved in the immune response and downregulation of genes involved in cell cycle, DNA replication, translation, and ribosome protein genes (Figure 7B). When we analyzed the number of enriched functions (with a GSEA adjusted $P < 0.05$) shared by embryonic and skin fibroblasts within each species, we discovered more functions perturbed in NMR fibroblasts (213 upregulated and 257 downregulated) than in mouse cells (61 upregulated and 42 downregulated), consistent with the results for every individual cell type.

We also tested if genes related to senescence-associated secretary phenotype (SASP) are differentially expressed in response to γ-irradiation in NMR and mice. We performed enrichment of differentially expressed genes by SASP gene set as characterized in (Coppé et al., 2010a, 2008, 2010b), and observed their consistent activation in all analyzed groups (GSEA $P < 10^{-3}$ for MSF, NEF, and NSF), except MEF samples (GSEA $P = 0.26$) (Figure 7B). Correlation and linear model analyses showed consistency between expression of SASP genes in the NMR and mouse with the Pearson correlation coefficient equal to 0.53 ($P = 2.8 \cdot 10^{-5}$) for SF and 0.63 for EF ($P = 2.9 \cdot 10^{-7}$).

In addition to common functions, we discovered many enriched pathways specific for certain species. Naked mole rat cells displayed unique downregulation of transcription, spliceosome, and mitochondrial translation, which may indicate a more profound inhibition of cellular metabolism. On the other hand, pathways involved in protein and glycoprotein metabolism, lipid metabolism, lysosome, extracellular matrix, and oxidative stress response were uniquely activated in the NMR. In addition, apoptotic processes were activated in the mouse (GSEA adjusted $P = 9 \cdot 10^{-3}$ for MEF and 10^{-3} for MSF), but not in the NMR (GSEA adjusted P = 0.125 for NEF and 0.302 for NSF), pointing to the avoidance of apoptosis by NMR cells when subjected to γ-irradiation (Figure 7B).

2.2.2 Identification of Common and Distinct Gene Expression Changes in Response to γ-Irradiation between NMR and Mouse

To obtain further insights into similarities and differences in the transcriptome response to γ-irradiation in mice and NMRs, we examined genes with the most similar and distinct expression changes across these species. With the Benjamini–Hochberg adjusted P value threshold equal to 0.05 and the fold change threshold equal to 2, we detected 224 genes with common changes and 782 genes with distinct changes between the NMR and mouse (Figure 8A). Interestingly, the majority of genes with distinct behavior were genes upregulated in the mouse but not in the NMR. These genes included apoptotic genes (GSEA adjusted P = 0.045), consistent with individual GSEA results (Figure 8B). Among them, we could identify the transcription factor *E2f1*, which mediates p53-dependent and -independent apoptosis, together with its positive regulator *Tfdp1*, apoptosis activators *Cflasr*, *Dapk1*, and *Pmaip1* (*Noxa*), with the latter known to be associated with radiation

response, cell-surface death receptor *Fas*, several cytoskeleton-related genes (*Plec, Lmnb1*, *Dsp*), as well as several genes related to proteasome structure and activity (*Psmb3, Psmc4*, *Psmd6, Psme4*). Other enriched pathways associated with genes activated in mice compared with NMR include transcription (GSEA adjusted $P = 3.87 \cdot 10^{-3}$) and spliceosome (GSEA adjusted $P = 8.2 \cdot 10^{-3}$). On the other hand, genes associated with ribosome (GSEA adjusted $P = 3.28 \cdot 10^{-3}$) and lysosome (GSEA adjusted $P = 3.28 \cdot 10^{-3}$) show significantly stronger inhibition in mice compared with the NMR.

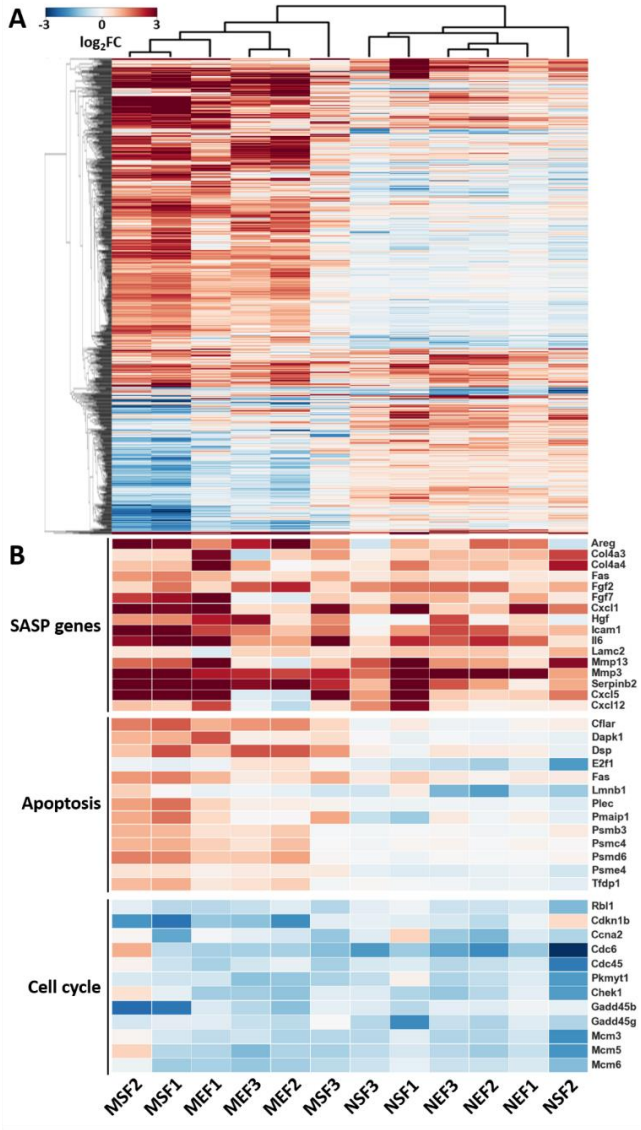

Figure 8. Genes with common and distinct gene expression response to γ-radiation in NMR and mouse

(A) Heatmap of genes identified as commonly or distinctly responded to irradiation in NMR and mouse (Benjamini-Hochberg adjusted p-value < 0.05, fold change > 2 in any direction). 224 genes were identified as commonly changed, and 782 as distinctly changed. **(B) Functions enriched by genes with common (SASP genes, Cell cycle) and distinct (Apoptosis) response to γ-irradiation in NMR and mouse fibroblasts (q-value < 0.05).** Differentially expressed genes (adjusted p-value < 0.05, fold change > 1.5 in any direction) are shown for each pathway. NEF: NMR Embryonic Fibroblasts; NSF: NMR Skin Fibroblasts; MEF: Mouse Embryonic Fibroblasts; MSF: Mouse Skin Fibroblasts; SASP: senescence-associated secretory phenotype.

GSEA performed on the list of commonly changed genes showed that pathways such as tumor necrosis factor (TNF) signaling (GSEA adjusted $P < 3.53 \cdot 10^{-5}$), ribosome (GSEA adjusted $P < 1.43 \cdot 10^{-5}$), and cell cycle (GSEA adjusted $P < 1.43 \cdot 10^{-5}$) together with SASP genes are commonly changed not only at the level of functional enrichment, but also at the level of the same individual genes involved in these pathways (Figure 8B).

Together, these results indicate that NMR and mice share many common gene expression signatures in response to γ-irradiation, both at the level of individual genes and at the level of enriched pathways. They include DNA replication, transcription, translation, cell cycle, and immune response. At the same time, some biological processes, such as apoptosis, glycoprotein metabolism, lysosome, extracellular matrix, and oxidative stress response, show distinct behavior in these species, pointing to unique adaptations of NMR fibroblasts to DNA damage. Generally, mouse fibroblasts demonstrate more substantial and variable transcriptome remodeling at the level of individual genes, whereas response of NMR fibroblasts seems to be less drastic and more robust.

2.2.3 Attenuated Senescence and Apoptosis in NMR Fibroblasts in Response to γ-Irradiation

To validate results obtained by RNAseq and observe if NMR cells recapitulate behavior of mice fibroblasts in response to DNA damage, we subjected MEF, MSF, NEF and NSF to 2 different doses of γ-irradiation, being 10 and 20 Gy. Senescence was quantified by SA-β-gal staining and BrdU incorporation. All four cell types showed SA-β-gal–positive staining in response to γ-irradiation. Notably, at 10 Gy of γ-irradiation NMR showed fewer SA-β-gal–positive cells than mouse cells. At the higher 20-Gy dose both

mice and NMR displayed similar numbers of SA-β-gal–positive cells (Figure 9A,B). Consistent with the SA-β-gal staining result, at 10 Gy NMR cells did not show a significant drop in BrdU incorporation, while in mouse cells BrdU incorporation dropped significantly. In the NMR cells, a significant drop in BrdU incorporation occurred only at 20 Gy (Figure 9C), consistent with the RNAseq results, where cell cycle pathway was found to be commonly downregulated in both species. Taken together, these results suggest that NMR cells are more resistant to induction of SIPS than mouse cells and require a higher dose to achieve the same percentage of senescent cells.

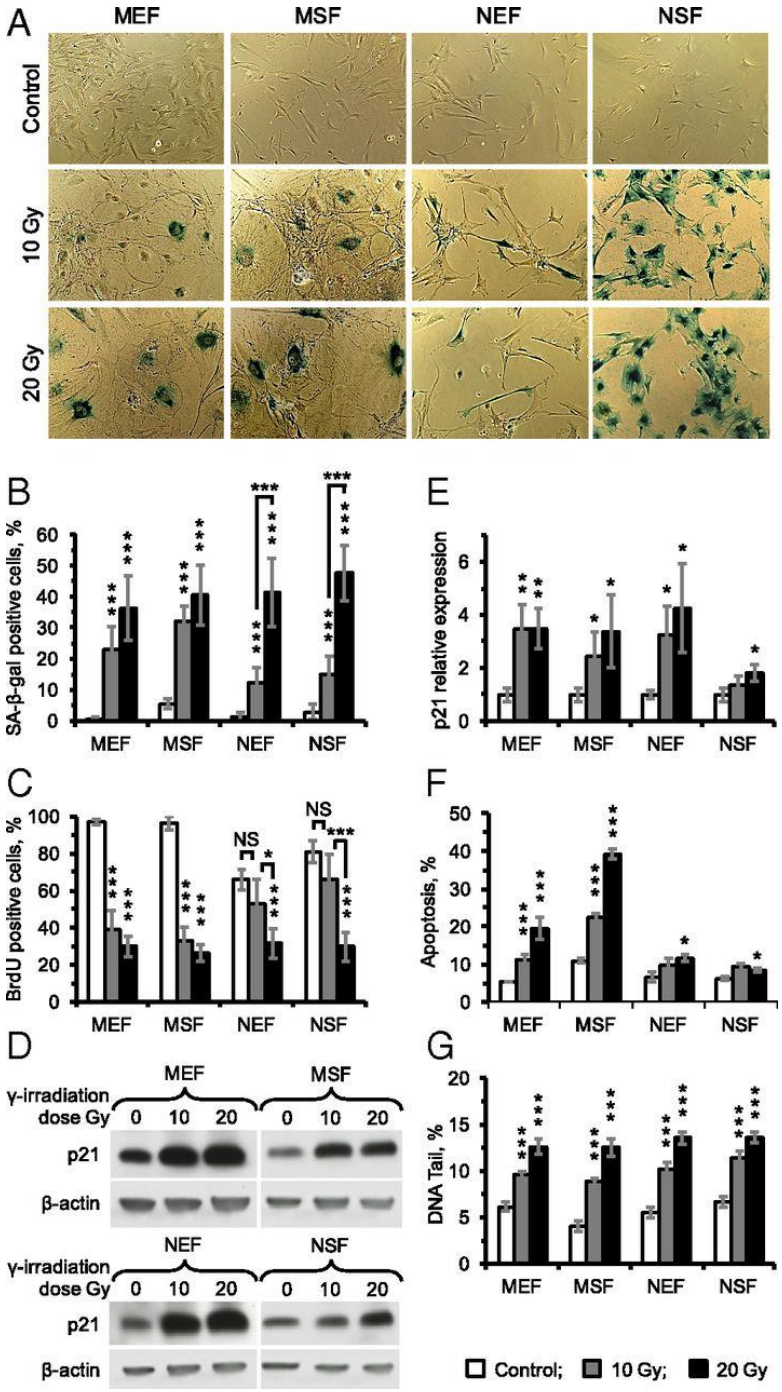

Figure 9. The γ-irradiation–induced CS of mouse and NMR fibroblasts

(A) Images of SA-β-gal staining of mouse and NMR embryonic and skin fibroblasts in response to 10 or 20 Gy of IR. (B) Quantification of β-gal–positive cells of mouse and NMR fibroblasts in response to IR. (C) BrdU incorporation in mouse and NMR fibroblasts 2 d after IR. (D) Expression of p21 in response to IR. Samples were harvested 2 d after IR and tested using Western blot. (E) Quantification of p21 expression. (F) Apoptosis of mouse and NMR

fibroblasts in response to IR. Three days after IR, cells were harvested and subjected to an Annexin V apoptosis assay using FACS. (G) Comet assay quantifying DNA damage in mouse and NMR fibroblasts induced by IR. MEF, mouse embryonic fibroblasts; MSF, mouse skin fibroblasts; NEF, NMR embryonic fibroblasts; NSF, NMR skin fibroblasts. For all except G, results are mean ± SD (n = 5); for comet assay (G), results are mean ± SEM (n = 100). *P < 0.05, **P < 0.01, ***P < 0.001.

Cell-cycle arrest and SIPS are triggered by the induction of p21 cyclin-dependent kinase inhibitor. Strong p21 induction occurred in MEF and NEF cells, but the p21 response was lower in the NSF cells compared with the NEF and MSF cells (Figure 9D, E).

In addition to senescence, cells may undergo DNA-damage–induced apoptosis, particularly when the DNA damage is severe (Childs et al., 2014). Both MEF and MSF cells underwent massive apoptosis in a dose-dependent manner while NEF and NSF cells showed only a slight increase in apoptosis after 20Gy irradiation, and no significant apoptosis was observed under 10Gy irradiation (Figure 9F), suggesting that NMR cells are resistant to γ-irradiation (IR)-induced apoptosis, consistent with the RNAseq results, where apoptosis activation was observed only in mice cells.

To examine if the NMR and mouse fibroblasts experienced the same physical DNA damage in response to γ-irradiation, we subjected cells to 10 and 20 Gy of γ-irradiation and collected immediately for comet assay. All four types of cells had similarly increased tail DNA in response to γ-irradiation (Figure 9G), suggesting that NMR and mouse cells sustain similar levels of DNA damage. Taken together, these results completely confirmed RNAseq findings and further showed that NMR fibroblasts undergo SIPS in response to γ-irradiation, but senescence and apoptotic responses are attenuated.

2.3 Discussion

CS plays important roles in developmental tissue remodeling (Muñoz-Espín et al., 2013) and tumor suppression in response to DNA damage (Campisi, 2005). We previously showed that NMRs, similarly to mice and other small-bodied rodents, do not display replicative senescence and continuously express telomerase (Seluanov et al., 2007, 2008). Here, we demonstrate that NMR cells undergo IR-induced senescence. These results show that despite their exceptional longevity and resistance to age-related diseases, NMRs still possess CS program.

Senescent cells accumulating in adult organisms have been linked to multiple age-related pathologies including cancer (Campisi, 2005), atherosclerosis (Childs et al., 2016), and osteoarthritis (Jeon et al., 2017). Elimination of senescent cells in mice displaying premature aging due to genomic instability increases animal life span, and elimination of senescent cells in wild-type mice increases their health span (Baar et al., 2017; Baker et al., 2016). However, our results indicate that the naked mole rat did not achieve longevity by eliminating the process of CS. Remarkably, senescent NMR cells exhibit a typical signature of SASP response including the conserved SASP factor CXCL-1 (GRO-α), which is believed to promote the growth of premalignant epithelial cells (Coppé et al., 2010b). Thus, the SASP response, which is linked to the proinflammatory and disease-promoting effects of senescence, is also preserved in the NMR.

NMRs may be somewhat protected from the induction of SIPS due to their higher resistance to the damaging agents. We observed that at 10 Gy of IR NMR cells displayed markedly fewer senescent cells then at 20 Gy, while mouse cells displayed a high level of

senescent cells at both IR doses. Thus, NMRs may accumulate fewer SIPS senescent cells during aging. This could be partly a result of better repair mechanisms or the protective role from the high-molecular-mass hyaluronan (HA) secreted by NMR cells (Tian et al., 2013). Ultimately, it would be interesting to quantify senescent cells in aged NMRs. This would shed light on whether senescent cells accumulate in vivo at similar rates to the shorter-lived species. This experiment, however, is logistically challenging as aged, 20- to 30-year-old NMRs are not readily available.

Furthermore, NMR fibroblasts were resistant to IR-induced apoptosis. Our RNAseq data demonstrated clearly that, unlike the mouse fibroblasts, in the NMR p53 and apoptosis signaling pathways were not induced by IR. Therefore, we hypothesize that the resistance of NMR cells to IR-induced apoptosis may be due to the blunted induction of p53 signaling. Reaching confluence and cell-cycle extension have been shown to promote resistance to apoptosis by allowing additional time to repair damage (Childs et al., 2014; Rochette and Brash, 2008). The NMR fibroblasts have a very slow rate of cell proliferation in culture, with early contact inhibition associated with the induction of $p16^{INK4a}$ and the additional INK4a/b hybrid product $pALT^{INK4a/b}$ (Seluanov et al., 2009; Tian et al., 2015). The $pALT^{INK4a/b}$ hybrid product induces stronger cell-cycle arrest in response to UV and IR (Tian et al., 2015). The strong cell-cycle arrest in NMR cells likely plays important roles in resistance to apoptosis. Generally, the resistance to IR-induced apoptosis in NMR may reflect its higher threshold for stress tolerance due to better DNA repair mechanisms or the protective effects of HA.

Since the naked mole rat is extremely cancer-resistant and long-lived, a question that could be raised is whether the resistance to apoptosis provides any benefit for cancer resistance or longevity. In terms of eliminating preneoplastic cells, apoptosis seems to have stronger ability to prevent tumorigenesis (Childs et al., 2014). However, too much apoptosis may deplete stem-cell reserves and contribute to frailty in old age (Gatza et al., 2007; Tyner et al., 2002).

Gene expression analysis of NMR cells made senescent by IR exposure (Figure 10) showed that many gene expression changes upon CS were conserved with mice such as induction of SASP, TNF response, and inhibition of protein translation and the cell cycle. The changes unique to NMR included induction of lysosomal genes, oxidative stress response, changes in extracellular matrix, and inhibition of transcription, spliceosome, and mitochondrial translation. These unique changes may have a cytoprotective effect. Induction of lysosomal genes suggests activation of autophagy. Autophagy plays important roles in response to DNA damage (Czarny et al., 2015; Wang et al., 2016). Previous study has shown that NMR has higher autophagy (Zhao et al., 2014). Here, we show that NMR fibroblasts are likely to undergo autophagy and induction of oxidative stress response upon exposure to IR, possibly contributing to NMR resistance to stresses. Furthermore, inhibition of transcription and mitochondrial translation, observed only in the NMR, suggests that senescent NMR cells inhibit metabolic activities, thereby reducing pathogenesis of senescent cells. It has been observed that downregulation of the mTOR pathway in senescent cells ameliorates the senescent phenotype (Laberge et al., 2015; Leontieva et al., 2014).

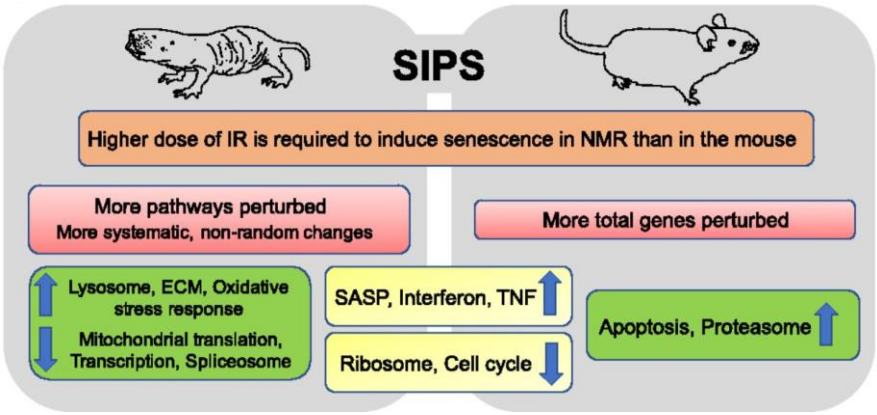

Figure 10. Summary of common and distinct features of IR-induced SIPS between the NMR and the mouse

Interestingly, fewer genes were changed in the senescent NMR cells, compared with mouse cells, but these genes organized in markedly more functional pathways. This result suggests that the senescence-related gene expression changes in the NMR are more systematic and nonrandom. Taken together, these unique features of NMR senescent cells may reduce the pathogenic properties of senescent cells and contribute to NMR longevity.

In summary, we have demonstrated that NMR cells undergo stress-induced senescence. This result shows that evolution of a long lifespan does not eliminate the CS response. On the contrary, NMR cells were more resistant to apoptosis than mouse cells, suggesting that NMR cells favor senescence to apoptotic response. While the SASP phenotype was conserved in the NMR cells, these cells displayed a unique transcriptional signature that may reduce the pathogenic effects of senescent cells and contribute to naked mole rat longevity and cancer resistance.

Chapter 3. Global Remodeling of the Mouse DNA Methylome during Aging and in Response to Calorie Restriction

3.1 Materials and methods

3.1.1 Reduced Representative Bisulfite Sequencing

Reduced Representation Bisulfite Sequencing (RRBS) of mouse blood samples was performed previously (Petkovich et al., 2017). Quality of high throughput sequence libraries was verified using "FastQC v.0.10.1" package (www.bioinformatics.babraham.ac.uk/projects/fastqc/). Trim Galore! v.0.4.0 was used for adapter removal and quality trimming. The TrimGalore tool (www.bioinformatics.babraham.ac.uk/projects/trim_galore/) was performed with settings optimized for RRBS. Methylation sites were detected using Bismark v.0.14.5 according to the program's manual.

3.1.2 Genomic Databases

We used several databases to annotate CpG sites. RnBeads R package (Assenov et al., 2014) was employed to annotate genes (Genes-1) and promoters (Promoters-1), and the RnBeads package used Ensembl gene definitions and defined promoters as regions spanning 1,500 bases upstream and 500 bases downstream of the transcription start site (TSS) of the corresponding gene. We used annotatr R package (Cavalcante and Sartor, 2017) to annotate genes (Genes-2; original database: UCSC genes), promoters (Promoters-2; 1 kb upstream of the TSS), CpG islands (CGIs), CGI shores (CGI-shores; 2 kb upstream/downstream from the ends of CGIs), CGI shelves (CGI-shelves, 2 kb upstream/downstream of the farthest upstream/downstream limits of CGI shores), the

remaining CGI Open Sea genomic regions (CGI-open-sea), 1-5 kb upstream of the TSS (Genes-upstream-1-to-5-kb), 3'- and 5'-untranslated regions (3'UTRs, 5'UTRs), exons (Exons), first exons (First-exons), introns (Introns), intergenic regions (Intergenic), exon-intron and intron-exon boundaries (Exon-intron-boundaries, Intron-exon-boundaries; defined as 200 bp up/downstream of any boundary between an exon and intron), enhancers (Enhancers-fantom5; original database FANTOM5 (Andersson et al., 2014)), long non-coding RNA (Long-noncoding-RNAs; original database: GENCODE). We used the Mouse ENCODE Consortium (Yue et al., 2014) data to annotate seven different histone modifications (Histone-H3K27m3, Histone-H3K36m3, Histone-H3K4m1-m3, Histone-H3K4m1-H3K36m3, Histone-H3K4m1, Histone-H3K4m3, Histone-Unmarked; the database was merged from 15 different mouse tissues and cell types), DNase hypersensitive sites (DHS), predicted promoters (Promoters-encode), predicted enhancers (Enhancers-encode), transcription factor binding sites (TFBS) and the mouse specific and human-mouse homologs of the listed genomic regions.

We downloaded genomic repetitive regions (Repeats) using the UCSC Table Browser (Karolchik et al., 2004; Rosenbloom et al., 2015), and super-enhancers from the SEA database (Super-enhancers-1) (Wei et al., 2016) and the dbSUPER database (Super-enhancers-2) (Khan and Zhang, 2016). Evolutionary conserved regions (Ecr) were defined as at least 100 bp long and 70% identity regions, and core evolutionary conserved regions (Core-ecr) were at least 350 bp and 77% identity regions between mouse and 10 different species (Human, Macaque, Chimp, Rat, Dog, Opossum, Chicken, Frog, Zebrafish, and Fugu). These regions were downloaded from https://ecrbase.dcode.org (Loots and

Ovcharenko, 2007). Ultra-conserved regions (UCR) were downloaded from http://ucbase.unimore.it (Bejerano et al., 2004; Lomonaco et al., 2014). Micro RNA (microRNAs) genomic coordinates were downloaded from http://www.mirbase.org (Kozomara and Griffiths-Jones, 2014). Genomic coordinates were mapped to mm10 with UCSC Batch Coordinate Conversion (liftOver) tool (Hinrichs et al., 2006) when the original genome assembly was not mm10 in certain databases. Genomic coordinates of regions were filtered out; if we could not detect DNA methylation, we kept the coordinates of the regions, in which at least one methylated CpG could have been measured.

3.1.3 Statistical Analysis

After data preprocessing and filtering, we used linear regression to examine the relationship between age and methylation levels and included 4 confounding factors: flow cell, library, adaptor and the number of aligned paired end reads of the samples. When site-by-site linear regressions and multiple data transformations were performed, we added the value 1 to every methylation fraction value to avoid incompatibility between the methylation value 0 and certain data transformations. We further chose the best fitting model based on the Akaike information criterion (Table 1). We declared a site to be significant, if the p-value, adjusted by the Benjamini-Hochberg procedure, was smaller than 0.05. To avoid overfitting, we excluded significant sites, for which there was a direction change in the regression slope upon comparison of the linear regression with all our confounders and without the confounders. To determine the enrichment of increasing or decreasing (I/D) sites in certain genomic regions, we created a contingency table including the number of I/D sites in the genomic region, the number of I/D sites outside

the region, the number of non-I/D sites in the region and the number of non-I/D sites outside the region, followed by a Fisher exact test.

To visualize the overall methylation change pattern in genes, we calculated relative positions for CpGs. The relative position 0 was assigned to the TSS, and 1 was the end of the gene. We also extended this analysis to the regions of the same length upstream and downstream of the gene and subjected them to the generalized additive model, using RnBeads R package, with a modification wherein we only included the significantly changing sites. To investigate the differences between the homolog elements, mouse-specific elements and all predicted elements, we performed Mann-Whitney U test between the regression slopes of every site in these regions and calculated adjusted p-values, using Benjamini-Hochberg procedure. When we examined the effect of the CpG islands, shores and shelves, we removed, from every region, the sites that could be assigned to (i) CGI, (ii) CGI and CGI shores, and (iii) CGI, CGI shore and CGI shelves, based on the built-in annotation of the RnBeads R package for these genomic regions, and performed a linear regression for every region using just the significantly changing sites. We included the four technical confounders, as described previously, and normalized every site by extracting the mean and dividing it by the standard deviation. In addition, we included, as confounders in every site, whether the site was present in a CGI shore, shelf or Open Sea region to avoid bias of the different aging trends.

Permutation tests were calculated by extracting the mean of the two compared groups, then merging the two groups into one. From the merged group, we randomly

selected values for two groups (including the same number of values as the original groups). We extracted the means and repeated the process 10,000 times. P-value was calculated by counting the number of cases, where the absolute value of the mean extraction of the randomly selected groups was larger than the absolute value of the original mean extraction, divided by 10,000. When testing the difference between increasing, decreasing and all sites, we aggregated the age groups by calculating the mean methylation across lifespan for every site.

3.1.4 Pathway Enrichment Analysis

To identify pathways associated with genes and promoters with changing methylation status during aging, we performed a pathway GSEA on a pre-ranked list of promoters and genes (Subramanian et al., 2005). This list included the sites annotated as promoters or gene bodies and z-scores, calculated as:

$$-ln(P) * S,$$

where P is the p-value of the linear regression of the site and S is the sign of the regression slope. For every promoter and gene, we calculated the mean of the z-scores of every site annotated to that genomic region. Kyoto Encyclopedia of Genes and Genomes (KEGG) and Gene Ontology (GO) Biological Process (BP) and Molecular Function (MF) databases were used in this analysis.

To identify pathways associated with age-related changes of methylation status, which can or cannot be explained by increasing entropy, we performed pathway

enrichment analysis for promoters and genes that showed changes based on the original methylation fraction (OMF) or the residual methylation fraction (RMF) using Database for Annotation, Visualization and Integrated Discovery (DAVID) (Huang et al., 2009a, 2009b). Z-scores were calculated by using the equation (1) for sites showing increasing or decreasing changes based on (i) just the OMF; and (ii) both in OMF and RMF. Increasing or decreasing trends were determined by the changes based on the OMF. Average z-score was calculated for every site annotated to promoters or genes. We used the first 2,000 genomic regions with the highest absolute z-scores as an input for the DAVID analysis. We used KEGG, GO BP and MF databases with the threshold FDR = 0.05.

3.1.5 Analyses of Calorie Restriction

Investigating the effect of the calorie restriction (CR), we analyzed 20 C57BL/6 male mice in 4 age groups (10, 18, 23, 27 months). Using the original 141 C57BL/6 mice (16 age groups) as controls, we built a linear model including age, CR (0 for control and 1 for CR) and the time after treatment (TAT), which is the difference between the age of mouse and 4 months (i.e. the start of CR) in the case of the intervention group and 0 in control animals. Using this model, we could estimate the initial shift (IS) at the beginning of the CR treatment (4 months) and calculate the difference in the rate of changes during aging in the CR group versus the control group, using the TAT which represents the cumulative change. We performed a site-by-site linear regression including the above mentioned variables and used a partial F-test to decide if IS and the TAT had a significant effect together (Benjamini-Hochberg FDR = 0.05). Partial F-test was calculated by fitting the reduced (including only the age) and the full (including the age, CR and TAT) models

separately and thereafter comparing them using Analysis of variance (ANOVA). Then we used the significant sites based on the F-test and determined, for every site, whether IS and TAT had a significant effect separately (Benjamini-Hochberg FDR = 0.05). To investigate the relation between the age-, initial shift- and cumulative effect-related changes we performed a linear regression between the linear model coefficients of these features.

We also investigated DNA methylation of blood samples from 22 (10 control and 12 CR) B6D2F1 male mice. Two age groups were analyzed in both subsets (20 and 27 months in controls, 21 and 27 months in CR). We applied a linear model and included age, intervention and flow cell as technical confounders. We compared the CR-related changes between the B6D2F1 and the C57BL/6 strain. To be able to make this comparison, we recalculated the C57BL/6 analysis, including only age and CR, but not TAT. Comparison between the two strains was by a linear regression between the CR-related linear model coefficients of the strains.

3.1.6 Analysis of Publicly Available Data

We downloaded publicly available human and mouse data for comparative analyses of our findings. The dataset of 656 human whole blood samples (Hannum et al., 2013) was downloaded from NCBI's Gene Expression Omnibus: GSE40279. We performed multidimensional scaling and 5 samples were identified as outlier samples and excluded from further analyses. Site-by-site linear regressions and multiple data transformations were performed as detailed above and four confounding factors were included in the linear regressions: gender, ethnicity, source and plate information. Entropy analysis was

performed on the human data as detailed above for mouse samples. We downloaded 24 mouse liver methylation data (Cole et al., 2017; Hahn et al., 2017) with accession numbers GSE89275 and GSE92486. We used the sites that were present in all samples and had higher coverage than 5x in more than 50% of samples in any age group and in calorie restriction samples. Furthermore, we used RnBeads R package to aggregate the measured sites, which belonged to the same CpG, to exclude high coverage outliers and sites that were overlapping with single nucleotide polymorphism. We built a linear model, including age (2, 5, 22, 26 months), calorie restriction (0 for control and 1 for CR), time after treatment and the source of the sample. To investigate the relationship between the age-, initial shift- and cumulative effect-related changes we performed linear regression between the linear model coefficients of these features.

3.2 Results

3.2.1 Global Trends in DNA Methylation during Aging

We assessed age-related changes in DNA methylation based on reduced representation bisulfite sequencing (RRBS) of blood of 141 C57BL/6 male mice representing 16 age groups (Petkovich et al., 2017). The youngest mice were 3 months old (young adults), and the oldest 35 months old (corresponding to the survival of the remaining 10% animals). After filtering and preprocessing, the dataset included approximately 800,000 CpG sites present in every sample. We performed multidimensional scaling to investigate global changes in the DNA methylome with age (Figure 11A). The average methylation status of CpG sites was slightly below 0.5 (one sample Student's t test, p-value = $1.99 \cdot 10^{-134}$), that is, the genome was slightly

hypomethylated. Linear regression was then performed, accounting for every site and possible confounding factors. There was a slight, but significant decrease in the global methylome with age (p-value = $6.05 \cdot 10^{-152}$; Figure 11b).

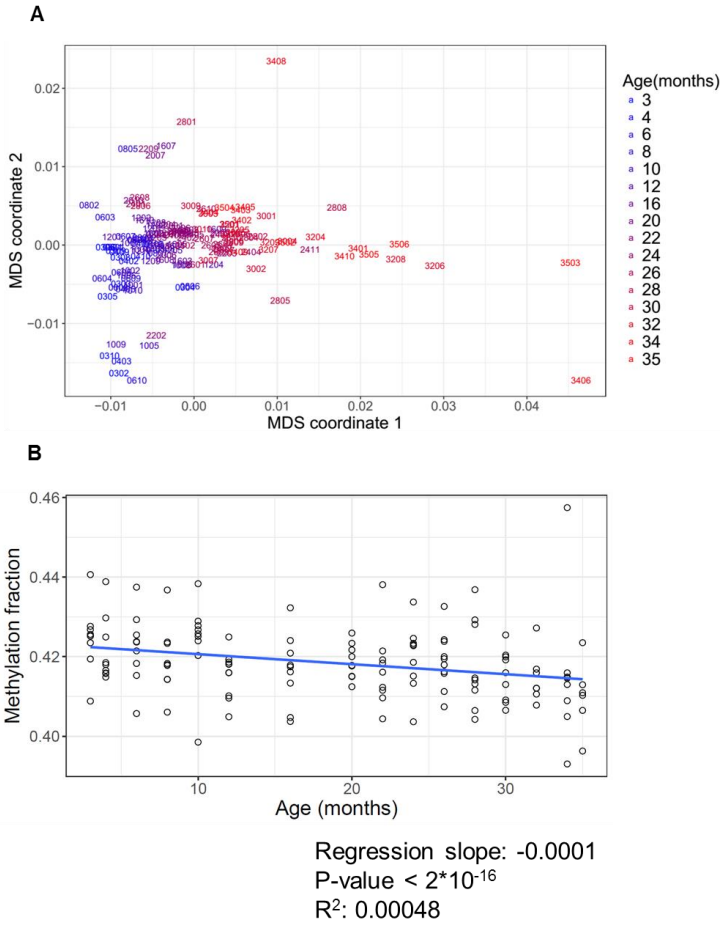

Figure 11. Global state of the mouse blood DNA methylome
(A) Multi-dimensional scaling (MDS) of 141 C57Bl/6 male samples. Colors represent ages as shown on the right. Samples are represented by sample ID, wherein the first two numbers represent age and the second two represent identification number in an age group. **(B) Mean methylation fraction of every site.** Linear regression parameters were calculated by using every site.

Linear regression (fraction methylated vs age of animal) was further performed in a site-by-site manner, again accounting for possible confounding factors, and multiple data

transformations were used to investigate nonlinear trends during aging, with Akaike information criterion (AIC) indicating the best fitting models (Table 1). We found that 21.2% of the sites were significantly correlated with age, including 10.2% that gained methylation and 11% that lost it. Linear regression for significant sites revealed a slight decrease in methylation level (p-value = $6.49 \cdot 10^{-17}$) with age. The best fitting model between significantly changing sites was age vs methylation percentage to the power of $-\frac{1}{3}$, observed in about 86% of the significant sites. These sites either gained methylation with age (41.6%; Figure 12a) or lost it (44.3%; Figure 12b) and changed predominantly in late life. In addition, 14% of the sites showed robust changes during early adulthood. We similarly investigated the dataset of 651 human samples from the age of 19 to 101 years (Hannum et al., 2013), and the best fitting models were highly consistent with the mouse data ($age \sim methylation^{-\frac{1}{3}}$: 81%, $\ln(age) \sim methylation^{-\frac{1}{3}}$: 19% of the significant sites).

Table 1. Models of methylation change with age

Data transformations used	Number of significant sites	Percent of significant sites (%)	Sites gaining methylation (%)	Sites losing methylation (%)
$\boldsymbol{age \sim methylation^{-\frac{1}{3}}}$	146067	85,9	41,6	44,3
$\boldsymbol{\ln(age) \sim methylation^{-\frac{1}{3}}}$	24059	14,1	6,5	7,6
$\boldsymbol{age \sim methylation}$	0	0	0	0
$\boldsymbol{\ln(age) \sim methylation}$	0	0	0	0
$\boldsymbol{age \sim methylation^2}$	0	0	0	0
$\boldsymbol{\ln(age) \sim methylation^2}$	0	0	0	0
$\boldsymbol{age \sim methylation^3}$	0	0	0	0
$\boldsymbol{\ln(age) \sim methylation^3}$	0	0	0	0

$age \sim methylation^{\frac{1}{2}}$	0	0	0	0
$ln(age) \sim methylation^{\frac{1}{2}}$	0	0	0	0
$age \sim methylation^{\frac{1}{3}}$	0	0	0	0
$ln(age) \sim methylation^{\frac{1}{3}}$	0	0	0	0
$age \sim ln(methylation)$	0	0	0	0
$ln(age) \sim ln(methylation)$	0	0	0	0
$age \sim methylation^2 + methylation$	0	0	0	0
$ln(age) \sim methylation^2 + methylation$	0	0	0	0
$age \sim methylation^{-1}$	0	0	0	0
$ln(age) \sim methylation^{-1}$	0	0	0	0
$age \sim methylation^{-2}$	0	0	0	0
$ln(age) \sim methylation^{-2}$	0	0	0	0
$age \sim methylation^{-3}$	0	0	0	0
$ln(age) \sim methylation^{-3}$	0	0	0	0
$age \sim methylation^{-\frac{1}{2}}$	0	0	0	0
$ln(age) \sim methylation^{-\frac{1}{2}}$	0	0	0	0

We further separately examined the sites that gained and lost methylation with age (Figure 12e). Sites with increasing methylation were characterized by the low methylation status, and those with decreasing methylation by high methylation, compared with the average methylation levels (permutation test, p-value < .0001 in both cases). The relationship between the regression slope and the mean methylation fraction for every site revealed a significant negative correlation (Pearson's correlation coefficient = -0.384, linear regression p-value < $2 \cdot 10^{-}16$). Again, sites with increasing methylation were hypomethylated, and those with decreasing methylation hypermethylated.

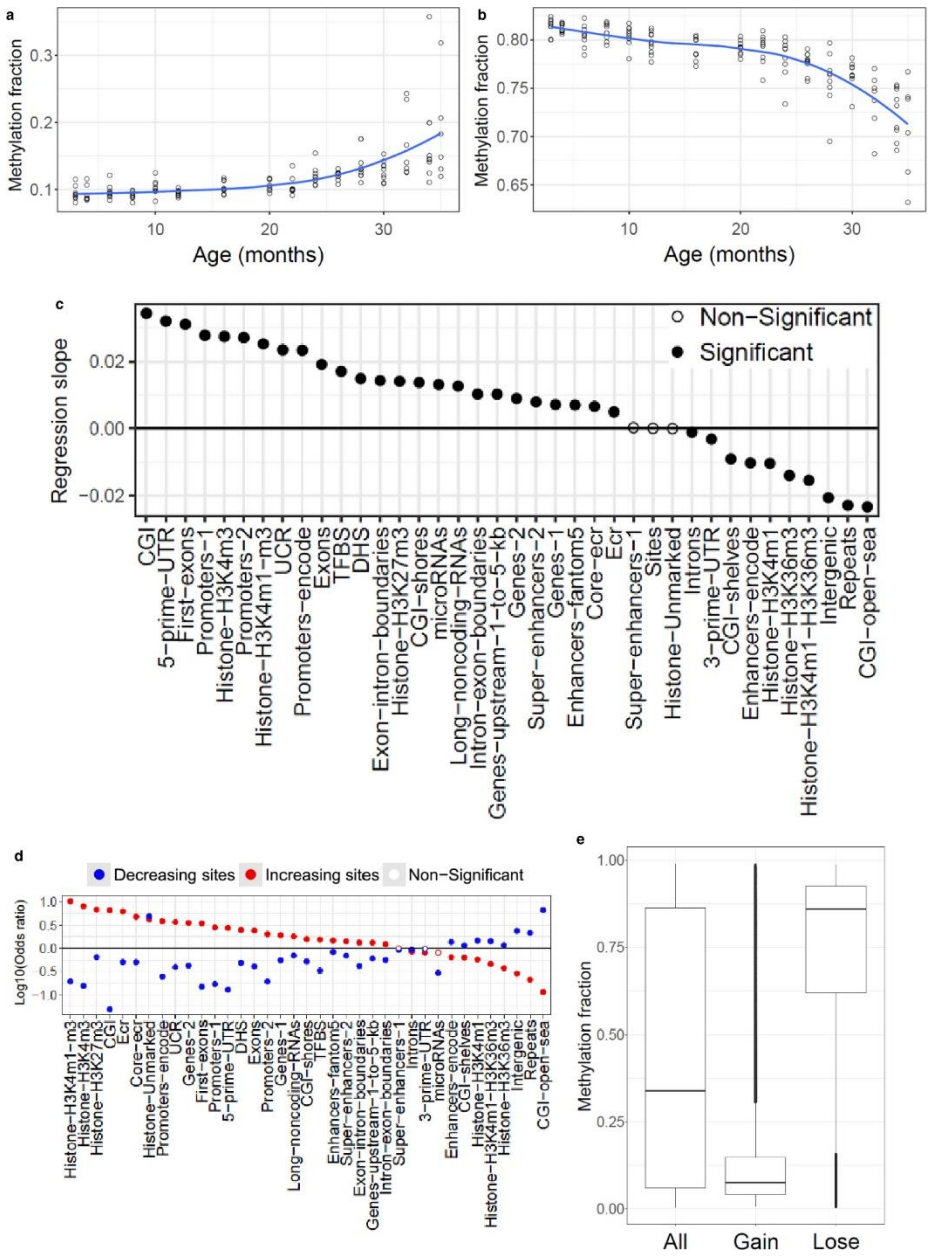

Figure 12. Global and region-specific changes in DNA methylation with age

(a) Mean of the increasing and accelerating sites with the best model: age~methylation$^{-\frac{1}{3}}$.

(b) Mean of the decreasing and accelerating sites with the best model: age~methylation$^{-\frac{1}{3}}$.

(c) Linear regression slope of CpG sites that changed with age based on their assignment to indicated regions of the genome. (d) Enrichment analysis of significantly changing sites in indicated genomic regions. (e) Boxplot of the average methylation fraction across lifespan for all (All), gaining (Gain) and losing (Lose) methylation sites.

3.2.2 Various Genomic Regions Show Distinct Remodeling Patterns in DNA Methylation

In addition to the global trends, we investigated changes in DNA methylation in distinct genomic regions. We performed linear regression analysis for various parts of the genome, following assignment of significant age-related sites to annotated genomic regions (Figure 12c). The CpG methylation fraction was normalized by extracting the mean and dividing it by the standard deviation. Using this approach, we could examine dominant changes based on the number of changing sites, diminishing the effect of the degree of change for different sites that could potentially bias the results. We observed a strong age-related gain in methylation in CpG islands (CGIs), 5'- UTRs, first exons of genes and gene promoters; a strong increase in methylation could also be observed around the transcription start sites (TSSs; Figure 13a). We observed an age-related methylation gain in many gene regions, such as exons and exon–intron boundaries, with the exception of introns and 3'-UTRs, which tended to lose methylation with age. More broadly, increasing methylation was observed at the 5'-ends and decreasing at the 3'-ends of genes. Regulatory elements, such as microRNAs, long noncoding RNAs, DNase hypersensitivity sites, and transcription factor binding sites (TFBS) tended to gain methylation during aging. We also observed increasing methylation in evolutionary conserved regions, core conserved regions, and ultra-conserved regions. Regions with decreasing methylation included intergenic and repetitive regions, the latter representing various classes of retrotransposons. Overall, the mouse blood DNA methylome was characterized by robust remodeling with age, and its patterns and directions of change were dependent on the location of CpG sites within various functional regions of the genome. We further investigated enrichment

(Fisher exact test) of increasing and decreasing sites in different genomic regions (Figure 12d). Increasing sites tended to be enriched in regions that gained methylation and decreasing sites in regions that lost it with age. After correction for cell type composition changes during aging (Houseman et al., 2016), we found somewhat fewer significant sites (7%), revealing a pattern reminiscent of the original regional regression analysis. Finally, we compared changes during aging (regression slope) in promoters (Promoters-Encode), enhancers (Enhancers-Encode), and TFBS between all sites, sites in regions with human–mouse homology and sites in mouse-specific regions (Figure 13b). Sites in homologous regions tended to gain, and sites in mouse-specific groups to lose methylation during aging compared to all sites in that region and to each other (Mann-Whitney U test, adjusted p-value < 0.05).

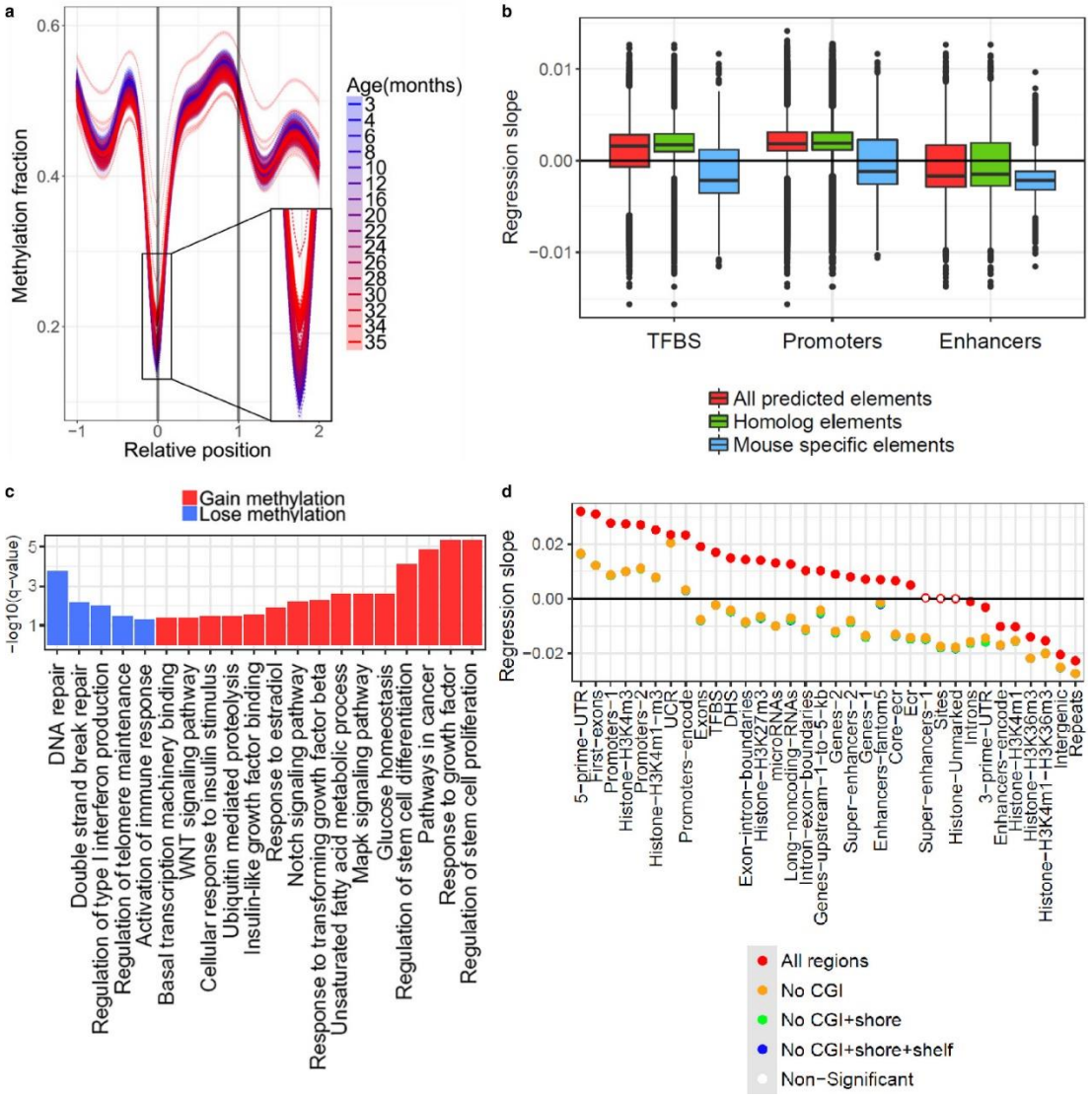

Figure 13. Genomic regions are characterized by distinct age-related changes

(a) Age-related changes in DNA methylation of genes. Relative position was calculated for every gene (0 corresponds to the TSS and 1 to the end of the gene) and extended in both directions up to the length of the gene. Dotted lines (individual samples) and thick lines (age groups) were calculated by generalized additive model using significant sites. **(b) Regression slope of significantly changing sites in three genomic regions and differences between all sites (all predicted elements), human–mouse homologs (homolog elements), and mouse-specific regions (mouse-specific elements). (c) Significantly enriched pathways in promoters that gained methylation (red) and lost it (blue) during aging.** KEGG and GO databases were used as pathway annotation for the analysis. **(d) Linear regression slope of genomic regions after removal of significant sites that overlap with CpG islands (CGI), CGI shores, or CGI shelves.**

Consistent with previous studies (Florath et al., 2014; Horvath et al., 2012; Rakyan et al., 2010), we found that the distance between the sites and CGIs strongly influenced methylation changes during aging, as CGIs gained and non-islands lost methylation. CGIs may overlap with other genome regions, and the aging changes in them may be driven by overlapping islands and may be less characteristic of the region itself or non-island parts of the genome. To examine this possibility, we removed, from every region, sites that could be assigned to (i) CGI, (ii) CGI and CGI shores, and (iii) CGI, CGI shore, and CGI shelves (Figure 13d). In most regions, CGIs had a strong effect on the overall pattern and mostly influenced regions that gained methylation. Many regions even changed their overall direction of change during aging after the removal of CGIs, but the most increasing regions, such as promoters, 5'-UTRs and first exons, still gained methylation with age. Methylation changes during aging in ultra-conserved regions tended to be less influenced by the overlapping CGIs than other regions that gained methylation. CGI island shores and shelves showed a minor additional effect.

3.2.3 Pathway Enrichment of Promoters and Genes with Age-associated Methylation Changes

To get a deeper understanding of the possible biological impact of methylation changes during aging, we carried out pathway GSEA (Subramanian et al., 2005) on promoters. We found 102 significantly enriched pathways (adjusted p-value < .05) associated with the loss of methylation and 1,162 pathways associated with its gain in promoters during aging. Among the pathways with decreased methylation were those related to DNA repair, immune processes, and inflammation. In the increasing group, the

most overrepresented pathways were related to developmental processes. There were also significantly enriched pathways related to aging and lifespan-extending interventions, such as the response to growth factors, insulin-like growth factor and TGFβ, MAPK cascade, WNT and Notch signaling pathway, regulation of stem cells, estradiol response, and fatty acid metabolism- and transcription regulation-related pathways (Figure 13c) (Carlson et al., 2008; Harrison et al., 2014; van Heemst, 2010; Heilbronn and Ravussin, 2003; Lopez-Otin et al., 2013; Ott and Grune, 2014).

We also investigated the enrichment for genes and found 39 significant pathways that lost methylation and 987 pathways that gained it during aging. We observed similar patterns in gene bodies compared to promoters. Pathways with decreasing DNA methylation included DNA repair, immune function, and inflammation-related pathways, and those with increasing methylation included various developmental pathways. There were aging-related enriched pathways in the increasing group, including regulation of cell aging and senescence, growth factor response such as the response to TGFβ stimulus, stem cell proliferation and differentiation, MAPK cascade, WNT, Notch signaling, and fatty acid metabolism-related pathways. In addition, a pathway involving DNA methylation itself was detected, including the gene DNMT1.

3.2.4 Increased Entropy of DNA Methylation Patterns during aging

As discussed above, a characteristic feature of age-related changes in DNA methylation was that the sites that gained methylation with age were initially hypomethylated, and those that lost it were hypermethylated. To further characterize age-related methylation changes, we prepared density plots for every age group, including all

sites (Figure 14a) or only the sites that showed significant changes with age (Figure 14b). Methylation levels for most sites were close to either 0 or 1; during aging, these extreme methylation states moved toward intermediate levels. These changes were even more pronounced among the sites that changed with age, pointing out to an age-related increase in entropy. We quantified these changes by calculating Shannon entropy (Hannum et al., 2013) for individual samples and performing linear regression against age and confounders, verifying a significant increase in entropy with age. The rise in Shannon entropy was found for all sites (Pearson's correlation coefficient = 0.468, p-value < $2{\cdot}10^{-16}$) and for the significant sites only (Pearson's correlation coefficient = 0.769, p-value < $2{\cdot}10^{-16}$), the latter with the stronger effect (permutation test, p-value < .0001; Figure 14c). We applied multiple data transformation to the age-entropy dependence in the same way as described above and identified $\text{age}\sim\text{entropy}^{-\frac{1}{3}}$ as the best fitting model based on AIC. We also found that entropy changed dominantly close to the end of life. Interestingly, there was a difference between entropy of the sites with increasing (Pearson's correlation coefficient = 0.682, p-value < $2{\cdot}10^{-16}$) and decreasing (Pearson's correlation coefficient = 0.801, p-value < $2{\cdot}10^{-16}$) methylation (Figure 14d): Entropy of the decreasing sites was higher for all age groups than of the sites with age-related increased methylation (permutation test, p-value < .0001). This could be seen in the density plots, wherein the peak with high methylation was wider than that with low methylation, and hypomethylated sites were more consistent in their methylation levels that the sites with high methylation. In addition, an analysis of 651 human samples revealed increasing entropy with the best model: $age\sim entropy^{-\frac{1}{3}}$, showing higher overall entropy of significant compared to

nonsignificant sites and higher overall entropy of decreasing compared to increasing sites. Overall, increased entropy during aging was reflected in the methylation patterns and differentially affected the sites with increasing, decreasing, and unaffected methylation.

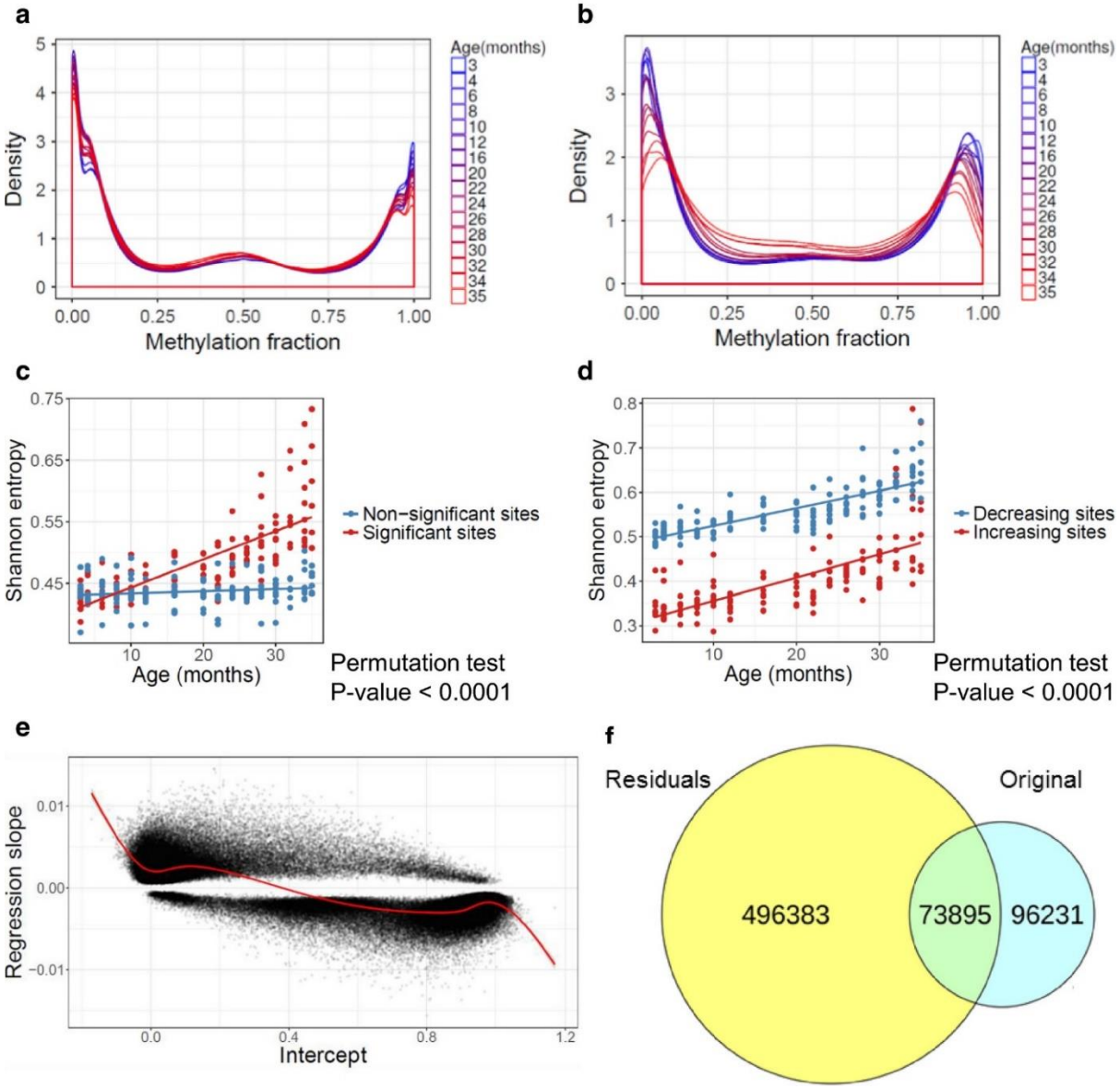

Figure 14. Age-related changes in entropy of the DNA methylome
(a) Age-related changes in DNA methylation, shown as a density plot accounting for all detected CpG sites. (b) Same as in (a), but the plots include only the CpG sites that significantly change with age. (c) Shannon entropy of the sites that significantly change (or do not change) with age. (d) Shannon entropy of the sites that significantly increase and

decrease with age. (e) Intercept of the linear regression vs. the regression slope for every site that significantly changed with age. The red curve represents generalized additive model fit. **(f) Venn diagram of significantly changed sites, based on the original age-related changes (Original) and entropy-normalized residuals (Residuals).**

To investigate sites, whose changes cannot be explained by the global change in entropy, we examined the relationship between the intercept of significant sites and the regression slope (Figure 14e) using a generalized additive model. Expected slope was then calculated for all sites, based on the intercept of linear regression and fitted values of generalized additive model, and the residual methylation fraction (RMF) was calculated by subtracting age 9 expected slope from the original methylation fractions (OMFs). After normalizing for the average entropy effect, linear regression was calculated for every RMF, accounting for confounding factors, using multiple data transformation, and choosing the best fitting model based on AIC. We found many sites (496,383 sites, 61.9%) without age-related changes in OMF, but the RMF changed with age (Figure 14f). These sites had low or high methylation levels and resisted changes during aging. We observed 96,231 sites (12%), where OMF changed with age, but the entropy-normalized RMF did not. Methylation of these sites changed during aging, but these changes could be explained by the average entropy effect. We also detected 73,895 (9.2%) sites that changed based on both OMF and RMF. These sites showed age-related changes: 32.8% changed more than the average entropy, 49.5% less than the average entropy, and 17.7% changed in the opposite direction, that is, these sites were already highly methylated, but further increased methylation during aging and vice versa. Finally, 16.9% of the sites did not change in either analysis: These sites showed intermediate methylation levels and did not change with age. We conclude that most of the sites retain the early age methylation state, some follow or

even exceed the average entropy trajectory, and few sites change in the direction against entropy.

Human data revealed a similar trend. We performed pathway enrichment analyses using the mouse samples and (i) sites that changed based on OMF and RMF, which showed age-related changes that cannot be explained by the average entropy; and (ii) sites that changed based on just the OMF, which could be fully explained by the average entropy. We detected similar trends during this analysis; both average entropy-driven and other sites were similarly enriched in pathways that changed during aging.

3.2.5 Regulation of the Blood DNA Methylome by Caloric Restriction

We further investigated the effect of calorie restriction (CR), a classical lifespan-extending intervention, on the blood DNA methylome by analyzing four groups of mice, from 10 till 27 months old, that were subjected to CR starting at the age of 4 months. We created a linear model and examined the sites characterized by the initial shift (IS) in response to CR (estimated shift at the age of 4 months) and the sites that changed with a different rate than the control group over time in response to treatment (designated time after treatment (TAT)), which represents the cumulative change (Figure 15). We detected 139,803 significant sites (22.6%; F test, adjusted p-value < .05), where both IS and TAT had a significant effect. We then examined which effect, instantaneous or cumulative, may characterize CR. Our analysis revealed 5,093 sites that changed with TAT and 14,516 with IS (adjusted p-value < .05). The identified sites were investigated in detail, revealing changes during (i) aging and IS, (ii) aging and TAT, and (iii) IS and TAT (Figure 16a). First, we examined the relationship between the sites that changed significantly during

aging in the control group and IS. There was a significant positive correlation between the linear model coefficients (Pearson's correlation coefficient = 0.681, p-value < $2 \cdot 10^{-16}$; Figure 16b). Thus, most sites with the initial shift following the intervention changed in the same direction as they did during aging.

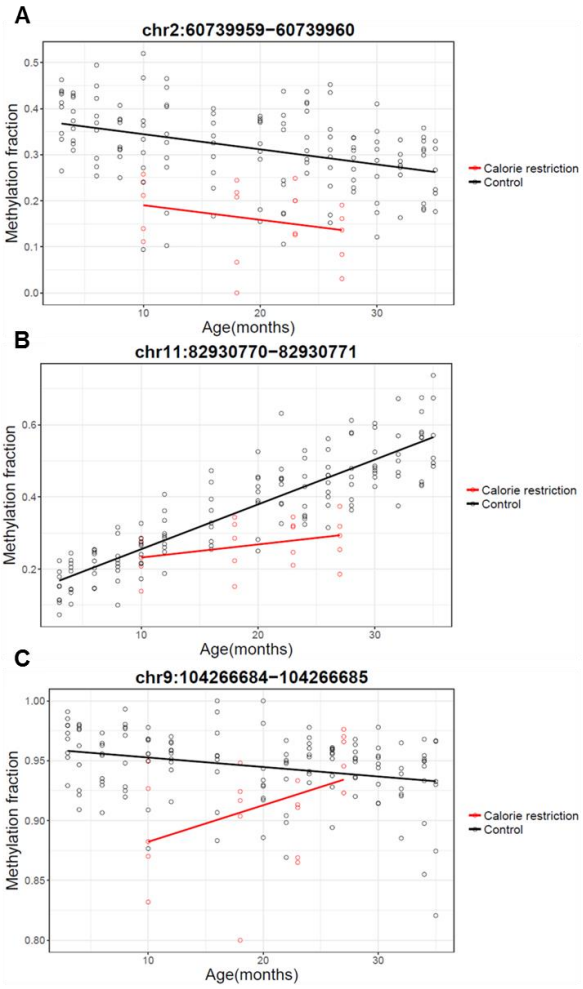

Figure 15. Examples of sites that change methylation with age following CR
(A) Site with the initial shift, but no significant cumulative effect. (B) Site with the cumulative effect, but without a significant initial shift. (C) Site with both significant initial shift and cumulative effect. In each case, the control group has a significant age-related change.

The same comparison between the sites changing both during aging and TAT showed a significant negative correlation (Pearson's correlation coefficient = -0.484, p-

value < $2 \cdot 10^{-16}$; Figure 16c). The cumulative effect during CR, represented by the TAT, seemed to exhibit an opposite direction than the age-related changes, and it slowed down the influence of aging on the methylome. We also investigated the sites, which change during both IS and TAT (including, but not limited to the sites with age-related changes), and observed a strong negative correlation (Pearson's correlation coefficient = -0.988, p-value < $2 \cdot 10^{-16}$; Figure 16d). The data suggest that these sites initially change after the start of the intervention, but then the cumulative effect drives methylation back to the level of the control group. In addition, we examined 24 publicly available mouse samples (Cole et al., 2017; Hahn et al., 2017), which revealed similar trends in response to CR. To get the end point of changes in the methylome in response to long-term CR, we compared the oldest CR group (27 months) with the age-matched control. For sites significantly changing during aging, we examined the relation between the regression slope throughout lifespan and the average difference in their methylation level between every control and CR site in the oldest age group. We observed a significant negative correlation, consistent with the idea that long-term CR slows down aging of the methylome. We further compared the average methylation difference between every control and CR site in the oldest age group and the age-related regression slope of every site in all CR samples (4 age groups) and observed a significant positive correlation, showing that the long-term cumulative changes shifted the methylome toward the direction of the cumulative effect itself. Based on these findings, we conclude that the initial and cumulative effects of CR show different effects and that the cumulative changes seem to slow down aging of the methylome during a long-term treatment.

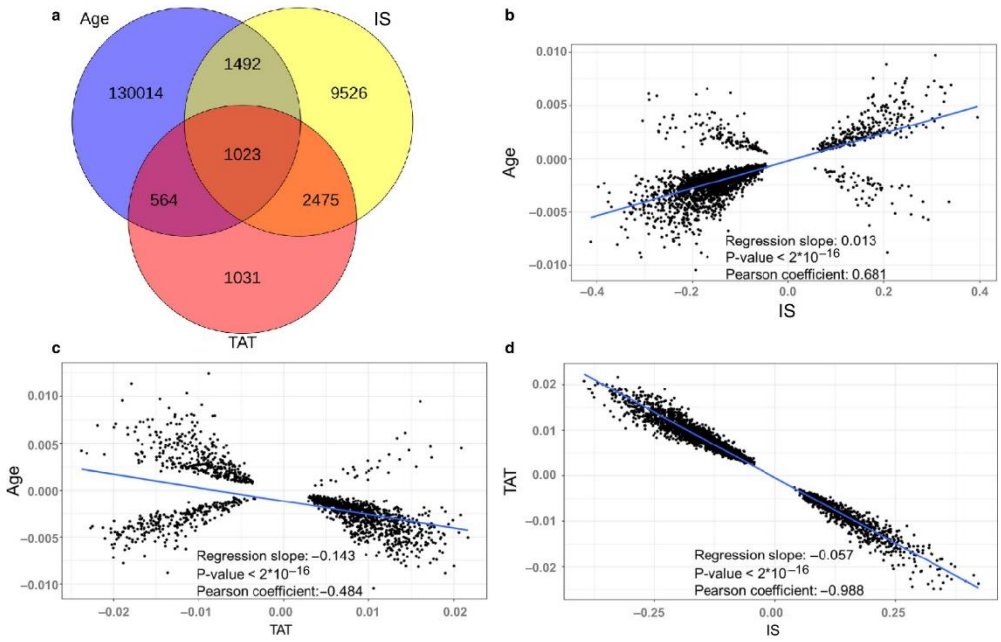

Figure 16. Age-related DNA methylation changes associated with CR effect
(a) Venn diagram of CpG sites that significantly change with age in the control group (Age), sites with the initial shift (IS) in response CR, and sites with cumulative changes following the intervention (TAT). (b) Correlation between linear model coefficients of significant age-related changes in the control group and significant IS changes. (c) Correlation between linear model coefficients of significant age-related changes in the control group and significant cumulative changes under the CR regime. (d) Correlation between the coefficients of significant cumulative changes and significant IS changes in response to CR (including, but not limited to sites with age-related changes).

To investigate whether our findings on CR apply to mice in a different genetic background, we investigated blood samples from 22 B6D2F1 male mice in two age groups. We detected 334 (0.048%) CpG sites differentially methylated between intervention and age-matched control mice. We further investigated whether CR affected the same sites in a similar way in mice in different genetic backgrounds, that is, in B6D2F1 and C57BL/6 mice. For this, we examined the relation between the linear model coefficients of significant CR-related changes in C57BL/6 mice and the same sites in B6D2F1 mice, assessing general relation of trends after CR in the two strains. Significant positive

correlation was observed (Pearson's correlation coefficient = 0.295, p-value < $2 \cdot 10^{-16}$). Then, we performed a similar analysis, but included only the sites, which showed significant CR-related changes in both strains, by focusing on most reliable 204 sites. We again detected a significant positive correlation (Pearson's correlation coefficient = 0.969, p-value < $2 \cdot 10^{-16}$). These data suggest that CR shifted the methylome in the same direction and generally affected the same sites in the two strains.

3.3 Discussion

3.3.1 Global and Local Changes in DNA Methylation throughout Adult Lifespan

Analysis of the blood DNA methylome of 141 mice representing 16 age groups spanning the entire adult lifespan (3-35 months of age) allowed us to examine changes in DNA methylation in great detail and at a high resolution. The Robust changes were observed in late (86% sites) and early (14% sites) life, whereas few changes were seen throughout middle ages, suggesting that the primary changes during aging are not linear and that they either accelerate or decelerate with age in both mice and humans. Accelerating nature of the majority of CpG changes is consistent with the exponential increase in molecular damage and with the model of the rising deleteriome (Gladyshev, 2016), whereas developmental processes appear to underlie the decelerating sites during aging.

We observed strong methylation gain with age at the 5'-ends of genes. In contrast, loss of methylation occurred at the 3'-UTRs and noncoding (introns) and intergenic regions. These findings in mice agree with previous human studies (Johansson et al., 2013; McClay et al., 2014), indicating conservation of age-related changes in DNA methylation

across species. We also observed increasing DNA methylation in other regulatory regions, such as microRNAs and long noncoding RNAs. CGI-related methylation was previously shown to suppress the expression of microRNAs and contribute to human cancers (Lujambio and Esteller, 2009). These observations support interactions between different epigenetic mechanisms of aging. Repetitive regions showed decreasing methylation with age. These changes in retrotransposons may promote the expression of these elements and increase damage to the genome in late life (Robertson and Wolffe, 2000; Yoder et al., 1997). Evolutionarily conserved elements, most notably ultra-conserved regions (100% sequence identity between human, mouse, and rat) gained methylation during aging. Increasing evidence suggests that these regions may be differentially expressed in human lymphomas and carcinomas (Calin et al., 2007). CGI hypermethylation suppresses the expression of the ultra-conserved regions, which is not uncommon in human cancers (Lujambio et al., 2010). Human–mouse homologs seemed to be mostly gaining, whereas mouse-specific regions losing methylation during aging. Overall, evolutionarily conserved elements tended to gain methylation during aging.

The presence of 5-methylcytosine at CpG dinucleotides created a fivefold depletion of this sequence during vertebrate evolution, probably due to spontaneous and enzyme-induced mutations (Bird, 1980; Gonzalgo and Jones, 1997). This may provide an explanation for hypomethylation of evolutionarily conserved regions and suggests that methylation gain during aging may promote mutations in the conserved elements in late life, contributing to the aging process. CGIs were found to be among the regions that gained methylation most, similar to the results of human studies (Jones et al., 2015), and

overlapping CGIs had a strong effect on the increasing regions. Regions with the strongest methylation gain, such as promoters, first exons, and 5'-UTRs, showed a general methylation increase with age even when the overlapping CGIs were removed. Methylation gain in promoters was frequently associated with overlapping CGIs (Saxonov et al., 2006), although our findings suggest that promoters even without overlapping CGIs gain methylation during aging. Pathway enrichment analysis of promoters and genes illuminated the biology behind the changes. Genes and promoters that lost methylation tended to be enriched in pathways that maintain cell homeostasis, for example, DNA repair-related pathways. These pathways are expected to become more expressed during aging, based on the idea of the inverse relationship between promoter methylation and gene expression (Jones et al., 2015). Many immunological and inflammation-related pathways were also enriched, in agreement with the known increase in inflammation in late life (Lopez-Otin et al., 2013). The most dominant pathways of genes and promoters gaining methylation during aging were developmental genes (Maegawa et al., 2017), which may indicate the decreasing expression of at least a subset of developmental genes during aging. There were also pathways in this group of promoters known to contribute to aging and lifespan-extending interventions, such as regulation of cell response to growth factor stimulus (Lopez-Otin et al., 2013), regulation of stem cell proliferation and differentiation (Heilbronn and Ravussin, 2003), insulin-like growth factor and response to insulin-related pathways (van Heemst, 2010), response to estradiol (Harrison et al., 2014), and ubiquitin-mediated proteolysis (Ott and Grune, 2014). Promoters involved in fatty acid metabolism (Hahn et al., 2017), and WNT-, Notch-, and TGFβ-related pathways also showed changes

during aging (Carlson et al., 2008). Methylation changes in the MAPK cascade were reported previously during aging in mice (Hahn et al., 2017). There were pathways gaining methylation in gene bodies that were enriched for regulation of cellular aging and senescence. We also observed methylation-related pathways enriched in gene bodies gaining methylation. Interestingly, a previous study showed decreased expression of DNMT1 (Ray et al., 2006) in mouse T cells during aging; this is the main DNMT expressed in adulthood that maintains DNA methylation of adult dividing cells (Armstrong et al., 2014). These changes may contribute to misregulation of methylation machinery and a consequent entropy increase during aging. Cancer-related pathways in promoters and gene bodies gained methylation, supporting the known relation between aging and cancer development (Lopez-Otin et al., 2013). These changes may contribute to misregulation of methylation machinery and a consequent entropy increase during aging. Cancer-related pathways in promoters and gene bodies gained methylation, supporting the known relation between aging and cancer development (Lopez-Otin et al., 2013). These enriched pathways indicate that DNA methylation may have a critical role during aging in mice.

3.3.2 Increased Entropy Alters the Developmental Pattern

Most CpG sites changed with age toward intermediate methylation states, pointing to altered entropy of the methylome. Previous studies revealed increased entropy in human DNA methylation (Hannum et al., 2013) and in mouse livers aged 0.2 to 7.1 months old (Wang et al., 2017). We were able to examine changes in entropy across the whole mouse and human lifespan at a high resolution. Interestingly, we observed acceleration of entropy changes in older ages, in agreement with the rise in accumulating damage and the

deleteriome (Gladyshev, 2016). Around 20% of the sites changed during aging, with the nearly equal numbers of those that increased and decreased methylation, but the global trend was associated with slightly decreased methylation with age, suggesting that the hypermethylated sites decrease somewhat more than the hypomethylated sites increase. Interestingly, however, hypomethylated sites that gained methylation were enriched in more pathways, including some with relevance to aging. The data suggest that these sites are more conserved and may underlie the features of aging associated with genetic programs, whereas the highly methylated sites that lost methylation with age may be associated with the more stochastic processes. After normalization for the average entropy effect, we observed that many sites fully resisted changes (61.9%), defining the extremes in methylation levels. Some sites changed slower than the entropy changes (4.6%), other sites followed the average entropy effect (12%), but some changed even faster than the average entropy (3%). There were also few sites that changed in the direction opposite to entropy changes (1.6%). A recent study of human aging found that the majority of DNA methylation changes were associated with epigenetic drift and accumulating damage, supporting the disposable soma theory of aging, whereas targeted changes in methylation also exist, as predicted by the mutation accumulation theory, and may mediate the effects of aging-related genes (Robins et al., 2017). Our results agree with these findings as the increasing and accelerating entropy, representing damage accumulation, disrupts the global methylation pattern, whereas fewer entropy-independent targeted changes were observed in mouse and human samples, which may drive aging-related biological functions. Interestingly, both entropy-driven and nonentropy-driven sites contributed similarly to the

pathways changed during aging, indicating that the entropy growth of the methylome may have biological consequences. The early developmental program may define global and region-specific methylation patterns and segregate functionally relevant CpG sites to fully methylated and unmethylated. This pattern may have multiple regulatory effects, with the respective sites contributing to certain biological functions. Other sites may follow entropy increase, which accelerates in late life and disrupt the developmental patterns.

3.3.3 Long-term CR Slows Down Aging of the Methylome

CR is known to extend lifespan of mice and many other species (Bordone and Guarente, 2005). We could detect two distinct responses to this longevity intervention. First, our analyses revealed that, initially, CR shifted the DNA methylome in the same direction as aging. This initial shift may be at least partly a response to stress caused by CR. Second, the cumulative change during CR affected the methylation pattern differently (compared to aging and compared to the initial shift by CR), and this cumulative trend seemed to shift the methylome toward a younger state (compared to control) and/or slow down aging of the methylome. Cumulative changes may influence the methylome in two different ways. On the one hand, they may affect sites with the initial shift caused by CR; in this case, the cumulative effect counteracts this shift. This effect may be compensatory with regard to the initial shift, as 98.2% of these sites do not differ from control in the oldest age group. On the other hand, the cumulative effect may influence the initially nonchanging sites and slow down the aging process. These sites appear to represent the long-term, lifespan-extending biological effect of CR. We observed that, initially, the methylome seemed to become older, whereas in the oldest age group the methylome

appeared to be younger in the CR group, suggesting that the cumulative effect has a larger longevity impact following long-term CR. The cumulative nature of CR is also confirmed by the meta-analysis of longevity studies in mice, wherein aging rate, but not vulnerability parameter, was shown to be a crucial coefficient of the Gompertz model explaining the CR influence on lifespan (Garratt et al., 2016). Furthermore, the earlier start of the treatment strongly increases the degree of lifespan extension via CR in mice (Simons et al., 2013).

Previous studies are consistent with our findings. Heterozygous DNMT1 knockout mice are characterized by slower immune senescence (Richardson, 2003). Young DNMT1 knockout mice feature general hypomethylation, the same trend as control mice during aging. On the other hand, older knockout mice showed hypermethylation and decreased immune senescence. Another study revealed that different sites change in response to CR in young and old mice (Hahn et al., 2017). A negative correlation was also shown between the methylation drift during aging and methylation changes following long-term CR in mice and monkeys (Maegawa et al., 2017), and the severity and duration of CR may have influenced the resulting methylation patterns. Based on these findings, the cumulative effect of CR seems to slow down the aging pattern of the methylome and it may have a more important role for lifespan extension, compared to the transient initial shift. In addition, the role of the cumulative effect in our and other studies suggests a strong link between DNA methylation and aging. It should also be noted that the pattern of methylome changes following CR was similar in mice in different genetic backgrounds.

Overall, we characterized changes in the blood DNA methylome of mice at unprecedented detail, uncovering nonlinear trends in DNA methylation remodeling during

aging. Promoters and genes with significant age-related changes in methylation turned out to be enriched in many known aging-related pathways, pointing to an important link between DNA methylation and control of the aging process at the molecular level. In addition, analyses of CR revealed differences between the initial and cumulative effects of the intervention on the DNA methylome, the latter being important for lifespan extension. Analysis of DNA methylation allowed us to quantify entropy that both increased and accelerated with age and altered the developmental methylation patterns, even though many CpG sites resisted these changes. Finally, sites with low methylation levels were more conserved, and associated with biological functions relevant to aging. Taken together, our findings define the biological relevance of DNA methylation to aging.

Chapter 4. Identification and Application of Gene Expression Signatures of Lifespan-Extending Interventions

4.1 Materials and Methods

4.1.1 Animal Samples

Mice were subjected for methionine restriction (MR) as following. Seven-weeks old male C57BL/6J mice were purchased from The Jackson Laboratory (Stock #000664, Bar Harbor, ME, USA) and housed in a conventional animal facility maintained at 20 ± 2°C and 50 ± 10% relative humidity with a 12 h light: 12 h dark photoperiod. During a 1-week acclimatization, mice were fed Purina Lab Chow #5001 (St. Louis, MO, USA). Mice were then weight matched and fed either a control (CF; 0.86% methionine w/w) or MR (0.12% methionine w/w) diet consisting of 14% kcal protein, 76% kcal carbohydrate, and 10% kcal fat (Research Diets, New Brunswick, NJ, USA) for 52 weeks. Body weight and food consumption were monitored twice weekly. Young mice were 8 weeks old (2 months) at the initiation of the experiments and 60 weeks old (14 months) upon termination. On the day of sacrifice, animals were fasted for 4 hours at the beginning of the light cycle. After mice were sacrificed by CO_2 asphyxiation, liver samples were collected, flash frozen, and stored at −80ºC until analyzed.

Other mice used in this study were obtained from the colonies at University of Michigan Medical School. Liver samples were taken at 6 and 12 months of age from male and females treated by drugs or exposed to caloric restriction (CR) diet from 4 months of age along with untreated littermate control mice of the same ages, being fed *ad libitum*.

Interventions analyzed at 6 months of age included 40% CR, Protandim™ (1200 ppm, as in (Strong et al., 2016)), rapamycin (42 ppm, as in (Miller et al., 2014)), 17-a-estradiol (14.4 ppm, as in (Strong et al., 2016)) and acarbose (1000 ppm, as in (Harrison et al., 2014)), while interventions analyzed at 12 months of age included 40% CR, acarbose (1000 ppm, as in (Harrison et al., 2014)) and rapamycin (14 ppm, as in (Miller et al., 2011, 2014)). Both males and females were subjected to the mentioned interventions. Genetically heterogenous UM-HET3 strain, in which each mouse had unique genetic background but shared the same set of inbred grandparents (C57BL/6J, BALB/cByJ , C3H/HeJ, and DBA/2J), was used in this setting.

Liver samples from Snell dwarf (Flurkey et al., 2001) and GHRKO (Coschigano et al., 2003) males, and their corresponding littermate controls, were taken from mice at 5 months of age belonging to (PW/J x C3H/HeJ)/F2 and (C57BL/6J x BALB/cByJ)/F2 strains, respectively.

In all cases, interventions continued until the animals were sacrificed. Each analyzed group, including both treated and control mice, contained 3 biological replicates, resulting in the total of 78 liver samples from different mice being sequenced in the work. RNA was extracted from liver tissues with PureLink RNA Mini Kit as described in the protocol and passed to sequencing.

4.1.2 RNAseq Data Processing and Analysis

Paired end sequencing was done on the Illumina HiSeq2000 platform generating approximately 25 to 50 million reads per sample, with read length of 100 nucleotides. Quality filtering and adapter removal were performed using Trimmomatic version 0.32.

Processed/cleaned reads were then mapped with STAR (version 2.5.2b) (Dobin et al., 2013). Read counting was performed by featureCounts (Liao et al., 2014). To filter out genes with low number of reads, only genes with at least 2 counts per million (cpm) in at least 3 samples were left, which resulted in 11053 detected genes according to Entrez annotation. Filtered data was then passed to RLE normalization (Anders and Huber, 2010).

Differential expression analysis was performed with R package edgeR (Robinson et al., 2009). For individual interventions, we declared gene expression to be significantly changed, if p-value, adjusted by Benjamini-Hochberg procedure (Benjamini and Hochberg, 1995), was smaller than 0.05 and fold change (FC) was bigger than 1.5 in any direction. When several doses and age groups were presented, we added separate factors accounting for that to the model and looked for genes significantly changed across these settings. As dose and age groups experiments were run separately and had their own controls, such factors allowed us to adjust for possible batch effect. The effects of certain interventions on different sexes were investigated separately. To determine the statistical significant of overlap between differentially expressed genes of certain interventions, we performed Fisher exact test separately for up- and downregulated genes, considering 11,053 detected genes as a background.

When performing analysis of feminizing effect, “feminizing changes” were defined as gene expression changes between control males and females from UM-HET3 strains. When calculating Pearson correlation between response to certain intervention in specific age group (6 or 12 months) and feminizing changes, the latter were calculated based on control males and females from the other age group (12 or 6 months, respectively). This

technique provided us with unbiased correlations, based on different control samples. In case of MR, GHRKO and Snell dwarf mice, which possess their own control, feminizing changes were aggregated across age groups. For that we used single edgeR model with the age specified as a separate factor. In cases of both individual and aggregated age groups, we declared the feminizing gene to be significantly changed, if p-value, adjusted by Benjamini-Hochberg procedure, was smaller than 0.05 and FC was bigger than 1.5 in any direction.

The statistical significance of Pearson correlation between feminizing changes and response to certain intervention ("feminizing effect") was calculated with Pearson correlation test and adjusted for multiple comparisons with Benjamini-Hochberg procedure. Difference in feminizing effect of certain intervention in certain age group between males and females was tested by Pearson correlation test, applied to the difference in $\log_2$FC of feminizing genes (from the other age group) in response to the specified conditions between males and females, and feminizing changes based on the other age group, with the following Benjamini-Hochberg adjustment. Overlap between statistically significant feminizing genes and gene differentially expressed in response to interventions was estimated by Fisher exact test similarly to comparison of individual interventions.

Heatmap of feminizing genes was created based on feminizing changes, aggregated across age groups, and $\log_2$FC of corresponding genes in response to individual interventions, aggregated across age groups as well (using edgeR). Only genes differentially expressed between control males and females (637 genes) were used to build

the heatmap. Clustering was performed with average hierarchical approach and Pearson correlation distance.

To investigate genes responsible for feminizing effect, we used single edgeR model to identify genes with changes associated with feminizing effect, calculated within unbiased correlation analysis. We declared a gene to be significantly changed, if its Benjamini-Hochberg adjusted p-value was smaller than 0.05. We then took an intersection of feminizing genes, aggregated across age groups, and genes associated with feminizing effect, separately for up- and downregulated genes, to obtain the final list of common genes. This resulted in 164 upregulated and 153 downregulated common genes.

4.1.3 Functional Enrichment Analysis

For identification of functions enriched by genes differentially expressed in response to individual interventions within our RNAseq data and aggregated across datasets (CR, rapamycin and GH deficiency interventions), commonly changed across interventions (common signatures) as well as associated with lifespan effect, we performed GSEA (Subramanian et al., 2005) on a pre-ranked list of genes based on z-scores, calculated as:

$$z\text{-}score = -\ln(pv) \times sgn(lfc),$$

where *pv* and *lfc* are p-value and logFC of certain gene, respectively, obtained from edgeR output, and *sgn* is signum function (is equal to 1, -1 and 0 if value is positive, negative and equal to 0, respectively). REACTOME, BIOCARTA, KEGG and GO biological process and molecular function from Molecular Signature Database (MSigDB) have been used as gene sets for GSEA (Subramanian et al., 2005). q-value cutoff of 0.1 was used to select

statistically significant functions. Adjusted z-scores of enriched functions were calculated as:

$$adjusted\ z\text{-}score = -\log_{10}(qv) \times sgn(NES),$$

where NES and qv are normalized enrichment score and q-value, respectively.

Horizontal and vertical barplots were shown for manually chosen statistically significant functions with size of barplot being dependent on value of adjusted z-score. For functions associated with lifespan effect, heatmap colored based on adjusted z-score was used. Clustering of functions enriched by individual interventions within RNAseq data was performed based on NES of functions with statistically significant enrichment (q-value < 0.1) by at least one intervention. Clustering has been performed with hierarchical average approach and Pearson correlation distance.

To identify functions enriched by genes shared by differences between males and females along with changes in response to lifespan-extending interventions in males, we performed Fisher exact test using Database for Annotation, Visualization and Integrated Discovery (DAVID) (Huang et al., 2009a, 2009b). INTERPRO, KEGG and GO BP and MF databases were used. We declared functions to be enriched if their Benjamini-Hochberg adjusted Fisher exact test p-value was smaller than 0.1.

To perform further functional enrichment analysis of molecular pathways by CR and GH deficiency, we applied iPANDA method (Ozerov et al., 2016) to every individual dataset related to these interventions and obtained corresponding pathway activation scores (PAS) for each of them. PAS is based on both statistical significance and the strength of activation of the certain pathway. As some of the individual datasets measure response to

certain intervention using the same control sampling, to calculate the aggregated PAS together with its p-value for the certain intervention, we used mixed-effect model, based on all single PAS values obtained from individual datasets with random term corresponding to the use of the same control sampling for calculation of gene expression change. Mixed-effect model was built with R package metafor (Viechtbauer, 2010). Obtained p-values were adjusted for multiple comparisons with Benjamini-Hochberg procedure. Functions were considered to be significantly enriched if their adjusted p-value was smaller than 0.1. Barplots with manually chosen enriched functions were built with the size of bars corresponding to the value of adjusted z-score, calculated as:

$$adjusted\ z\text{-}score = -\log_{10}(adj.\ pv) \times sgn(agPAS),$$

where $adj.\ pv$ and $agPAS$ are BH adjusted p-value and aggregated PAS obtained from mixed-effect model output, respectively.

4.1.4 Aggregation of RNAseq and Microarray Datasets for Meta-Analysis

To aggregate data across different platforms and studies, we developed the following method. First, data within each study is preprocessed independently and log-transformed to conform to normal distribution if needed. Then, filtering of low-covered genes is performed with soft threshold. Then, all identifiers are mapped to Entrez ID gene format, and genes not detected in our RNAseq data are filtered out. This results in the coverage of 11053 genes or less if some of these genes have been filtered out because of the low coverage. Afterwards, samples within every study are normalized by quantile and z-score normalization, followed by multiplication by the certain value to make it on the same scale as RNAseq data with more natural interpretation. Finally, mean and standard

error of logFC of every gene for every response to intervention is calculated together with p-value (along with Benjamini-Hochberg adjusted p-value) estimated by edgeR (Robinson et al., 2009) and limma (Ritchie et al., 2015) for RNAseq and microarrays datasets, respectively. This results in 2 values representing every gene from every dataset. Importantly, one study may lead to several datasets if several interventions or settings have been analyzed there. Sometimes, different interventions or doses share the same control sampling. This may lead to some batch effect, which we, however, removed at the subsequent steps. In total, our meta-analysis resulted in 17 different interventions presented in 77 control-intervention datasets from 22 different sources (including ours) (Figure 19D).

Z-score normalization of every sample, performed before calculation of logFC, results in similar and comparable distribution of gene changes across different studies and platforms. Importantly, z-score normalization is not performed after calculation of logFC as different interventions may lead to different scale of gene expression profile perturbation. Indeed, lifespan-extending genetic manipulations generally lead to bigger perturbation of transcriptome compared to diets and compounds (Figure 20). To demonstrate this effect, we calculated median and standard deviation of logFC distribution across the whole transcriptome for every individual dataset. Median may be interpreted as imbalance between up- and downregulated changes whereas standard deviation corresponds to the scale of perturbation. To visualize distribution of specified metrics for different kinds of interventions (pharmacological, dietary and genetic manipulations), we used violinplots. Unpaired Mann-Whitney test was used to compare medians and standard deviations of logFC distributions corresponding to different kinds of interventions.

4.1.5 Identification of Genes Associated with Individual Interventions

logFC calculated for every dataset were further used as inputs to the statistical tests for meta-analysis. To account for standard error of logFC and remove batch effect related to the belonging of several datasets to the same study or same control sampling within the study, we applied mixed-effect model using R package metafor (Viechtbauer, 2010). As an input, we used both mean and standard error of logFC. Such approach allowed us to account for the size of the effect and variance of estimated gene expression change within each individual dataset, which provides more sensitive and accurate analysis compared to previous studies focused on comparison of lists of differentially expressed genes.

When calculating gene expression changes of individual interventions across different sources (such as CR and rapamycin), to remove batch effect, we considered belonging to the same study or control group as random term. When calculating such changes for GH deficiency interventions, we also included type of intervention as a random term. Using this procedure, we obtained aggregated logFC and corresponding p-value for every gene. Besides standard p-value, we also calculated leave-one-out (LOO) and robust p-value. 'LOO p-value' is defined as the highest p-value after removal of every study one by one. On the other hand, 'robust p-value' is the lowest p-value after the same procedure. Benjamini-Hochberg procedure was used to adjust every type of p-value for multiple comparisons. We declared genes to be differentially expressed in response to CR, rapamycin and GH deficiency across datasets if adjusted p-value was smaller than 0.01 and their LOO p-value was smaller than 0.01. The significance of overlap between lists of differentially expressed genes obtained from meta-analysis was estimated by Fisher exact

test separately for up- and downregulated genes, considering 11,053 detected genes as a background.

To identify upstream regulators of detected gene expression response to CR, rapamycin and GH deficiency, we applied the Biobase Transfac platform (Matys, 2006). First, for every individual dataset, we identified transcription factors binding to sequences enriched in promoters of differentially expressed genes using the platform. This resulted in matrix, where every transcription factor was either enriched (1) or not (0) for the certain dataset. At this step, we excluded redundant IDs corresponding to different binding patterns of the same factor by considering factor to be enriched if at least one of its patterns is enriched. This resulted in 1466 different upstream regulators. To identify factors overrepresented across different datasets of the same intervention, we applied permutation version of binomial statistical test as described in (Plank et al., 2012). Briefly, to identify the p-value threshold corresponding to the desired FDR (equal to 0.01), permutation test is performed, where 1 and 0 (corresponding to enrichment of different transcription factors) are shuffled within each dataset and number of false positives for different binomial test p-value thresholds are calculated. Based on the obtained numbers, p-value threshold ensuring FDR threshold of 0.01 is determined. The significance of overlap between enriched upstream regulators of different interventions was estimated by Fisher exact test, considering 1466 non-redundant transcription factors as a background.

Similarly, aggregated logFC together with p-values were calculated for all interventions presented in our data by multiple sources. For interventions presented as a single dataset, logFC and p-values were obtained from individual datasets as described

previously. For interventions measured in several datasets from the same source, single edgeR or limma model was used depending on the origin of the data (RNAseq or microarray). This resulted in matrix containing aggregated log_2FC values of every gene in response to different interventions. To visualize change of each gene within each individual intervention, we built barplots representing aggregated log2FC of the certain gene in response to all intervention where it has been detected. Statistically significant changes were defined based on Benjamini-Hochberg adjusted p-value.

4.1.6 Analysis of Mutual Organization of Interventions

To assess similarity of gene expression response across interventions, we built a heatmap of aggregated log_2FC of genes significantly changed in response to CR, rapamycin and GH deficiency interventions (2507 genes in total). Complete hierarchical clustering was employed for the heatmap. Correlation matrix representing similarity between aggregated logFC of different interventions was calculated based on Pearson correlation coefficient.

To calculate correlations between interventions in unbiased way, we applied the following approach. For every pair of interventions, including comparison of intervention with itself, we examined all pairs of datasets from different sources. For each such pair we took a union of 100 genes with the most significant expression change (defined by p-values calculated for individual datasets) and calculated Spearman correlation coefficient between the datasets. We reiterated this algorithm and, as a result, for every pair of interventions obtained distribution of Spearman correlation coefficients, calculated between datasets from different sources. For CR and rapamycin, we visualized these distributions using

violinplot. One-sample Mann-Whitney test and Benjamini-Hochberg adjustment were used to check if means of correlation coefficients are different from 0 with statistical significance. We declared correlation coefficient to be significant if adjusted p-value was smaller than 0.1.

For correlation matrix we employed median values of Spearman correlation coefficients. By filtering out comparisons of datasets from the same source, we removed possible batch effect and ended up with independent and unbiased comparison of interventions. However, as some interventions were presented only within the same source, we couldn't estimate unbiased correlation for such cases. This missing data was visualized by grey boxes. The same was sometimes true for comparison of intervention with itself, as in this case we also employed only datasets from different sources. For this reason, correlation coefficient of intervention with itself was not equal to 1 in resulted unbiased correlation matrix. Complete hierarchical clustering approach was employed for visualization of correlation matrix. To demonstrate similarities between different interventions in network mode, we employed Cytoscape (Shannon et al., 2003). Only edges between interventions with significant positive correlation coefficients (median Spearman correlation coefficient > 0 and adjusted Mann-Whitney p-value < 0.1) were shown. The width of edge was defined by the $\log_{10}$(adjusted p-value). Smaller p-value led to wider edge.

4.1.7 Identification of Common Signatures and Genes Associated with Lifespan Effect

To identify genes with expression change shared across lifespan-extending interventions and, therefore, served as qualitative predictors of lifespan extension, we

filtered out all interventions and settings with unproved lifespan extension effect. Only settings, for which reliable longevity study was performed, were considered in the subsequent analysis. Therefore, for example, 40% CR in C57BL/6 females was excluded from the analysis as this setting doesn't lead to statistically significant lifespan extension, contrary to 20% CR applied to the same mouse strain.

First, for every single gene we calculated number of interventions, where it is differentially expressed based on adjusted aggregated p-value estimated as described previously. We considered gene to be differentially expressed if its adjusted aggregated p-value was smaller than 0.1. However, this approach overfits genes changed in response to similar interventions (such as GH deficiency interventions) and doesn't take into account possible consistent changes, which may be, however, not significant due to low sampling size or high variance. To overcome this problem, we applied single mixed-effect model to every gene as described previously and looked for genes, which aggregated logFC across lifespan-extending interventions is significantly different from 0. Here, however, we also included type of intervention as a random term together with correlation matrix specifying similarities between general response of the interventions. This correlation matrix was taken from unbiased mutual organization analysis described previously. We declared genes to be significantly shared across interventions if Benjamini-Hochberg adjusted robust p-value, obtained after removal of every type of intervention one by one, was smaller than 0.05. Heatmap with expression changes of significant genes across individual datasets was clustered with complete hierarchical approach.

To identify genes associated with lifespan effect, we estimated three main metrics of lifespan for every available setting, including median lifespan ratio (in logarithmic scale), maximum lifespan ratio (in logarithmic scale), defined as ratio of average lifespan of 10% most survived individuals, and median hazard ratio, defined as ratio of slopes of survival curves at the median point (timepoint where 50% of cohort is remained survived). We calculated these metrics for all available longevity studies related to the certain intervention setting (sex, dose and strain), and calculated average value across the studies to obtain most consistent and reliable value. Interventions or settings, for which no appropriate longevity study was available, were excluded.

Afterwards, we applied mixed-effect model as described previously to identify genes associated with each of the 3 numeric metrics of lifespan effect. Control group and type of intervention were considered as random term, and correlation matrix between interventions was used to define covariance matrix. We declared genes to be significantly associated with lifespan effect if Benjamini-Hochberg adjusted p-value and LOO p-value, obtained after removal of every intervention one by one, were both smaller than 0.05. The significance of overlap between lists of genes associated with different metrics of lifespan effect was estimated by Fisher exact test separately for genes with positive and negative association, considering 11,053 detected genes as a background. Complete hierarchical clustering was used to sort genes on heatmap, representing logFC of genes with significant association across individual datasets. Individual datasets were sorted there based on their effect on maximum lifespan.

4.1.8 Test on Association with Longevity Signatures

To test association of interventions with longevity signatures related to individual interventions (CR, rapamycin and GH deficiency), common changes and lifespan effect association, we employed GSEA-based approach. First, for every signature we specified 250 genes with the lowest p-values and divided them into up- and downregulated genes. These lists were considered as gene sets. Then we ranked genes related to interventions of interest based on their z-scores, calculated as described in functional enrichment section. When running association test for lifespan-extending interventions (Figure 21A), we used p-values obtained from aggregated analysis as described previously. For interventions without known association with lifespan (Figure 24E), we downloaded them from GEO under the following accession numbers: GSE21060 (Ramadoss et al., 2010), GSE77082 (Alonso et al., 2017), GSE15891 (Baze et al., 2010a), GSE11287 (Osburn et al., 2008) and GSE10421 (Kautz et al., 2008). We preprocessed each dataset, performed quantile normalization and Entrez ID transformation and applied limma model for calculation of p-values, which were converted to z-score as explained previously.

We calculated GSEA scores separately for up- and downregulated lists of gene set as described in (Lamb et al., 2006) and defined final GSEA score as a mean of the two. To calculate statistical significance of obtained GSEA score, we performed permutation test where we randomly assigned genes to the lists of gene set maintaining their size. To get p-value of association between certain intervention and longevity signature, we calculated the frequency of real final GSEA score being bigger by absolute value than random final GSEA scores obtained as results of 3,000 permutations. To adjust for multiple

comparisons, we performed Benjamini-Hochberg procedure. Resulted adjusted p-values were converted into adjusted z-scores as:

$$adjusted\ z\text{-}score = -\log_{10}(adj.\ pv) \times sgn(GSEA\ score),$$

where $adj.\ pv$ and $GSEA\ score$ are BH adjusted p-value and final GSEA score, respectively. Heatmaps were colored based on values of adjusted z-scores.

4.2 Results and Discussion

4.2.1 RNAseq Analysis across Lifespan-Extending Interventions

We subjected young adult mice to 8 interventions previously established to extend lifespan, including acarbose, 17-α-estradiol, rapamycin, Protandim, CR (40%), MR (0.12% methionine w/w), GHRKO and *Pit1* knockout (Snell dwarf mice) (Figure 17A). This set included 4 interventions that have never been analyzed at the gene expression level (acarbose, 17-α-estradiol, Protandim and MR). All compounds and diets were applied to genetically heterogeneous UM-HET3 mice and started at 4 months of age, except for MR, which was applied to 2-month-old C57BL6/J mice. Duration of treatment exceeded 8 months in at least one age group for all compounds and diets and was equal to 5 months for the long-lived mutants. We then performed RNAseq on liver samples of these mice, together with corresponding controls, analyzing both males and females, except for MR, GHRKO and Snell dwarf mice, where only males were examined. Since some of these interventions are known to be effective when used at different concentrations and different ages (Harrison et al., 2009, 2014; Mercken et al., 2014; Miller et al., 2014; Mitchell et al., 2016; Strong et al., 2016), we used 2 different age groups for CR, rapamycin and acarbose

(6- and 12-month-old, representing 2- and 8-month treatment, respectively), and 2 different effective concentrations of rapamycin (14 and 42 ppm) (Figure 17A).

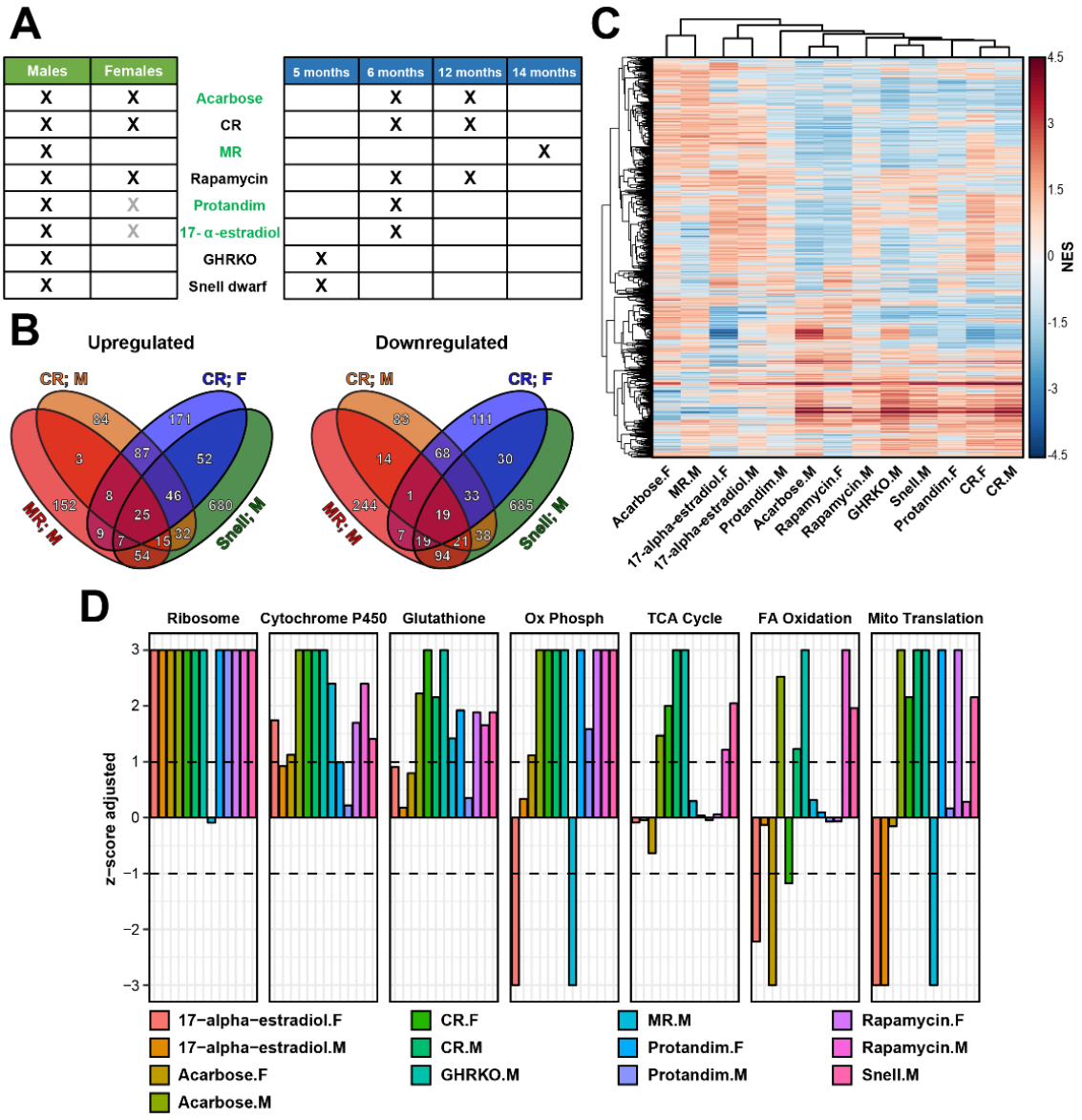

Figure 17. RNAseq analysis of hepatic gene expression in mice subjected to lifespan-extending interventions

(A) RNAseq dataset. Mice were subjected to indicated lifespan-extending interventions for several months (from 2 to 12 for different interventions and age groups; n=3 for each control and treatment group within each sex and age setting resulting in 78 samples in total). Interventions, which have not been previously analyzed at the level of gene expression, are colored in green. Sex and age of mice corresponding to each intervention is shown with X marks. Cases where an intervention failed

to extend lifespan with statistical significance in females are shown with grey X mark. **(B) Overlap of gene expression changes in response to longevity interventions.** Overlap of differentially expressed genes (BH adjusted p-value < 0.05 and FC > 1.5 in any direction) in response to MR in males, CR in males and females and in Snell dwarf males is shown. 44.3% of upregulated and 41.8% of downregulated genes in response to MR are shared with at least one other lifespan-extending intervention. **(C) Heatmap of functions enriched by gene changes in response to lifespan-extending interventions.** Normalized enrichment score (NES) of functions are shown for every intervention. All functions enriched by at least one intervention are presented. FDR threshold of 0.1 was used to filter out functions nonsignificant for every individual intervention. Clustering has been performed with hierarchical average approach and Pearson correlation distance. **(D) Functions enriched by upregulated (up) and downregulated (down) genes across different interventions based on GSEA.** Z-score, calculated as $\log_{10}$(FDR q-value) corrected by sign of regulation, is plotted on the y axis. FDR threshold of 0.1 is shown by dotted lines. Shown functions were selected manually. Ribosome: Ribosome (KEGG); Cytochrome P450: Drug metabolism by cytochrome P450 (KEGG); Glutathione: Glutathione metabolism (KEGG); Ox Phosph: Oxidative phosphorylation (KEGG); TCA cycle: Citrate Cycle/TCA Cycle (KEGG); FA oxidation: Fatty acid β-oxidation (GO); Mito Translation: Mitochondrial translation (GO); MR: Methionine Restriction; CR: Caloric Restriction; Snell: Snell dwarf mice; F: Females; M: Males.

Differentially expressed genes associated with each intervention were initially examined separately for males and females. With false discovery rate (FDR) threshold of 0.05 and fold change (FC) threshold of 1.5, we detected 230 upregulated and 92 downregulated genes for MR males, 364 upregulated and 270 downregulated genes for acarbose males, 289 upregulated and 69 downregulated genes for acarbose females, 207 upregulated and 34 downregulated genes for 17-α-estradiol males, 313 upregulated and 268 downregulated genes for 17-α-estradiol females, 30 upregulated and 2 downregulated genes for Protandim males and 90 upregulated and 70 downregulated genes for Protandim females. Many differentially expressed genes were found to be common to interventions. For example, almost half of MR genes (44.3% upregulated and 41.8% downregulated genes) were altered significantly and in the same direction in Snell dwarf males and CR males and females (Figure 17B). Moreover, genes affected only in Snell dwarfs covered

37% of MR upregulated and 36.5% of MR downregulated genes (Fisher exact test p-value $< 2.2 \cdot 10^{-16}$ in both cases). This observation supports the idea of common molecular mechanisms shared by MR and other interventions such as CR and Snell dwarf mice. It is also consistent with the previous findings that the lifespan extension effect of CR in flies is highly dependent on the presence of methionine in the diet and can be abrogated by the addition of amino acids only if they include methionine (Grandison et al., 2009).

Analysis of enriched functions using gene set enrichment analysis (GSEA) (Subramanian et al., 2005) revealed many similarities among the interventions (Figure 17D). For example, ribosomal protein genes were upregulated in response to all interventions except MR (q-value < 0.001), and other commonly upregulated functions included drug metabolism by cytochrome P450, glutathione metabolism, oxidative phosphorylation and TCA cycle. These patterns are consistent with the reports on individual lifespan-extending interventions, including Ames and Snell dwarf mice, Little mice, GHRKO, CR and rapamycin (Amador-Noguez et al., 2004; Miller et al., 2014; Steinbaugh et al., 2012).

In addition to common strategies, we detected distinct signatures. For example, 17-α-estradiol in females and MR resulted in downregulation of oxidative phosphorylation. Although ribosomal protein genes, in general, represented the most common upregulated pattern across the interventions, this was not the case for mitochondrial ribosomal protein genes. Some interventions, including CR, GHRKO, Snell dwarf mice and acarbose in males, showed significant upregulation of these genes, whereas 17-α-estradiol in both sexes and MR showed their downregulation. Finally, fatty acid oxidation, which is known

to be positively associated with the lifespan extension effect of several interventions (Amador-Noguez et al., 2004; Plank et al., 2012; Tsuchiya et al., 2004), was significantly downregulated when applied to females (Figure 17D). 17-α-estradiol, acarbose and CR showed significant downregulation of fatty acid oxidation genes in females, whereas in males we observed an opposite effect for acarbose and CR.

Interestingly, although MR mice resemble CR mice in stress resistance and endocrine changes, and MR mice share many differentially expressed genes with CR and growth hormone (GH) deficiency-associated interventions (i.e. GHRKO and Snell dwarf mice), MR displayed a quite distinct pattern at the level of functional enrichment (Figure 17C, D). It shared some common signatures with CR and GH-associated mutants, including upregulation of glutathione metabolism, drug metabolism by cytochrome P450 and regulation of telomere maintenance and downregulation of complement and coagulation cascades. However, it also exhibited upregulation of PI3K, insulin receptor and mTOR pathways and downregulation of oxidative phosphorylation and genes coding structural constituents of ribosome, which was distinct from CR and most other interventions. Data from other tissues, once they become available, may add to the understanding of similarities and differences across these interventions.

To get a more global view on the similarities among interventions in terms of regulation of cellular pathways, we built a heatmap of normalized enrichment scores (NES) of all functions enriched by at least one intervention and clustered the data using an average hierarchical approach (Figure 17C). MR clustered separately from other interventions, but together with acarbose in females (unfortunately, we lacked tissues of female mice

subjected to MR). Not surprisingly, GHRKO and Snell dwarf mice, which are both associated with growth hormone deficiency, showed a very similar pattern of gene expression both at gene and functional enrichment levels, consistent with previous studies that examined gene expression response of GH deficiency (Amador-Noguez et al., 2004). Finally, females and males showed a similar response to CR and 17-α-estradiol at the level of functional enrichment, whereas their responses to acarbose and Protandim were quite different. Interestingly, although both 17-α-estradiol and Protandim lead to statistically significant lifespan extension only in males, similarities in the response to them across sexes seem to be different at the level of cellular pathways. High similarity in the functional response to 17-α-estradiol between males and females together with its substantial effect on median lifespan in males (increase by 19%) and absence of effect in females (Strong et al., 2016) point to the role of sex in the lifespan effect even when molecular changes induced by interventions are similar across sexes.

4.2.2 Feminizing Effect of Lifespan-extending Interventions

The finding of sex-specific changes in gene expression in response to longevity interventions allowed us to examine this question in more detail. Several previous studies noted a feminizing effect of CR and GH deficiency on gene expression in males (Buckley and Klaassen, 2009; Estep et al., 2009; Fu and Klaassen, 2014; Li et al., 2013). To test sex-specific effects in our broad dataset of interventions, we first identified "feminizing" changes, defined as significant gene expression changes between control males and females from UM-HET3 strains in 6- and 12-month-old age groups. We then examined if interventions in different sexes feminize the gene expression profile. To test this in an

unbiased way, for every intervention in a certain age group, we calculated the correlation of its response with feminizing changes, calculated for another age group (feminizing effect), except for Snell dwarf mice, GHRKO and MR, where we used feminizing changes aggregated across both ages for correlation calculation, as these interventions had separate controls.

We detected a tendency for genetic (GHRKO and Snell dwarf mice) and dietary (CR and MR) interventions in males to produce statistically significant feminizing-like patterns at the gene expression level (Figure 18A). Indeed, sex-specific changes calculated for the 12-month-old age group shared more than 45% of up- and downregulated genes with GHRKO and 6-month-old CR males and showed a statistically significant overlap with both (Fisher exact test adjust p-value < $4.1 \cdot 10^{-8}$) (Figure 18B). The feminizing effect was especially strong for genetic mutants, reaching 70.1% correlation for GHRKO (Pearson correlation test adjusted p-value = $4.8 \cdot 10^{-94}$; Figure 18C). Besides mutants and diets, acarbose applied for 8 months in males also produced a significant feminizing effect. Interestingly, it was similar to the CR effect, as acarbose prevents the digestion of starch and disaccharides to glucose in the intestine by inhibiting α-glucosidases (Balfour et al., 1993), and it is the only drug showing the feminizing effect in males in our data. Other drugs didn't lead to a significant feminizing effect in males or even produced a significant negative effect, such as rapamycin in 12-month-old males (Pearson correlation test adjusted p-value = 0.012; Figure 18A).

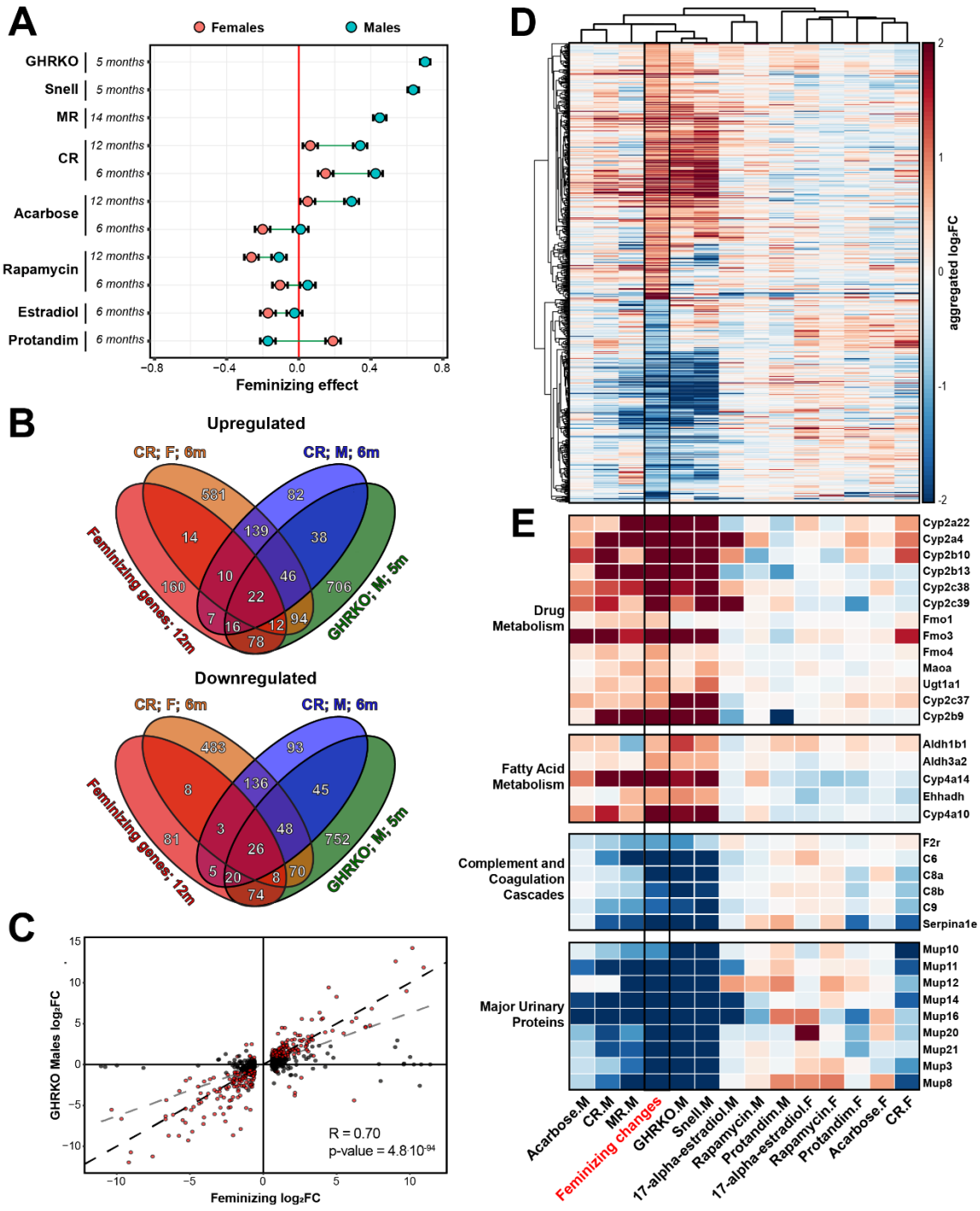

Figure 18. Feminizing effect of lifespan-extending interventions

(A) Feminizing effect across interventions and age groups. Genetic (GHRKO, Snell dwarf mice) and dietary (CR, MR) interventions together with acarbose at 12 months of age show a significant feminizing effect in males. For all interventions and age groups, except for Protandim, males show a significantly higher feminizing effect than females (Pearson correlation test adjusted p-value <

$8.4 \cdot 10^{-3}$ for all interventions and age groups). The feminizing effect is defined as correlation of $\log_2$FC of feminizing genes between response to intervention and feminizing changes in the other age group. **(B) Overlap of genes differentially expressed between males and females and in response to feminizing lifespan-extending interventions.** Fisher exact test BH adjusted p-value $< 4.1 \cdot 10^{-8}$ for overlap of all presented interventions with feminizing genes. **(C) Correlation between feminizing changes and changes induced by GHRKO in males.** $\log_2$FC of genes differentially expressed between males and females (BH adjusted p-value < 0.05 and FC > 1.5 in any direction) aggregated across age groups are shown. Genes statistically significantly changed in response to GHRKO (BH adjusted p-value < 0.05 and FC > 1,5 in any direction) are colored in red. Regression and identity lines are shown as grey and black dotted line, respectively. **(D) Heatmap with $\log_2$FC of genes differentially expressed between females and males (Feminizing genes) and in response to different interventions within each sex.** $\log_2$FC of genes differentially expressed between females and males (BH adjusted p-value < 0.05 and FC > 1.5 in any direction) aggregated across age groups are shown. **(E) Functional enrichment of feminizing genes significantly associated with feminizing effect across interventions.** Drug metabolism, fatty acid metabolism and complement and coagulation cascades are annotated by KEGG database; major urinary proteins are annotated by INTERPRO database. Estradiol: 17-α-estradiol; GHRKO: Growth hormone receptor knockout; MR: Methionine Restriction; CR: Caloric Restriction; Snell: Snell dwarf mice; F: Females; M: Males; 12m: 12 months; 6m: 6 months; 5m: 5 months.

To better understand the nature of the feminizing pattern of genetic and dietary interventions, we identified sex-specific genes, whose change in response to interventions is, at the same time, associated with the feminizing effect. With the FDR threshold of 0.05 and FC threshold of 1.5, we detected 355 sex-specific genes differentially expressed at a higher level in females and 282 genes expressed at a lower level (Figure 18D). Among them, 153 (out of 355) and 164 (out of 282) genes were positively and negatively associated with the feminizing effect, respectively. Functional enrichment of these genes using DAVID (Huang et al., 2009a, 2009b) revealed upregulation of drug metabolism (Fisher exact test BH adjusted p-value = $1.5 \cdot 10^{-9}$) and fatty acid metabolism (Fisher exact test BH adjusted p-value = 0.026) (Figure 18E). Cytochrome P450 genes, involved in drug metabolism, are well known to be differentially expressed between sexes in mice and be regulated by GH, and in particular by sex-specific differences in daily GH pulse frequency

and amplitude (Waxman and Holloway, 2009). However, it was previously unclear whether the same xenobiotic metabolizing enzyme (XME) genes are altered in response to different lifespan-extending interventions. Here, we show that this is indeed the case. Among downregulated genes, we detected enrichment of complement and coagulation cascades (Fisher exact test BH adjusted p-value = $9.8 \cdot 10^{-3}$) and major urinary proteins genes (Fisher exact test BH adjusted p-value = 0.021) (Figure 18E).

In females, the effect on sex-specific genes was mostly similar to that in males. For example, 6-month-old CR females also exhibited a significant feminizing-like pattern (Pearson correlation test adjusted p-value = $7.7 \cdot 10^{-4}$), and rapamycin females showed a significant masculinizing pattern in both age groups (Pearson correlation test adjusted p-value = $3.3 \cdot 10^{-10}$ and 0.02 for 12 and 6 months, respectively) (Figure 18A). Interestingly, one of the strongest masculinizing patterns in females was produced by 17-α-estradiol, while it had no significant effect on sex-specific genes in males, hinting that its selective effect on males is not due to simple recapitulation of the female hormonal profile. Based on our data, feminization does not explain the effect of interventions on lifespan extension. Indeed, 17-α-estradiol does not lead to any feminizing changes in males but increases their median (by 19%) and maximum (by 12%) lifespan (Strong et al., 2016). Besides, in females rapamycin and 17-α-estradiol showed a similar and significant masculinizing effect, although the first drug extended lifespan in females even stronger than in males (Miller et al., 2014), whereas the second compound did not lead to lifespan extension in females (Strong et al., 2016). Therefore, it seems that feminizing, or masculinizing, effects are neither necessary nor sufficient for lifespan extension, although a number of

interventions, including GH mutants and diets, regulate some pathways associated with sex-specific differences.

Although various interventions had a different effect on feminizing genes across sexes, we detected a consistently stronger feminizing effect in males compared to females for every individual intervention and age group, except for Protandim (Pearson correlation test adjusted p-value < $6.8 \cdot 10^{-3}$) (Figure 18A). In other words, regardless of the direction and size of the effect of certain intervention on sex-specific genes in males, it will most likely lead to more masculinizing changes in females. Moreover, lifespan-extending interventions seem to converge gene expression profiles of males and females to some middle "asexual" state. This finding may suggest that the survival state, induced by lifespan-extending interventions, is mainly universal across sexes, and sex-specific differences of organisms start disappearing when moving to that state. Therefore, we believe that different sexes share general mechanisms of lifespan extension, although they have different initial states defined by sex-specific features.

Overall, the data show that the feminizing effect is shared by genetic and dietary lifespan-extending interventions in males, and that there are certain common genes and functions that define this effect. The feminizing effect does not explain lifespan extension, but is consistently higher in males compared to females subjected to the same intervention, regardless of its direction and size, pointing to the converging effect of lifespan-extending interventions on sex-specific gene expression differences.

4.2.3 Signatures of CR, Rapamycin and Growth Hormone Deficiency

To obtain a comprehensive picture of gene expression responses to interventions, we collected all publicly available microarray datasets for mouse liver and conducted a meta-analysis across aggregated data. We first focused on 3 interventions for which many independent studies were previously performed: CR, rapamycin and interventions related to GH deficiency (Snell and Ames dwarf mice, GHRKO and Little mice). The latter group was combined, as these interventions, although targeting different genes involved in GH production and sensing, result in a similar effect on liver due to inability to activate GHR. In addition to this mechanistic notion, similarity among these interventions could also be seen at the level of hepatic gene expression as demonstrated by other groups (Amador-Noguez et al., 2004) and our results (Figure 19F and Figure 21C). As we were interested in the general effects of interventions regardless of experimental design and effect on lifespan, we combined all data across different sexes, strains, ages, durations of interventions and doses. In total, data from 29 datasets (across 13 different studies), 9 datasets (across 3 different studies) and 20 datasets (across 7 different studies) were aggregated for CR, rapamycin and GH deficiency, respectively.

To overcome issues associated with differences in platforms across different studies, along with batch effects, we developed an integrative method, based on independent preprocessing and normalization of individual datasets and following aggregation of means and standard deviations of logFC for all genes detected in our RNAseq data (resulting in 11,053 genes). Importantly, to account for possible differences in the general effect of interventions on mouse transcriptome, we did not normalize

distributions of logFC across datasets. To include information about standard deviations of logFC and account for possible batch effects due to the use of several datasets sharing the same control (e.g., if several doses were tested), we applied a mixed-effect model, considering shared control as a random term. We used this method to identify genes up- or downregulated across datasets (and, as a result, different doses, strains, age groups, etc.) of the same intervention type. Our approach, contrary to the comparison of lists of differentially expressed genes used in previous meta-analyses (Plank et al., 2012; Swindell, 2008), accounts for the size of the effect and variance of gene expression change within each individual dataset and, therefore, provides a more accurate and sensitive analysis. Besides standard p-value, obtained from the mixed-effect model test, we calculated "leave-one-out" (LOO) p-value as the largest (least significant) p-value after removal of every study one by one.

In this procedure, genes were designated statistically significant if their BH adjusted p-value was < 0.01 and LOO p-value was < 0.01. With these thresholds, we identified 419 up- and 370 downregulated genes for CR, 894 up- and 879 downregulated genes for GH deficiency, and 127 up- and 100 downregulated genes for rapamycin (Figure 19A). Interestingly, CR and GH interventions significantly overlapped (37% of CR upregulated and 26.3% of CR downregulated genes were shared with GH interventions; Fisher exact test p-value < 10^{-28} for both up- and downregulated genes), whereas rapamycin did not show a statistically significant overlap. Upregulated genes shared by CR and GH deficiency were enriched for oxidative phosphorylation (Fisher exact test BH adjusted p-value = $1.52 \cdot 10^{-9}$), and downregulated genes were enriched for complement and

coagulation cascades (Fisher exact test BH adjusted p-value = $5.21 \cdot 10^{-6}$). The difference in the gene expression response between CR and rapamycin was previously noted (Fok et al., 2014; Miller et al., 2014), but is not well understood. Our data provide a clear case for largely distinct mechanisms by which these interventions act in the liver. Not surprisingly, all GH deficiency interventions showed downregulation of *Igf1* and its stabilizer *Igfals* along with upregulation of 2 genes encoding its inhibitors, IGF-binding proteins *Igfbp1* and *Igfbp2*. Interestingly, *Igf1* expression showed no significant changes in response to CR and was even slightly upregulated in response to rapamycin. Both its binding proteins (*Igfbp1* and *Igfbp2*), however, were significantly upregulated in response to CR. Therefore, inhibition of the *Igf1* pathway in response to CR seems to happen due to the increased repression of *Igf1* by its binding proteins and not due to a change in its expression. GH-deficient mutants, on the other hand, repress the pathway by both downregulation of *Igf1* (along with its stabilizer *Igfals*) and upregulation of its inhibitors.

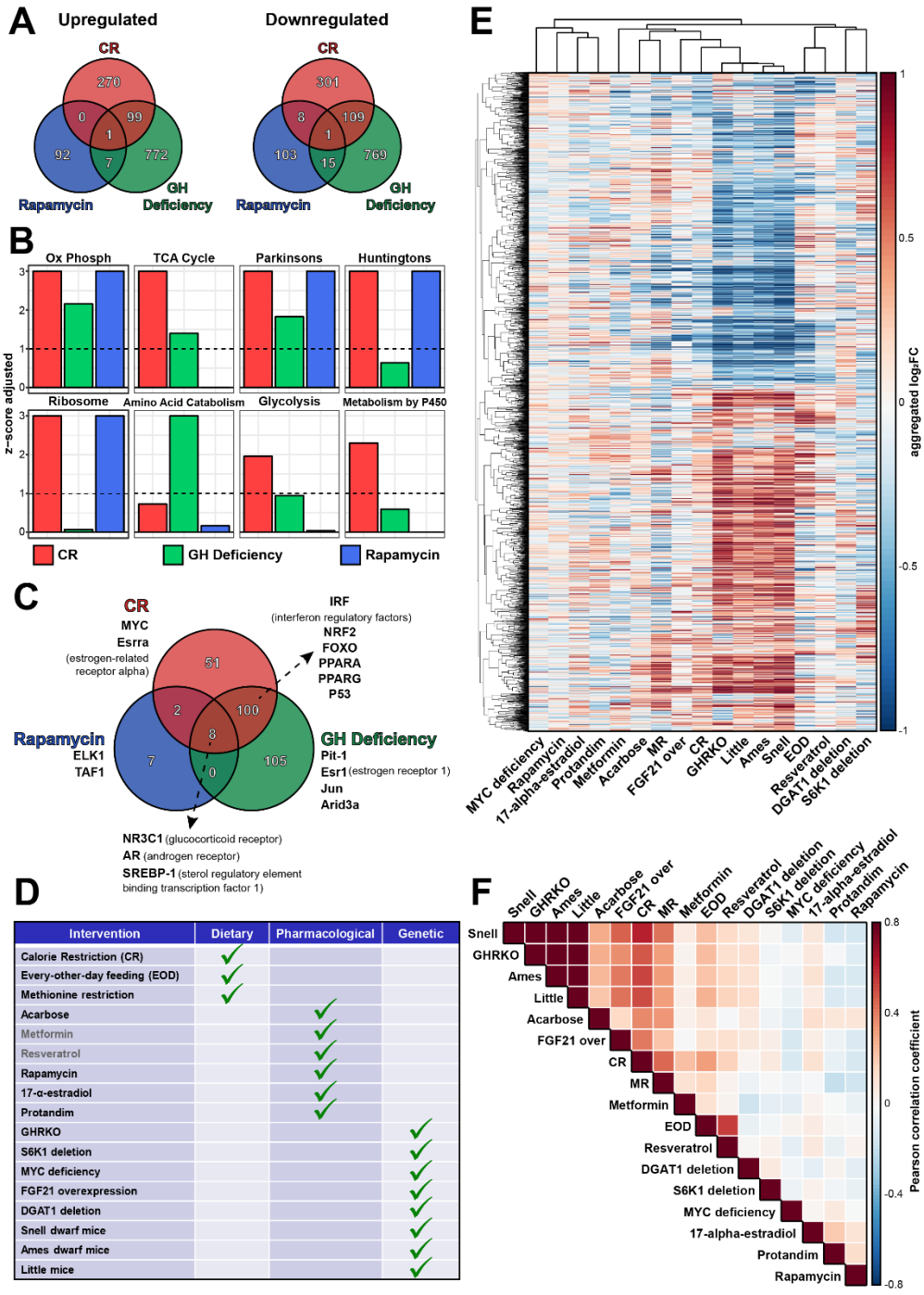

Figure 19. Genes significantly changed in response to CR, rapamycin and GH-deficiency across multiple datasets

(A) Genes identified as significantly up- and downregulated in response to CR, rapamycin and GH deficiency. FDR threshold of 0.01 and p-value LOO threshold of 0.01 were used to select significant genes. There is significant overlap between the genes changed in response to

CR and GH deficiency (Fisher exact test p-value < $2.2 \cdot 10^{-16}$). **(B) Functions enriched by upregulated and downregulated genes in response to CR, rapamycin and GH deficiency based on GSEA.** Z-score, calculated as $\log_{10}$(FDR q-value) corrected by sign of regulation, is plotted on y axis. q-value threshold of 0.1 is shown by dotted lines. Presented functions were selected manually. Ox Phosph: Oxidative phosphorylation (KEGG); TCA cycle: Citrate Cycle/TCA Cycle (KEGG); Parkinsons: Parkinson's Disease (KEGG); Huntingtons: Huntington's Disease (KEGG); Ribosome: Ribosome (KEGG); Amino Acid Catabolism: Cellular Amino Acid Catabolic Process (GO); Glycolysis: Glycolysis/Gluconeogenesis (KEGG); Metabolism by P450: Drug metabolism by cytochrome P450 (KEGG). **(C) Overlap of transcription factors IDs enriched by genes differentially expressed in response to CR, rapamycin and GH deficiency.** Permutation FDR of 0.01 was used to obtain the list of overrepresented IDs. Transcription factors specified in the text were selected manually. **(D) Interventions included into meta-analysis.** 17 interventions associated with increased lifespan or healthspan are included in the aggregated dataset. Two interventions (metformin and resveratrol, shown in grey) are included into the dataset despite their inability to significantly increase lifespan in healthy mice as shown by the ITP program. **(E) Fold changes of genes up- and downregulated in response to CR, rapamycin and GH deficiency across different lifespan- and healthspan-extending interventions.** GH-deficiency interventions form a tight cluster with similar transcriptome profile behavior, pointing to the same molecular mechanisms. Union of genes differentially expressed in response to CR, rapamycin and GH-deficiency interventions (BH adjusted p-value < 0.01 and p-value LOO < 0.01) and $\log_2$FC scale was used to create the heatmap. Complete hierarchical clustering approach was employed. **(F) Pearson correlation between genes differentially expressed in response to CR, rapamycin and GH deficiency.** The major cluster is formed by GH deficiency (Snell and Ames dwarf mice, GHRKO, Little mice), dietary interventions (CR, MR, EOD), FGF21 overexpression and others. Pearson correlation coefficient was calculated based on gene logFC aggregated across different datasets for every intervention. Complete hierarchical clustering approach was employed. Snell: Snell dwarf mice; Ames: Ames dwarf mice; Little: Little mice; CR: Caloric Restriction; GH: Growth Hormone; GHRKO: Growth Hormone Receptor Knockout; FGF21 over: FGF21 overexpression.

By applying GSEA, we further identified several pathways shared by 2 or all 3 analyzed interventions (Figure 19B). Oxidative phosphorylation was commonly upregulated across these interventions (q-value < 0.008 in all cases). Other shared upregulated functions included TCA cycle, ribosome and genes involved in age-associated diseases (Parkinson's and Huntington's), consistent with the RNAseq data.

To obtain further details on the regulation of molecular pathways by CR and GH deficiency, we used the iPANDA algorithm (Ozerov et al., 2016), which is another method of functional enrichment that utilizes the sign of the effect of a certain gene on pathway activation or inhibition. We applied it to every individual dataset included in our meta-analysis and calculated an aggregated pathway activation score (PAS) along with its statistical significance using the mixed effect model described previously. Consistent with the GSEA output, we observed activation of TCA cycle (BH adjusted p-value = $1.5 \cdot 10^{-4}$ and $2.2 \cdot 10^{-4}$), respiratory electron transport chain (BH adjusted p-value = 0.013 and 0.023), urea cycle (BH adjusted p-value = 0.036 and 0.068) and PPAR pathway (BH adjusted p-value = 0.06 and $7.6 \cdot 10^{-3}$) along with inhibition of the alternative complement (BH adjusted p-value = $8.9 \cdot 10^{-4}$ and $5.8 \cdot 10^{-7}$), interferon (BH adjusted p-value = 0.032 and 0.024) and insulin processing (BH adjusted p-value = 0.035 and 0.034) pathways in both CR and GH deficiency. Pathways activated in response to CR also included transcriptional activation of mitochondrial biogenesis (BH adjusted p-value = $1.3 \cdot 10^{-3}$), triglyceride biosynthesis (BH adjusted p-value = 0.032) and circadian clock (BH adjusted p-value = $6.6 \cdot 10^{-3}$), while inhibited pathways included translational initiation regulated by mTOR signaling (BH adjusted p-value = 0.028). GH deficiency interventions, in turn, showed activation of caspase cascade (BH adjusted p-value = $1.8 \cdot 10^{-8}$) and GSK3 signaling pathway (BH adjusted p-value = $3.4 \cdot 10^{-7}$) together with inhibition of IGF1R signaling (BH adjusted p-value = $1.5 \cdot 10^{-14}$) and MAPK (BH adjusted p-value = $7.9 \cdot 10^{-7}$), biosynthesis of mineralocorticoids (BH adjusted p-value = $6.8 \cdot 10^{-10}$) and cholesterol (BH adjusted p-value

= $9.2 \cdot 10^{-3}$), mTOR (BH adjusted p-value = $1.5 \cdot 10^{-9}$) and estrogen (BH adjusted p-value = $9.4 \cdot 10^{-6}$) pathways.

To identify upstream regulators of observed gene expression changes, we analyzed enrichment of transcription factors associated with differentially expressed genes using the Biobase Transfac platform (Matys, 2006). First, for each individual dataset we identified transcription factors binding to sequences enriched in promoters of genes differentially expressed in the corresponding dataset. We then applied a binomial statistical test to identify factors whose enrichment was overrepresented across datasets within the same type of intervention. A permutation FDR threshold of 0.01 resulted in the identification of 161 transcription factor IDs enriched for CR, 213 IDs enriched for GH-deficient interventions and 17 IDs enriched for rapamycin (Figure 19C). As at the level of individual genes, CR and GH-deficient interventions shared many transcription factors (>50% of their enriched transcription factors were shared; Fisher exact test p-value < 10^{-26}). However, in this case rapamycin also showed significant overlap with other interventions (58.8% and 47.1% of enriched transcriptional factors were shared with CR and GH deficiency, respectively; Fisher exact test p-value < 0.002 in both cases). Interestingly, 8 factors shared by all 3 interventions included receptors related to glucose sensitivity and sterol metabolism, such as glucocorticoid receptor NR3C1 and sterol regulatory element binding transcription factor SREBP-1. Factors shared by CR and GH deficiency included NRF2, PPARα, PPARγ and a number of interferon regulatory factors, consistent with the results observed at the level of functional enrichment.

4.2.4 Mutual Organization of Gene Expression Profiles of Lifespan-extending Interventions

We next performed a meta-analysis of the dataset that included, in addition to the gene expression data we generated, all publicly available microarray data on lifespan-extending interventions in mouse liver. We also included resveratrol and metformin, which are interventions that did not increase lifespan in the ITP mouse cohort at the concentrations used (Miller et al., 2011; Strong et al., 2013, 2016), but are known to share some molecular mechanisms with lifespan-extending CR (Barger et al., 2008; Dhahbi et al., 2005; Martin-Montalvo et al., 2013; Pearson et al., 2008a), increase healthspan of mammals, including improvement of cardiovascular function and physical performance along with inhibition of inflammation (Baur and Sinclair, 2006; Martin-Montalvo et al., 2013; Pearson et al., 2008a), and lead to increased longevity of the nematode *Caenorhabditis elegans* (De Haes et al., 2014; Viswanathan et al., 2005; Wood et al., 2004), short-lived fish *Nothobranchius furzeri* in case of resveratrol (Valenzano et al., 2006), and mice under certain conditions (Baur et al., 2006; Martin-Montalvo et al., 2013; Pearson et al., 2008a). After integration of all available data, our dataset included 17 different interventions and 77 control-intervention comparisons across 22 different sources (Figure 19D). Importantly, our list of analyzed interventions included multiple representatives of each of the different intervention types, i.e. dietary, genetic (mutations, overexpression) and pharmacological.

Aggregation of data was performed using the approach discussed above. Interestingly, comparison of standard deviations of gene expression fold change

distributions in response to different interventions showed that genetic manipulations had the largest effects on gene expression profile (Mann-Whitney test p-value = 0.003 between dietary and genetic intervention groups), whereas pharmacological interventions had the smallest effect (Mann-Whitney test p-value = $1.71 \cdot 10^{-6}$ between pharmacological and dietary intervention groups) and dietary interventions were in the middle (Figure 20A). As control, we examined possible differences between medians of gene fold change distributions, and did not observe significant differences between any pair of intervention groups (Figure 20B). As expected, genetic manipulations caused more significant changes of transcriptome profiles compared to diets and, especially, to drugs. Therefore, it was particularly important to avoid normalization of mean fold change distributions across different datasets, as in that case the described important features of different interventions would be lost.

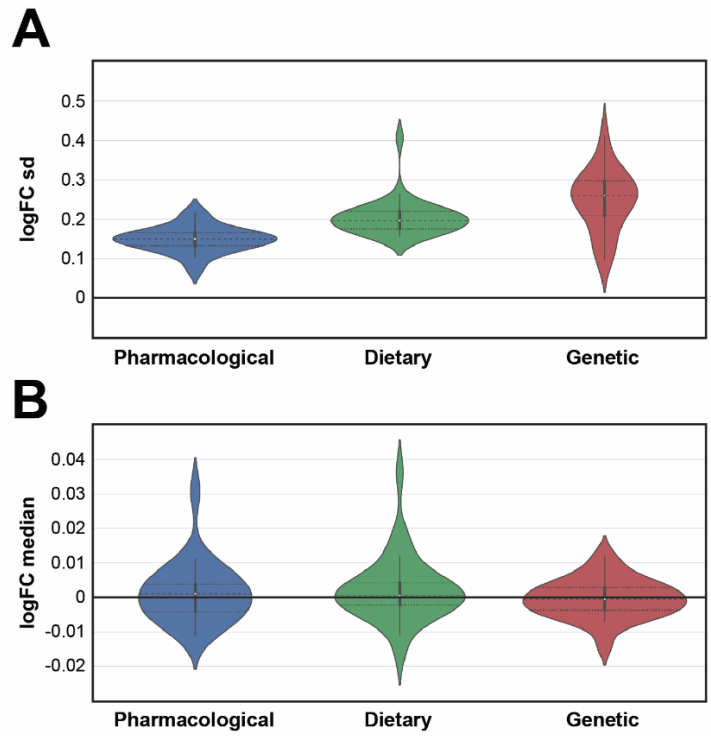

Figure 20. Amplitude of gene expression changes induced by different types of interventions (A) Standard deviations of gene expression changes (log_2FC) across three main types of interventions. All differences are statistically significant (Mann-Whitney test p-value is equal to $1.71 \cdot 10^{-6}$ between pharmacological and dietary and 0.003 between dietary and genetic). **(B) Medians of gene expression changes (log_2FC) across three main types of interventions.** Medians of gene expression changes are distributed similarly across different types of interventions (Mann-Whitney test p-value > 0.05 for all three comparisons)**.**

To examine how similar various interventions are in terms of gene expression signatures identified for CR, GH deficiency and rapamycin, we created a heatmap representing aggregated gene expression data across interventions for the identified genes (Figure 19E). Not surprisingly, interventions associated with GH deficiency formed a tight cluster, indicating convergence of their molecular mechanisms in the liver. In general, we found that interventions resemble changes induced by CR, GH deficiency and rapamycin. Indeed, we observed positive Pearson correlation between aggregated gene expression changes for most interventions (Figure 19F). However, some interventions turned out to

show distinct gene expression patterns. Thus, we observed a small separate cluster formed by rapamycin, Protandim and 17-α-estradiol, in which only the latter intervention showed positive correlation with the interventions representing the main cluster. Furthermore, acarbose and 17-α-estradiol showed positive correlation with both major and minor clusters, pointing to the existence of certain gene expression patterns within each of them, which do not necessarily conflict with each other. To see if different interventions recapitulate the gene expression changes separately induced by CR, rapamycin and GH deficiency, we performed GSEA for every intervention, using genes identified as signatures of the 3 specified interventions as input subsets. Using a BH adjusted permutation test p-value threshold of 0.1, we identified interventions with statistically significant positive association with CR, rapamycin and GH deficiency (Figure 21A). Interestingly, the majority of interventions, including all GH deficiency interventions, all diets (CR, every-other-day feeding (EOD) and MR), acarbose, FGF21 overexpression, 17-α-estradiol and resveratrol, shared the changes induced by CR and GH deficiency, pointing to the commonality of gene expression responses to these interventions. On the other hand, rapamycin again showed a distinct pattern, which was, however, partially shared by some interventions (acarbose, GHRKO, Snell dwarf mice, 17-α-estradiol and Protandim). This approach, however, may include some batch effects resulting from comparison of datasets from the same source and even because of the use of the same, shared, controls (e.g., resveratrol and EOD along with Protandim and 17-α-estradiol obtained from the same data and compared against common controls).

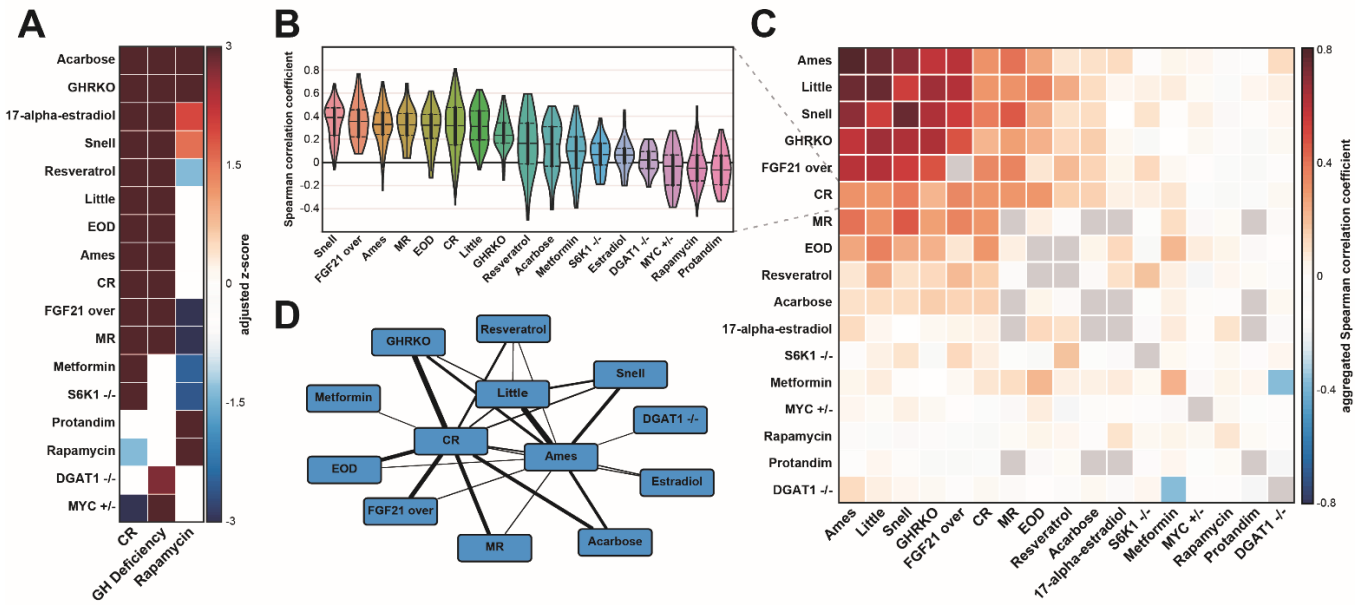

Figure 21. Mutual organization of gene expression profiles of lifespan-extending interventions

(A) GSEA enrichment of interventions by genes regulated by CR, rapamycin and GH deficiency. Each cell represents adjusted z-score calculated based on GSEA against subsets of genes significantly affected by CR, rapamycin and GH-deficient interventions. Only statistically significant associations (BH adjusted p-value < 0.1) are colored. **(B) Spearman correlation coefficient distribution between gene expression profiles of CR and other interventions.** At the level of gene expression, CR showed statistically significant (BH adjusted Mann-Whitney test p-value < 0.1) positive correlation with the majority of interventions, including itself (median Spearman correlation coefficient = 0.32; BH adjusted Mann-Whitney test p-value = $2.9 \cdot 10^{-93}$). For every intervention, violinplot shows distribution of Spearman correlation coefficients between gene expression changes of every dataset of CR and the indicated interventions. Union of 100 genes with the lowest p-value in each pair of examined datasets was used for calculation. **(C) Gene expression profile correlation matrix aggregated for every intervention pair.** The majority of lifespan-extending interventions show significant positive correlation at the level of gene expression changes. For each pair of interventions, the matrix represents median Spearman correlation value across all possible comparisons of datasets representing corresponding interventions from different sources. Union of 100 genes with the lowest p-value in each pair of examined datasets was used for calculation. To make results unbiased, only data from different sources was used for calculation. For this reason, correlation couldn't be estimated for interventions, for which no independent pair of datasets from different sources was available. This missing data is shown by grey boxes. **(D) Network of interventions based on similarity of their gene expression profiles.** Protandim, rapamycin, MYC +/- and S6K1 -/- didn't show statistically significant positive association with any other intervention. The width of edge is defined by BH adjusted Mann-Whitney test p-value of Spearman correlation between interventions (in logarithmic scale). Only statistically significant

(BH adjusted Mann-Whitney test p-value < 0.1) connections are shown. Estradiol: 17-α-estradiol; Snell: Snell dwarf mice; Ames: Ames dwarf mice; CR: Caloric restriction; MR: Methionine Restriction; EOD: Every-other-day feeding; FGF21 over: FGF21 overexpression; Little: Little mice; GHRKO: Growth Hormone Receptor Knockout.

To overcome the batch effect and investigate mutual organization of gene expression profiles of different interventions at the level of whole transcriptomes, we compared interventions pairwise, considering, for every pair of interventions, only pairs of control-intervention comparisons from different sources. For each of them, we calculated the Spearman correlation coefficient using the union of their 100 most statistically significant differentially expressed genes. We then examined the distribution of these correlation coefficients among all pairs of control-intervention comparisons. Using this approach, we could get rid of the batch effect in that datasets from the same study were not compared when calculating the correlation coefficient. We also used the same unbiased procedure to obtain the distribution of correlation coefficients between different datasets of the same intervention. This let us investigate how consistent gene expression response to certain intervention is across different studies and experimental design settings.

CR showed a statistically significant positive correlation with the majority of interventions, including all GH deficiency interventions (BH adjusted Mann-Whitney p-value < $1.5 \cdot 10^{-8}$ for all of them), dietary interventions, such as MR (BH adjusted Mann-Whitney p-value = $1.8 \cdot 10^{-6}$), EOD (BH adjusted Mann-Whitney p-value = $1.9 \cdot 10^{-6}$) and itself (BH adjusted Mann-Whitney p-value = $2.9 \cdot 10^{-93}$), FGF21 overexpression (BH adjusted Mann-Whitney p-value = $2.5 \cdot 10^{-7}$), acarbose (BH adjusted Mann-Whitney p-value = $6.1 \cdot 10^{-6}$), 17-α-estradiol (BH adjusted Mann-Whitney p-value = 0.023), metformin (BH adjusted Mann-Whitney p-value = 0.039) and resveratrol (BH adjusted Mann-Whitney p-

value = $4.8 \cdot 10^{-4}$) (Figure 21B). Interestingly, although rapamycin was thought to be a CR mimetic, it, instead, showed a slight (median Spearman correlation coefficient = -0.049) but significant (BH adjusted Mann-Whitney p-value = $2 \cdot 10^{-3}$) negative correlation with CR when compared at the gene expression level, consistent with the previous findings (Figure 19A, F and Figure 21A). The same analysis applied to rapamycin revealed its significant positive correlation only with itself (median Spearman correlation coefficient = 0.099; BH adjusted Mann-Whitney p-value = $5.9 \cdot 10^{-3}$).

Using the same approach, we obtained a matrix with median Spearman correlation coefficients for every pair of interventions aggregated across all control-intervention comparisons from different sources (Figure 21C). We detected a tight cluster formed by GH deficiency interventions and *Fgf21* overexpression. Dietary interventions, including CR, MR and EOD, showed positive correlation with this cluster and each other. Other interventions showed either week positive correlation with the main cluster (resveratrol, 17-α-estradiol, acarbose, metformin and S6K1 -/-) or quite distinct gene expression patterns with no significant positive correlation with the group of highly correlated interventions defined by CR and GH deficiency (DGAT1 -/-, MYC +/-, Protandim and rapamycin). To clearly visualize similarity between gene expression profiles of different interventions, we built a network where the width of an edge connecting a pair of interventions reflected the level of statistical significance of Spearman correlation between them across datasets (Figure 21D). Here, only the edges with statistically significant positive associations (BH adjusted Mann-Whitney p-value < 0.1) are shown. Consistent with the results discussed above (Figure 21A), most interventions shared similarity with

CR and GH deficiency interventions (such as Ames and Little dwarf mice) at the level of gene expression (Figure 21D). The lack of statistically significant associations between many interventions may be explained by insufficient number of independent datasets. The relatively high value of median Spearman correlation between interventions forming the main cluster (Figure 21C) suggests that increase in the number of datasets will fill many edges missing in the network.

Overall, most lifespan-extending interventions showed similar gene expression patterns both at the level of whole transcriptomes and particular genes. However, some interventions, such as rapamycin, Protandim, S6K1 -/- and MYC +/-, showed quite distinct transcriptional patterns in liver, and did not demonstrate statistically significant positive correlation with any other intervention (Figure 21D). This was especially interesting in the case of rapamycin, which, although thought to be a CR mimetic, showed positive correlation neither with CR nor with GH deficiency interventions, consistent with the results of other groups (Fok et al., 2014; Miller et al., 2014), and even showed statistically significant negative correlation with CR. The data suggest distinct molecular mechanisms at the level of gene expression that mediate the effects of rapamycin and other interventions. However, based on the unbiased comparison of rapamycin datasets, we detected low (although significant) positive correlation of this intervention with itself (median Spearman correlation coefficient = 0.099), which may point to high variability of the response to rapamycin at the level of gene expression and a large effect of experimental design on the response. The higher level of noise observed in the transcriptome response to rapamycin may also be a consequence of the generally lower extent of gene expression

changes in response to drugs compared to diets and genetic manipulations (Figure 20A). Therefore, a more comprehensive study of the rapamycin effect on the transcriptome is needed to validate our findings and better understand cellular mechanisms responsible for this unique pattern.

4.2.5 Common Signatures across Lifespan-extending Interventions

To identify gene signatures commonly up- or downregulated by lifespan-extending interventions, which could serve as an approximation of 'necessary' features and qualitative predictors of lifespan extension, we first identified statistically significant genes regulated by each individual intervention using the same approach as in case of CR, rapamycin and GH deficiency interventions, where datasets from several independent sources were present. Here, we only considered the datasets and interventions with the experimental design (strain, dose and sex), statistically proven to lead to lifespan extension. Using this intervention-wise approach, for every gene we calculated the number of interventions, where it was up- or downregulated (Figure 22A). One gene (*Gsta4*) was statistically significantly upregulated in 9 different interventions (out of 15) and 7 genes (*Gstt3, Abcb1a, Slc22a29, Slc15a4, Ak4, Serpina6 and Cers6*) were upregulated in 8 interventions (BH adjusted p-value < 0.1). These genes are involved in xenobiotic (*Gsta4*, *Gstt3, Abcb1a and Slc22a29*), glucocorticoid (*Serpina6*) and sphingolipid (*Cers6*) metabolism. In addition, 2 genes (*C9* and *C8a*, both are complement components) were identified as significantly downregulated in 9 and 8 interventions, respectively. However, this approach has several disadvantages. First, it does not account for the difference in the number of datasets associated with every intervention along with the difference in quality

of individual datasets (e.g., number of samples). Second, it does not consider possible similarity of different interventions at the level of global gene expression (as in case of GH deficiency interventions which showed very similar effects on the hepatic transcriptome). Therefore, this method leads to overfitting of common signatures by genes differentially expressed in response to GH deficiency.

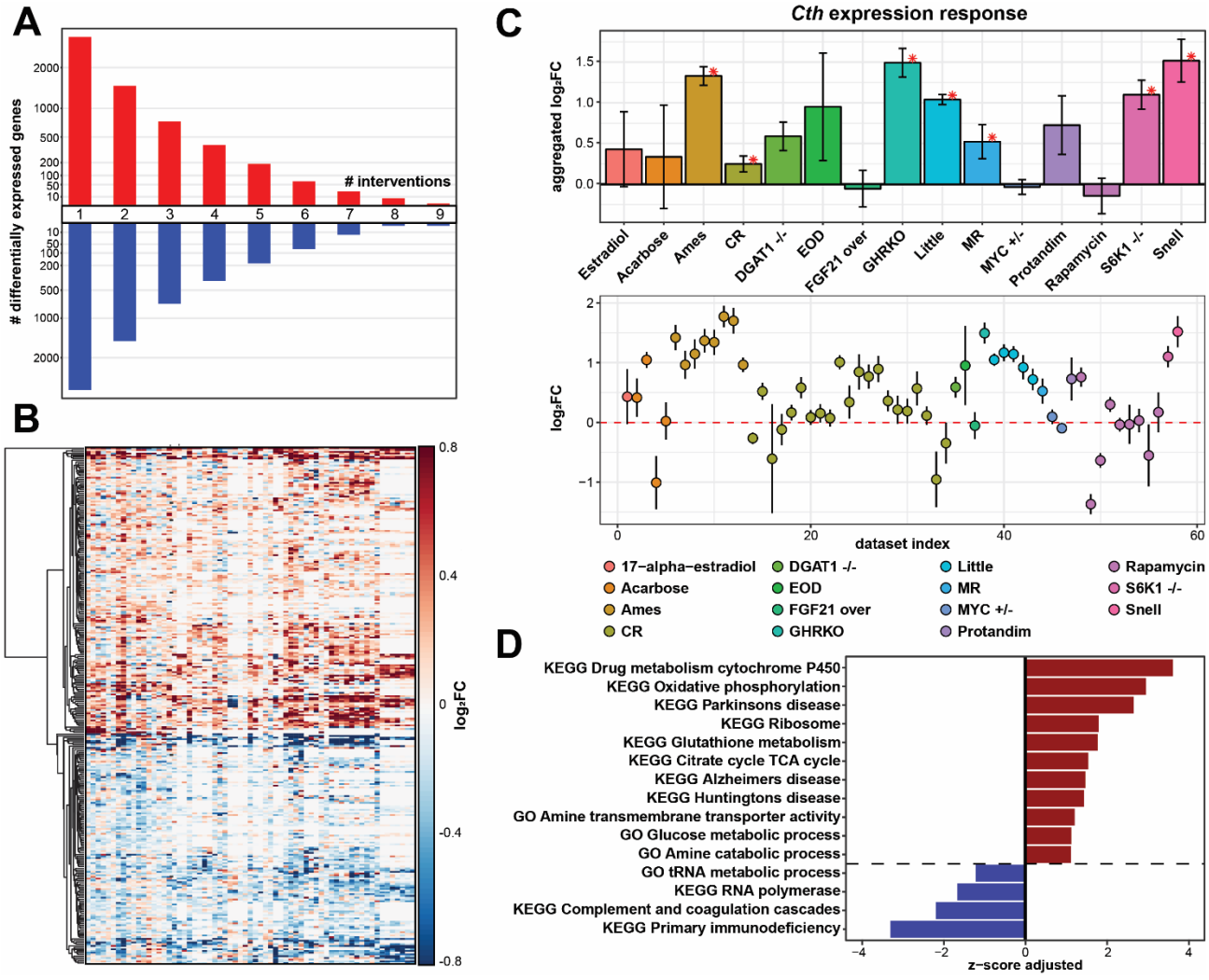

Figure 22. Common signatures of lifespan-extending interventions

(A) Number of genes identified as statistically significantly up- (red) and downregulated (blue) in response to different lifespan-extending interventions. Genes effected by the largest number of individual interventions encode cytochrome P450s and glutathione metabolism

proteins. FDR threshold of 0.1 was used to select significant genes within each intervention. **(B) Fold change of genes commonly regulated in response to lifespan-extending interventions.** 166 upregulated and 134 downregulated genes were identified as common signatures of lifespan-extending interventions. Genes significantly regulated across interventions (BH adjusted robust p-value < 0.01) were included in the heatmap. Individual control-intervention datasets are shown on the x axis. **(C) *Cth* fold change across different lifespan-extending interventions (upper panel) and across individual datasets used in the analysis (lower panel).** Cystathionine gamma-lyase (*Cth*) gene is significantly upregulated across different lifespan-extending interventions (BH adjusted robust p-value = 0.0033) and within 7 individual interventions. On the upper barplot, red asterisk denotes interventions with the BH adjusted p-value < 0.05. On the lower plot, dots representing gene fold change within each individual dataset are colored based on the intervention type. Estradiol: 17-α-estradiol; Snell: Snell dwarf mice; Ames: Ames dwarf mice; Little: Little mice; CR: Caloric restriction; MR: Methionine Restriction; EOD: Every-other-day feeding; FGF21 over: FGF21 overexpression; GHRKO: Growth Hormone Receptor Knockout. **(D) GSEA functional enrichment of up- (red) and downregulated (blue) genes associated with common changes across lifespan-extending interventions.** Statistically significantly enriched functions (FDR q-value < 0.1) are shown. Adjusted z-score, calculated as $\log_{10}$(FDR q-value) corrected by sign of regulation, is presented on x-axis. Presented functions were selected manually.

To overcome this problem, we searched for genes shared by different interventions using a single mixed-effect model with an additional random term corresponding to intervention type and correlation matrix for this term composed from means of correlation coefficients of gene expression changes between the corresponding interventions across all possible pairs of datasets (Figure 21C). This approach addresses the shortcomings of the previous method by increasing the weight of well-represented interventions and decreasing the weight of similar interventions (e.g., GH deficient mutants). Therefore, gene expression changes induced only by GH deficiency will have a higher probability of being realized by null hypothesis and, as a consequence, higher p-values. Using this method, we detected only 7 up- and 5 downregulated genes shared by all interventions with BH adjusted p-value < 0.05. In other words, although there may be shared molecular mechanisms among different interventions, they are usually supported by different gene expression changes.

To detect genes commonly shared by most interventions, we weakened the criteria by letting one intervention to be an outlier. We realized it by removing each intervention one by one and taking the best remaining p-value ("robust p-value" approach). Using the BH adjusted robust p-value threshold of 0.05, we identified 166 upregulated and 134 downregulated genes (Figure 22B). Interestingly, one of the most significant commonly upregulated genes was *Cth* (BH adjusted robust p-value = 0.0033) (Figure 22C). It encodes cystathionine gamma-lyase, which participates in the conversion of cystathionine (derived from methionine) to cysteine, which is an important step in glutathione synthesis and H_2S production (Kabil et al., 2011). *Cth* has previously been shown to be upregulated in response to DR-mediated stress and sulfur amino acid restriction (Hine et al., 2015). Our data suggest that, at least at the transcript level, this gene is increased in liver by most lifespan-extending interventions and could be used as a simple test for the shift in gene expression associated with longevity.

Another interesting example of a gene commonly upregulated across lifespan-extending interventions is *Brca1* (BH adjusted p-value = 0.04). This well-known tumor suppressor, whose loss-of-functions mutations are associated with breast and ovary cancer in humans with frequency of 80% and 40%, respectively (Narod and Foulkes, 2004), has also been found in several studies to be related to longevity in mice. In particular, its haploinsufficiency (*Brca1* +/-) led to shortened lifespan (by 8% in mean lifespan) with 70% tumor incidence vs about 10% in wild-type animals (Cao et al., 2003). Interestingly, besides being related to DNA repair, BRCA1 was also shown to physically interact with NRF2 and increase its stability and activation (Gorrini et al., 2013). Consequently, it may

act by activating the NRF2-dependent antioxidant response. Thus, the common upregulation of *Brca1* may be due to activation of NRF2 signaling, which is one of the shared signatures of lifespan-extending interventions (Figure 19C and Figure 22D).

Several glutathione S-transferase genes were also significantly upregulated across lifespan-extending interventions, including *Gstt2* (BH adjusted robust p-value = 0.014), *Gsto1* (BH adjusted robust p-value = 0.037) and *Gsta4* (BH adjusted robust p-value = 0.013). All of them are involved in glutathione metabolism, known to be activated at the gene expression level in response to CR (Fu and Klaassen, 2014) and several GH deficiency states (Sun et al., 2013; Tsuchiya et al., 2004). Administration of GH was shown to decrease GST activity in several tissues including liver (Brown-Borg et al., 2005). Overall, upregulation of *Gst* genes is a common signature of lifespan-extending interventions and they are significantly changed not only by GH deficiency and CR, but also by FGF21 overexpression, acarbose, MR, MYC deficiency and others.

To identify pathways associated with common up- and downregulated gene signatures, we performed functional GSEA (Figure 22D). Consistent with the RNAseq findings, most significant upregulated functions included metabolism of xenobiotics by cytochrome P450 (q-value = 0.0055) and glutathione metabolism (q-value = 0.017) mainly regulated by the NRF2 pathway, oxidative phosphorylation (q-value = 0.001), ribosome (q-value = 0.016), TCA cycle (q-value = 0.028), glucose (q-value = 0.074) and amino acid metabolism (q-value = 0.075). Downregulated functions included primary immunodeficiency (q-value = $4.8 \cdot 10^{-4}$), RNA polymerase (q-value = 0.022) and tRNA metabolic process (q-value = 0.061). Interestingly, several age-related diseases associated

at the molecular level with age-dependent changes in regulation of many cellular pathways, including mitochondrial function, oxidative phosphorylation, apoptosis and proteolysis, such as Alzheimer's (q-value = 0.034), Parkinson's (q-value = $2.2 \cdot 10^{-3}$) and Huntington's (q-value = 0.036) diseases, were enriched for common signatures, pointing to direct connection between changes induced by aging and lifespan-extending interventions.

4.2.6 Signatures Associated with the Degree of Lifespan Extension

To identify genes positively and negatively associated with the degree of lifespan extension, serving as quantitative predictors of this effect, we applied a previously described mixed-effect regression model with the response value equal to one of 3 commonly used metrics of lifespan extension: median lifespan ratio, maximum lifespan ratio, calculated as the ratio of average lifespan of 10% longest-surviving individuals, and the median hazard ratio, calculated as the ratio of slopes of survival curves at the timepoint where 50% of cohort is alive. We used these metrics as they seem to be the most consistent and robust to the effects of sampling size (Moorad et al., 2012). As in the case of common signatures, we considered source and type of intervention as random terms and used the correlation matrix of interventions to account for similarity between them. Using thresholds of BH adjusted p-value and LOO p-value, obtained after removal of every intervention one by one, equal to 0.05, we detected 351, 258 and 183 genes with positive and 264, 191 and 108 genes with negative association with maximum lifespan ratio, median lifespan ratio and median hazard ratio, respectively (Figure 23A and Figure 24D). These gene sets showed a significant overlap (Fisher exact test p-value < 10^{-18} in all cases), which was especially large between median and maximum lifespan. Indeed, 65.1% and 47.9% of

genes with positive and 52.9% and 38.3% with negative association with median and maximum lifespan, respectively, were shared between them. As the median hazard ratio is more volatile compared to other metrics, median and maximum lifespan provide more reliable sets of genes. One of the strongest positive associations with maximum and median lifespan was found for *Hint3* (BH adjusted p-value = $3.2 \cdot 10^{-7}$ and $2.5 \cdot 10^{-4}$, respectively) encoding nucleotide hydrolase (Figure 23C). On the other hand, *Irf2* encoding interferon regulatory transcription factor showed a significant negative association with these metrics (BH adjusted p-value = $2.57 \cdot 10^{-6}$ and $1.2 \cdot 10^{-5}$, respectively) (Figure 23D).

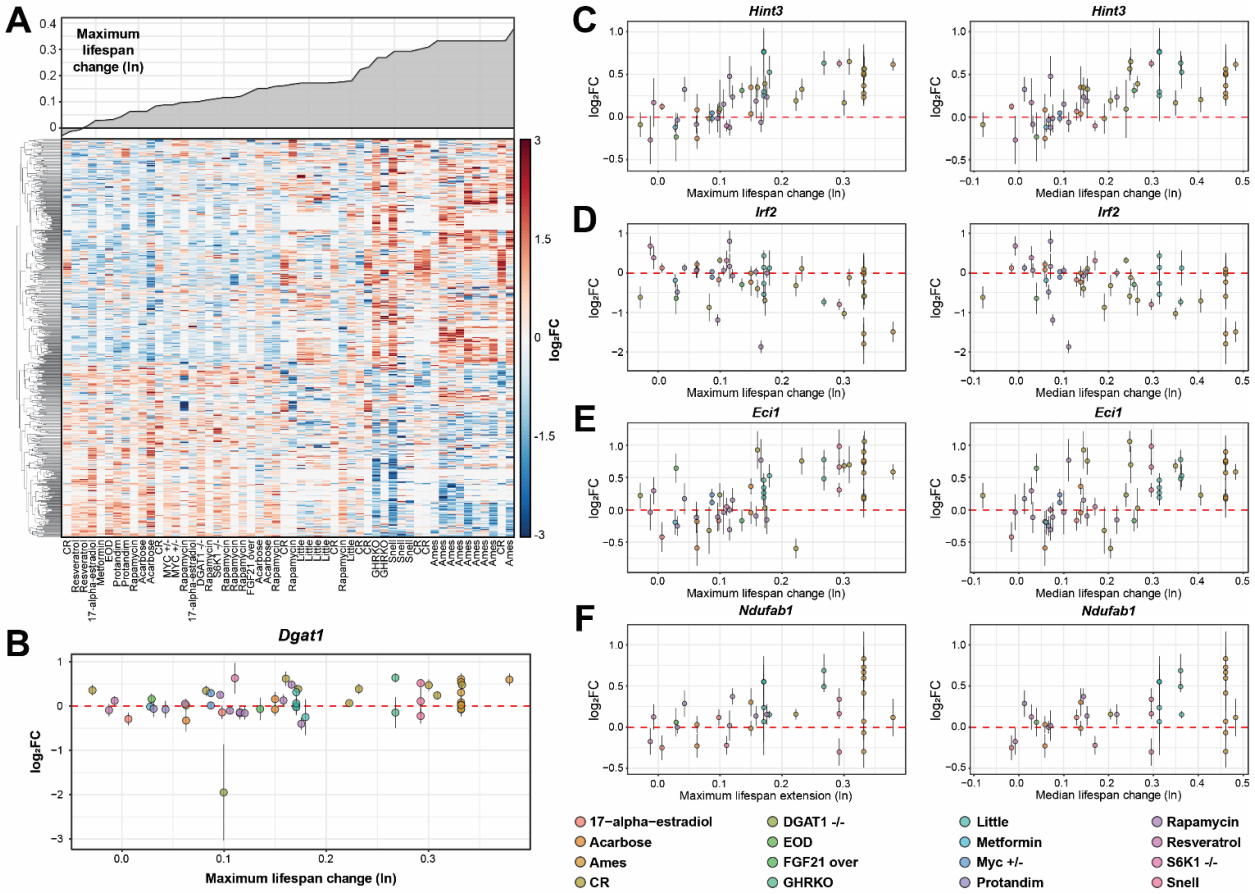

Figure 23. Gene expression signatures associated with the degree of lifespan extension
(A) Fold change of genes associated with the maximum lifespan effect across different datasets. Genes identified as significantly associated with maximum lifespan effect (BH adjusted

p-value < 0.05 and p-value LOO < 0.05), calculated as ln(maximum lifespan ratio), are shown in the heatmap. 351 and 264 genes were found to have positive and negative association with maximum lifespan effect, respectively. Plot on the top shows maximum lifespan effect for corresponding dataset. **(B) Association of *Dgat1* fold change with maximum lifespan.** Although *Dgat1* deletion is associated with lifespan extension in female mice, its fold change shows a slight positive association with the maximum lifespan ratio (slope coefficient = 0.38 and BH adjusted p-value = 0.007). **(C-F) Association of *Hint1* (C), *Irf2* (D), *Eci1* (E) and *Ndufab1* (F) fold change with maximum (left) and median (right) lifespan ratio.** All specified genes show statistically significant associations with both maximum and median lifespan. CR: Caloric Restriction; FGF21 over: FGF21 overexpression; EOD: Every-Other-Day Feeding; Snell: Snell dwarf mice; Ames: Ames dwarf mice; Little: Little mice; GHRKO: Growth Hormone Receptor Knockout.

Interestingly, the fat synthesis enzyme *Dgat1*, those knockout is associated with extension of average and maximum lifespan in female mice by 23% and 8%, respectively (Streeper et al., 2012), was found to be slightly positively associated with median and maximum lifespan effects across interventions (slope coefficient = 0.38 and 0.29 and BH adjusted p-value = 0.007 and 0.04 for maximum and median lifespan, respectively) (Figure 23B). However, the change in expression of *Dgat1* is relatively small compared to all lifespan-extending interventions, except for *Dgat1* deletion. This example demonstrates that different initial targets of lifespan-extending interventions can be unique and not shared across them, but may lead to similar downstream systemic responses, which define the lifespan extension effect.

Other genes positively associated with changes in both maximum and median lifespan included members of fatty acid metabolism, including acyl-coenzyme A dehydrogenase *Acadm* (BH adjusted p-value = 0.001 and 0.005 for maximum and median lifespan, respectively) and enoyl-coenzyme A delta isomerase *Eci1* (BH adjusted p-value = $2.2 \cdot 10^{-6}$ and $6.4 \cdot 10^{-6}$) (Figure 23E), and oxidative phosphorylation pathway, including the

b subunit of ATP synthase *Atp5f1* (BH adjusted p-value = $5.3 \cdot 10^{-4}$ and 0.004), cytochrome c oxidase assembly protein *Cox17* (BH adjusted p-value = $5 \cdot 10^{-4}$ and 0.01) along with dehydrogenase 1 subcomplexes *Ndufb3* (BH adjusted p-value = $2.6 \cdot 10^{-5}$ and 0.048) and *Ndufab1* (BH adjusted p-value = 0.005 and 0.003) (Figure 23F).

To identify pathways enriched by genes positively and negatively associated with the lifespan extension effect, we ran GSEA for all 3 metrics of lifespan extension and observed general consistency among them in terms of functional enrichment (Figure 24C). Thus, genes related to TCA cycle (q-value < 10^{-3} for all metrics), oxidative phosphorylation (q-value < 0.015 for all metrics), amino acid catabolism (q-value < 0.02 for all metrics) and Huntington's (q-value < 0.093 for all metrics) and Parkinson's diseases (q-value < 0.004 for all metrics) were significantly positively associated among all three metrics used in the analysis, whereas fatty acid (q-value < 0.003) and propanoate metabolism (q-value < 0.081) genes showed significant positive association with maximum and median lifespan changes. On the other hand, regulation of interleukin 1 beta production showed significant negative associations with specified metrics (q-value < 0.096 for median lifespan and median hazard ratio) (Figure 24C). However, some functions, such as peroxisome (q-value = 0.03 for maximum lifespan) and DNA replication (q-value = 0.026 for median hazard ratio), were specific to single lifespan extension metrics. This may explain how certain interventions increase specific lifespan characteristics without affecting others.

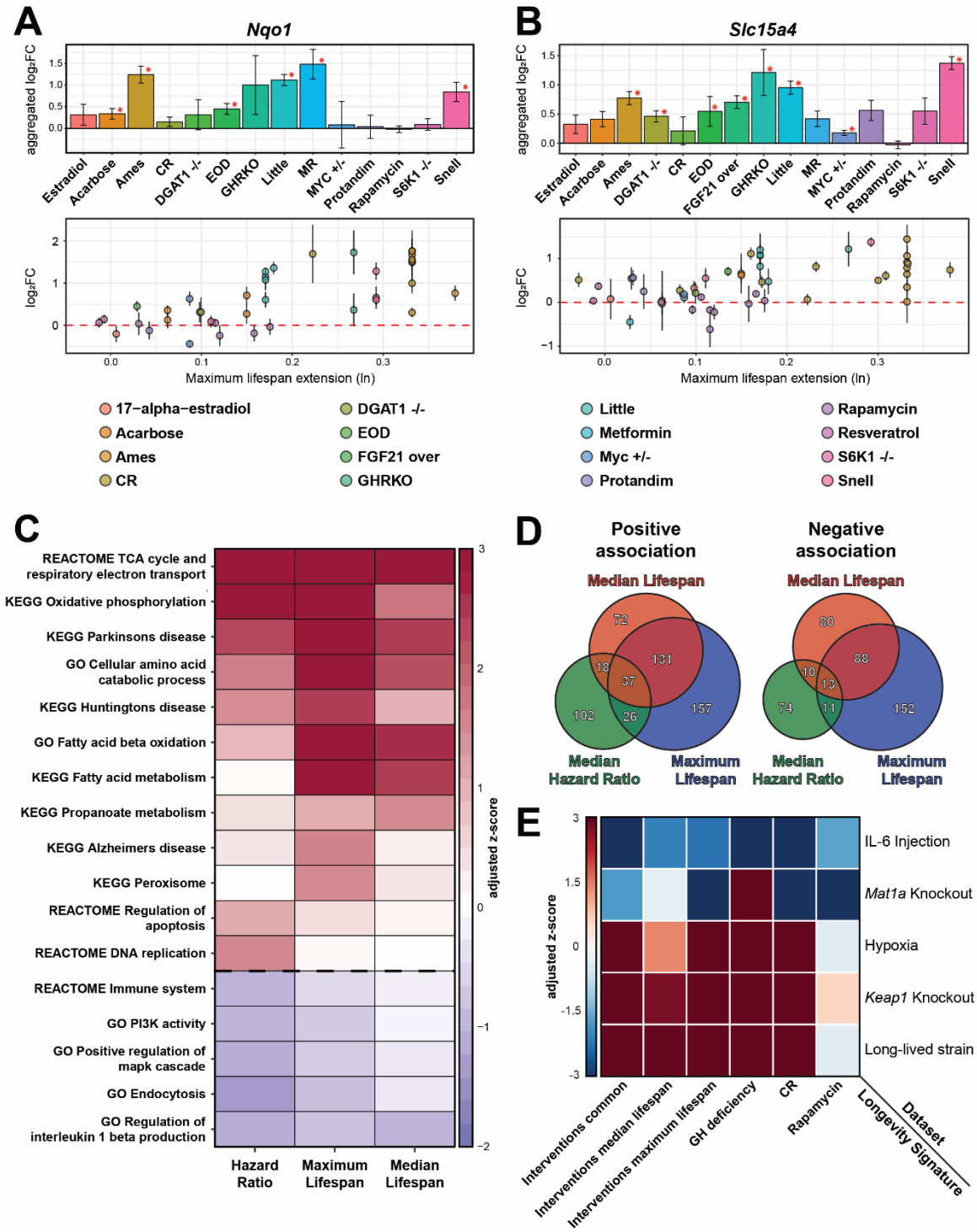

Figure 24. Analysis of signatures associated with lifespan extension effect and identification of new lifespan-extending interventions

(A-B) Fold change of *Nqo1* (A) and *Slc15a4* (B) across different interventions and their association with the maximum lifespan extension effect. *Nqo1* (coding for NADH

dehydrogenase 1) and *Slc15a*4 (coding for lysosomal amino acid transporter) are examples of genes both significantly shared by lifespan-extending interventions (BH adjusted robust p-value = 0.011 and 0.008, respectively) and positively associated with the lifespan extension effect (BH adjusted p-value = 0.002 and 0.02, respectively). Red asterisk denotes interventions with BH adjusted p-value < 0.1. Estradiol: 17-α-estradiol; Snell: Snell dwarf mice; Ames: Ames dwarf mice; Little: Little mice; CR: Caloric restriction; MR: Methionine Restriction; EOD: Every-other-day feeding; FGF21 over: FGF21 overexpression; GHRKO: Growth Hormone Receptor Knockout. **(C) GSEA functional enrichment of genes positively (upper) and negatively (lower) associated with the lifespan extension effect.** Functions statistically significantly associated with at least one lifespan extension metric (FDR q-value < 0.1) are shown. Cells are colored based on adjusted z-score, calculated as $\log_{10}$(FDR q-value) corrected by sign of regulation. Presented functions were selected manually. **(D) Number of genes showing positive (left) and negative (right) association with different metrics of the lifespan extension effect.** Generally, different metrics show significant overlap in genes significantly associated with them (Fisher exact test p-value < 10^{-18} in all cases). Genes were considered significantly associated if BH adjusted p-value < 0.05 and p-value LOO < 0.05. **(E) Association of individual interventions from publicly available datasets with the identified longevity signatures.** Longevity signatures include genes aggregated across individual interventions (CR, rapamycin and GH deficiency interventions), common signatures and signatures associated with the lifespan extension effect (maximum and median lifespan change). Cells are colored based on adjusted z-score, calculated as $\log_{10}$(BH adjusted p-value) corrected by sign of regulation.

Interestingly, some of the genes or pathways could serve as both qualitative and quantitative predictors of lifespan extension, being both common signatures and signatures associated with the lifespan extension effect or enriched by these signatures. We identified 26 genes being both commonly changed across interventions and associated with either median or maximum lifespan extension effect in the same direction (Table 2). 17 of them were upregulated and positively associated with lifespan extension, while 9 were downregulated and negatively associated. The identified genes are involved in regulation of apoptosis (*Aatk*, *Net1*, *Rb1*, *Sgms1*), immune response (*C4bp*, *P2ry14*, *Slc15a4*, *Tap2*, *Rb1*), transcription (*Pir*, *Sall1*), stress response (*Net1*, *Nqo1*, *Pck2*, *Rb1*), glucose metabolism (*Pck2*, *Pgm1*) and cellular transport (*Ldlrad3*, *Slc15a4*, *Slc25a30* and *Tap2*).

Table 2. Genes being both common signatures and signatures associated with the degree of lifespan extension effect

Gene	Description	Sign of association	Function
Aatk	apoptosis-associated tyrosine kinase	Negative	Apoptosis; Growth arrest
Agpat9	1-acylglycerol-3-phosphate O-acyltransferase 9	Positive	Triglyceride biosynthesis
C4bp	complement component 4 binding protein	Negative	Complement cascades; Innate immune response
Cpn2	carboxypeptidase N, polypeptide 2	Negative	-
Dbt	dihydrolipoamide branched chain transacylase E2	Positive	Amino acid breakdown (isoleucine, leucine, valine)
Fam167b	family with sequence similarity 167, member B	Positive	-
Gorasp1	golgi reassembly stacking protein 1	Negative	Golgi apparatus organization
Hps4	Hermansky-Pudlak syndrome 4	Negative	Lysosome organization
Ldlrad3	low density lipoprotein receptor class A domain containing 3	Positive	Receptor-mediated endocytosis
Megf9	multiple EGF-like-domains 9	Positive	-
Net1	neuroepithelial cell transforming gene 1	Positive	Stress response; DNA repair; Regulation of apoptosis
Nqo1	NAD(P)H dehydrogenase, quinone 1	Positive	Oxidative stress response; Oxidative phosphorylation
P2ry14	purinergic receptor P2Y, G-protein coupled, 14	Positive	G-protein coupled receptor for UDP-glucose; Immune response
Pck2	phosphoenolpyruvate carboxykinase 2 (mitochondrial)	Positive	Gluconeogenesis; Stress response
Pgm1	phosphoglucomutase 1	Positive	Glucose metabolism
Pir	pirin	Positive	Regulation of transcription and replication
Postn	periostin, osteoblast specific factor	Positive	Cell adhesion; Regeneration
Psmd9	proteasome (prosome, macropain) 26S subunit, non-ATPase, 9	Positive	Proteolysis
Rb1	retinoblastoma 1	Negative	Stress response; Negative regulation of cell cycle and apoptosis; tumor supression; macrophage differentiation
Rdh9	retinol dehydrogenase 9	Positive	Retinol metabolism
Sall1	sal-like 1 (Drosophila)	Positive	Histone deacetylase (HDAC); Regulation of transcription
Sgms1	sphingomyelin synthase 1	Positive	Sphingolipid biosynthesis; Regulation of apoptosis
Slc15a4	solute carrier family 15, member 4	Positive	Amino acid transport (histidine and oligopeptides); Innate immune response; Regulation of endolysosomal pH
Slc25a30	solute carrier family 25, member 30	Negative	Mitochondrial transport
Tap2	transporter 2, ATP-binding cassette, sub-family B (MDR/TAP)	Negative	Adaptive immune response; Antigen presentation; Protein transport
Vwa5a	von Willebrand factor A domain containing 5A	Negative	Tumor suppression (putative)

Abbreviations: HDAC: Histone deacetylase; UDP: Uridine diphosphate; EGF: Epidermal growth factor

For example, *Nqo1*, encoding NAD(P)H-dependent quinone oxidoreductase involved in oxidative stress response, showed a significant positive association with maximum and median lifespan (BH adjusted p-value = 0.002 and $7.74 \cdot 10^{-5}$, respectively) and was also commonly upregulated across lifespan-extending interventions (BH adjusted robust p-value = 0.011) (Figure 24A). Interestingly, this gene is one of the well-known targets of the transcription factor NRF2, an upstream regulator of gene expression response to various lifespan-extending interventions (Leiser and Miller, 2010; Mutter et al., 2015) (Figure 19C).

Another interesting example is *Slc15a4*, which codes for lysosome-based proton-coupled amino-acid transporter of histidine and oligopeptides from lysosome to cytosol. In

dendritic cells, this protein regulates the immune response by transporting bacterial muramyl dipeptide (MDP) to cytosol and, therefore, activating the NOD2-dependent innate immune response (Nakamura et al., 2014). In addition, its activity affects endolysosomal pH regulation and probably v-ATPase integrity, required for mTOR activation (Kobayashi et al., 2014). Our data shows that *Slc15a4* is a common signature of lifespan-extending interventions (BH adjusted robust p-value = 0.008) along with some other transporters (Figure 22D) and is positively associated with maximum lifespan (BH adjusted p-value = 0.02) (Figure 24B), pointing to importance of lysosomal integrity and amino acid transport in lifespan extension.

As for the pathways, oxidative phosphorylation showed positive association with both common and lifespan effect associated signatures, and some functions involved in liver regulation of immune response showed negative association (Figure 22D and Figure 24C). The role of oxidative phosphorylation in lifespan extension may explain the effect of some direct regulators of the electron transport chain, such as methylene blue, leading to 6% increase in female maximum lifespan in mice (Harrison et al., 2014). Indeed, serving as an alternative electron carrier in the electron transport chain in mitochondria, the compound increases its activity together with cellular oxygen consumption (Wen et al., 2011). This is a nice example of an intervention with a distinct molecular mechanism, whose effect, however, converges at the level of regulated cellular pathways.

4.2.7 Application of Longevity Signatures for the Identification of New Candidates for Lifespan Extension

In this work, we obtained gene expression patterns (signatures) associated with the response to particular well-studied interventions (CR, rapamycin and GH deficiency interventions), as well as signatures based on gene sets commonly regulated across different lifespan-extending interventions and associated with the lifespan extension effect. We considered the possibility that these 'longevity signatures' could be used as predictors of new lifespan-extending interventions at the gene expression level. To test this possibility, we examined 4 publicly available datasets containing data on hepatic gene expression in response to certain *in vivo* interventions and ran a GSEA-based association test using longevity signatures as input subsets (Figure 24E). These datasets included injection of interleukin 6 (IL-6) (GSE21060) (Ramadoss et al., 2010), knockout of methionine adenosyltransferase gene (Mat1a) (GSE77082) (Alonso et al., 2017), hypoxia conditions (GSE15891) (Baze et al., 2010b) and knockout of *Keap1*, coding for an inhibitor of acute stress regulator NRF2 (GSE11287) (Osburn et al., 2008).

Interleukin-6 (IL-6) is one of the best studied pro-inflammatory cytokines secreted by T cells and macrophages to support the immune response. It was shown to stimulate the inflammatory and auto-immune response during progression of diseases, including diabetes (Kristiansen and Mandrup-Poulsen, 2005), Alzheimer's disease (Swardfager et al., 2010), multiple myeloma (Gadó et al., 2000) and others. Moreover, IL-6 was shown to induce insulin resistance directly by inhibiting insulin receptor signal transduction (Senn et al., 2002). Finally, functions related to liver regulation of the immune response

stimulated by IL-6 were enriched for genes both commonly downregulated and negatively associated with the lifespan extension effect of longevity interventions. We tested if the intraperitoneal injection of interleukin-6 into mouse bloodstream leads to hepatic gene expression changes associated with longevity signatures and detected a significant negative association with all longevity signatures (BH adjusted p-value < 0.025) (Figure 24E), pointing to a potential negative effect of IL-6 on mouse lifespan.

Methionine adenosyltransferase 1A (Mat1a) is an enzyme that catalyzes conversion of methionine to S-adenosylmethionine. This gene plays a crucial role in methionine and glutathione metabolism. Its activity in liver is increased 205% in Ames dwarf mice compared to wild-type animals (Uthus and Brown-Borg, 2003), and the introduction of GH to these mice led to ~40% decrease in MAT activity in liver (Brown-Borg et al., 2005). Moreover, due to the role of MAT in methionine metabolism, MAT deficiency in liver leads to persistent hypermethioninemia (Ubagai et al., 1995), which can be thought of as the opposite of MR. Therefore, we expected that knockout of *Mat1a* could be negatively associated with longevity signatures. Indeed, the test for longevity association revealed a negative association of this intervention with 4 out of 6 longevity signatures, the exceptions being GH deficiency and median lifespan effect signatures (BH adjusted p-value < 0.02) (Figure 24E). Therefore, *Mat1a* knockout leads to the changes in gene expression opposite to those caused by longevity signatures, and is expected to diminish mouse longevity.

Hypoxia, a reduction in oxygen levels, has suggestive associations with longevity that are not yet well understood. First, aging is associated with hypoxia, e.g. showing 38% reduction in oxygen levels in adipose tissue (Zhang et al., 2011). Second, studies

investigating the effect of hypoxia on longevity show contrasting results. Thus, one group showed that, in *C. elegans*, growth in low oxygen and mutation of VHL-1, a negative regulator of the main modulator of hypoxia HIF-1, extended worm lifespan up to 40% (Mehta et al., 2009). However, another group reported an increased lifespan in *C. elegans* following the deletion of HIF-1 gene under slightly different conditions (Chen et al., 2009). Also, by generating reactive oxygen species (ROS), hypoxia leads to activation of NRF2, one of the upstream regulators associated with the response to lifespan-extending interventions (Figure 19C). Finally, hypoxia was found to be among the most effective protectors against mitochondrial disfunction associated with virtually all age-related degenerative diseases (Balaban et al., 2005; Jain et al., 2016). In mammals, chronic hypoxia leads not only to a compensatory increase in oxygen delivery due to increased production and affinity to hemoglobin, decreased weight, higher ventilation rate and capillary density and larger mass of lung, liver and left ventricle (Aaron and Powell, 1993; Baze et al., 2010b), but also to a decrease in demand for oxygen through alterations in metabolism, including increased rate of anaerobic metabolism (glycolysis) along with decreased whole animal metabolic rate and body temperature (Gautier, 1996; Steiner and Branco, 2002). Therefore, we were particularly interested to investigate whether chronic hypoxia would affect hepatic gene expression in mice in ways that were correlated to lifespan gene expression signatures. We examined changes in gene expression in mice subjected to 11.5 kPa Po_2 hypoxia (11.8% oxygen in the air) for 32 days, and detected a significant positive association of hypoxia with all longevity signatures, except for rapamycin (BH adjusted p-

value < 0.034) (Figure 24E), suggesting a potential positive effect of this intervention on mouse healthspan and/or lifespan.

NRF2 is one of the key acute stress regulators, which, among others, activates XMEs (Baird and Dinkova-Kostova, 2011) commonly upregulated at the level of gene expression across different lifespan-extending interventions (Figure 22D). Overexpression of the NRF2 ortholog SKN-1 in *C. elegans* leads to a 5-20% increase in average lifespan (Tullet et al., 2008), whereas mutation of its inhibitor, *Keap1*, was shown to increase median lifespan by 8-10% in *Drosophila melanogaster* males (Sykiotis and Bohmann, 2008). Moreover, Protandim, a mixture of 5 botanical extracts known to stimulate *Nrf2* activation, was proved to increase median lifespan in male mice by 7% (Strong et al., 2016). However, whether *Nrf2* directly affects longevity of mammals remain unclear. We examined how hepatic gene expression is changed by hepatocyte-specific conditional knockout of *Keap1* in mice and identified statistically significant positive association with almost all longevity signatures, except for rapamycin (BH adjusted p-value < 0.0015) (Figure 24E). This finding points to a potential positive effect of NRF2 activation on mouse healthspan and lifespan.

Finally, we tested if longevity signatures could be used to predict the difference in lifespan between different mouse strains, known to have such a difference. The GSE10421 dataset includes gene expression of for livers of male mice of 2 mouse strains tested at the same chronological age (7 weeks old): C57BL/6 and DBA/2 (Kautz et al., 2008). We ran a statistical model testing for genes with significant difference between these strains and subjected them to the longevity association test. All longevity signatures except for

rapamycin showed a significant positive association with C57BL/6 gene expression profile compared to that of DBA/2 (BH adjusted p-value < $5.3 \cdot 10^{-4}$) (Figure 24E). Lifespan of C57BL/6 mice (median lifespan = 901 days) is significantly higher than that of DBA/2 (median lifespan = 701 days) (Yuan et al., 2009). This difference was captured by the longevity signatures, which predicted the strain with greater lifespan. These findings further support the notion that the longevity signatures can be used for the prediction of new lifespan-extending interventions as well as for the assessment of differences in expected lifespan.

To conclude, we collected and characterized RNAseq data on several lifespan-extending interventions, including four that had never been analyzed at the level of gene expression, across sexes, doses and age groups. We observed a significant feminizing pattern of gene expression changes in males in response to genetic (GHRKO and Snell swarf mice) and dietary (CR and MR) interventions along with acarbose in 12-month-old males. We identified functional gene groups responsible for this feminizing effect, most notably drug metabolism by cytochrome P450 and complement and coagulation cascades. However, the feminizing effect is neither necessary nor sufficient for lifespan extension, as other interventions showed no such effect in males or even demonstrated a significant masculinizing effect (e.g., rapamycin in 12-month-old males). However, we also observed consistent tendency of lifespan-extending interventions to induce more masculinizing changes in females compared to males, therefore, leading to convergence of gene expression profile across sexes.

Expanding this analysis to encompass all available microarray data on longevity interventions allowed us to define gene expression signatures associated with individual interventions or groups of related interventions (rapamycin, CR and GH deficiency) as well as functions commonly changed across different lifespan-extending interventions. We observed that, despite some differences, most lifespan-extending interventions share altered genes and pathways, including upregulation of genes encoding XMEs regulated by NRF2 along with TCA cycle, oxidative phosphorylation, glucose and amino acid metabolism, and ribosome protein genes, and downregulation of complement and coagulation cascades. Interestingly, some genes, involved in stress response, apoptosis, glucose metabolism, transcription and immune response, and pathways, such as oxidative phosphorylation and hepatic regulation of the immune response, were found to be commonly regulated by interventions and associated with lifespan extension effect, serving as both qualitative and quantitative predictors of the lifespan extension effect. These genes and processes seem to be the most reliable and consistent determinants of longevity in mouse and deserve further exploration. By comparing the response to different interventions at the level of gene expression, we observed that the majority of interventions showed significant positive correlations with each other, although others, including rapamycin, showed a distinct pattern.

Finally, we employed gene expression signatures to identify new lifespan-extending interventions based on gene expression data. Here, our algorithm could distinguish two strains of mice differing in lifespan. It was also applied to several interventions considered to be positively or negatively associated with changes in lifespan,

suggesting that they indeed may influence lifespan. Thus, we propose hypoxia and hepatocytes-specific *Keap1* knockout to be significantly associated with longevity signatures at the level of gene expression and, therefore, to be strong candidates for experimental validation. Based on our findings, we believe that the described approach may be used to identify promising candidates with the potential lifespan extension effect among environmental, genetic and pharmacological interventions. Thus, it may facilitate a search for new interventions and help screen candidate genes and drugs prior to costly lifespan analyses.

Chapter 5. Conclusion

In this work we expanded our understanding of mechanisms behind lifespan extension on both across- and within-species level. Using high-throughput approach and different models of lifespan extension, we identified molecular signatures associated with longevity and validated them through experiments and proper predictions.

By performing RNAseq analysis of response of naked mole rat fibroblasts to DNA damage, induced by γ-irradiation, we identified common and unique gene expression signatures of this long-lived rodent compared to mice. We observed common upregulation of senescence-associated secretory phenotype (SASP) genes together with downregulation of cell cycle. On the other hand, apoptosis and p53 pathways were upregulated in mice significantly stronger than in NMR. We validated these findings experimentally by showing that both species undergo cell arrest but NMR fibroblasts are highly resistant to IR-induced apoptosis and favor cellular senescence over apoptosis, contrary to the mouse. We also showed that NMR cells were significantly more resistant to γ-irradiation than mice despite the comparable level of DNA damage. Unique transcriptional changes in NMR indicate that this effect may be linked to certain cytoprotective mechanisms, including activation of autophagy and antioxidative response.

By performing analysis of the blood DNA methylome of 141 mice representing 16 different age groups, we identified reliable aging methylation patterns at a high resolution. We observed acceleration of methylation change along with accelerated increase in entropy with age, consistent with the exponential behavior of Gompertz mortality model and deleteriome theory of aging, explaining aging through accumulation of damage with time.

We further identified pathways enriched by genes with significant change of methylation status with age and observed number of longevity-related processes there, including DNA repair, inflammation, insulin and IGF1 signaling (IIS), fatty acid metabolism and stem cell proliferation. Finally, we demonstrated anti-aging effect of caloric restriction (CR) on significant methylation changes. Its effect was cumulative, gradually slowing down the aging-related changes with time. This finding is consistent with meta-analysis of longevity studies in mice, proposing that CR acts on aging rate, but not vulnerability, parameter of Gompertz model in mouse, contrary to the rapamycin.

Finally, we identified gene expression signatures of existing lifespan-extending interventions in mouse. By performing RNAseq analysis of 8 lifespan-extending interventions in liver, we observed regulation of some common processes. We also detected significant feminizing pattern in males in response to genetic and dietary interventions and acarbose, while other drugs showed no feminizing or even slightly masculinizing pattern (e.g., rapamycin), suggesting that feminizing effect is neither necessary nor sufficient for lifespan extension. Most interestingly, we observed that lifespan-extending interventions consistently induced more feminizing changes in males compared to females, resulting in convergence of gene expression profile across sexes.

By aggregating our data with publicly available datasets on longevity interventions in mouse liver, we identified consistent signatures associated with individual interventions, such as rapamycin, CR and GH deficiency, as well as common signatures across lifespan-extending interventions, including upregulation of xenobiotic metabolizing enzymes (XMEs) regulated by NRF2, TCA cycle and oxidative phosphorylation, and

downregulation of immune-response-related functions. We then detected signatures associated with the degree of lifespan extension effect and demonstrated that some genes and functions seem to be both qualitative and quantitative predictors of lifespan, including stress response, apoptosis, glucose metabolism, immune response and oxidative phosphorylation. We observed that the majority of genetic and dietary interventions along with some drugs turned out to be positively correlated at the level of gene expression, while other interventions including rapamycin showed a distinct pattern. Finally, we applied obtained longevity signatures to identify new lifespan-extending interventions based on their transcriptome profile. Using the signatures, we successfully distinguished between two strains of mice with differences in lifespan and proposed pro- or anti-longevity effect for several interventions considered to be positively or negatively associated with lifespan, such as hypoxia and conditional *Keap1* knockout in hepatocytes.

Based on analyzed models, we observe that longevity phenotype may be achieved through regulation of common and distinct mechanisms across- and within the species. One of the common mechanisms turned out to be acute stress response and antioxidant defense activated by NRF2. Indeed, this pathway distinguished NMR response to γ-irradiation compared to mouse and was one of the most significantly upregulated pathways across lifespan-extending interventions. Apoptosis-related genes also showed unique pattern in NMR cells and were associated with lifespan extension within the species. However, many cellular processes appear to be uniquely associated with longevity across NMR and interventions models. Thus, autophagy seems to play important cytoprotective role in NMR resistance to DNA damage, as confirmed by other studies. On the other hand,

regulation of oxidative phosphorylation and TCA cycle, glucose metabolism and immune response are significantly associated with lifespan extension by interventions in mouse. Notably, we observe that these effects are generally negatively correlated with aging as shown by effect of CR on methylation profile and detection of differences in biological age between two mouse strains by longevity signatures. Moreover, identified gene expression signatures may be applied for prediction of new lifespan-extending interventions and methylation profile may be used for validation of identified signatures. Therefore, investigated longevity-associated molecular signatures may not only shed the light on crucial mechanisms lying in the basis of lifespan extension but also substantially facilitate research and development of new antiaging therapies.

Bibliography

Aaron, E. a, and Powell, F.L. (1993). Effect of chronic hypoxia on hypoxic ventilatory response in awake rats. J. Appl. Physiol. *74*, 1635–1640.

Abegglen, L.M., Caulin, A.F., Chan, A., Lee, K., Robinson, R., Campbell, M.S., Kiso, W.K., Schmitt, D.L., Waddell, P.J., Bhaskara, S., et al. (2015). Potential Mechanisms for Cancer Resistance in Elephants and Comparative Cellular Response to DNA Damage in Humans. Jama *314*, 1850.

Alers, S., Loffler, A.S., Wesselborg, S., and Stork, B. (2012). Role of AMPK-mTOR-Ulk1/2 in the Regulation of Autophagy: Cross Talk, Shortcuts, and Feedbacks. Mol. Cell. Biol. *32*, 2–11.

Alonso, C., Fernández-Ramos, D., Varela-Rey, M., Martínez-Arranz, I., Navasa, N., Van Liempd, S.M., Lavín Trueba, J.L., Mayo, R., Ilisso, C.P., de Juan, V.G., et al. (2017). Metabolomic Identification of Subtypes of Nonalcoholic Steatohepatitis. Gastroenterology *152*, 1449–1461.e7.

Amador-Noguez, D., Yagi, K., Venable, S., and Darlington, G. (2004). Gene expression profile of long-lived Ames dwarf mice and Little mice. Aging Cell *3*, 423–441.

Anders, S., and Huber, W. (2010). Differential expression analysis for sequence count data. R106.

Andersson, R., Gebhard, C., Miguel-Escalada, I., Hoof, I., Bornholdt, J., Boyd, M., Chen, Y., Zhao, X., Schmidl, C., Suzuki, T., et al. (2014). An atlas of active enhancers across human cell types and tissues. Nature *507*, 455–461.

Apfeld, J., O'Connor, G., McDonagh, T., DiStefano, P.S., and Curtis, R. (2004). The AMP-activated protein kinase AAK-2 links energy levels and insulin-like signals to lifespan in *C. elegans*. Genes Dev. *18*, 3004–3009.

Armstrong, V.L., Rakoczy, S., Rojanathammanee, L., and Brown-Borg, H.M. (2014). Expression of DNA methyltransferases is influenced by growth hormone in the long-living Ames dwarf mouse in vivo and in vitro. J. Gerontol. A. Biol. Sci. Med. Sci. *69*, 923–933.

Asdell, S. a, Doornenbal, H., Joshi, S.R., and Sperling, G. a (1967). The effects of sex steroid hormones upon longevity in rats. J. Reprod. Fertil. *14*, 113–120.

Assenov, Y., Muller, F., Lutsik, P., Walter, J., Lengauer, T., and Bock, C. (2014). Comprehensive analysis of DNA methylation data with RnBeads. Nat Meth *11*, 1138–1140.

Ayyadevara, S., Alla, R., Thaden, J.J., and Shmookler Reis, R.J. (2008). Remarkable longevity and stress resistance of nematode PI3K-null mutants. Aging Cell *7*, 13–22.

Azpurua, J., Ke, Z., Chen, I.X., Zhang, Q., Ermolenko, D.N., Zhang, Z.D., Gorbunova, V., and Seluanov, A. (2013). Naked mole-rat has increased translational fidelity compared with the mouse, as well as a unique 28S ribosomal RNA cleavage. Proc. Natl. Acad. Sci. *110*, 17350–17355.

Baar, M.P., Brandt, R.M.C., Putavet, D.A., Klein, J.D.D., Derks, K.W.J., Bourgeois, B.R.M., Stryeck, S., Rijksen, Y., van Willigenburg, H., Feijtel, D.A., et al. (2017). Targeted Apoptosis of Senescent Cells Restores Tissue Homeostasis in Response to Chemotoxicity and Aging. Cell *169*, 132–147.e16.

Baird, L., and Dinkova-Kostova, A.T. (2011). The cytoprotective role of the Keap1-Nrf2 pathway. Arch. Toxicol. *85*, 241–272.

Baker, D.J., Childs, B.G., Durik, M., Wijers, M.E., Sieben, C.J., Zhong, J., A. Saltness, R., Jeganathan, K.B., Verzosa, G.C., Pezeshki, A., et al. (2016). Naturally occurring p16 Ink4a-positive cells shorten healthy lifespan. Nature *530*, 184–189.

Balaban, R.S., Nemoto, S., and Finkel, T. (2005). Mitochondria, oxidants, and aging. Cell *120*, 483–495.

Balfour, J.A., Mctavish, D., Dean, J.D., Infirmary, M.R., Fiilsch, U.R., Klinik, M., Kiel, K.D.C., and Republic, F. (1993). Acarbose. An Update of its Pharmacology and Therapeutic Use in Diabetes Mellitus. Drugs *46*, 1025–1054.

Barger, J.L., Kayo, T., Vann, J.M., Arias, E.B., Wang, J., Hacker, T.A., Wang, Y., Raederstorff, D., Morrow, J.D., Leeuwenburgh, C., et al. (2008). A low dose of dietary resveratrol partially mimics caloric restriction and retards aging parameters in mice. PLoS One *3*.

Bartke, A. (2011). Growth hormone, insulin and aging: The benefits of endocrine defects. Exp. Gerontol. *46*, 108–111.

Bartke, A., Wright, J.C., Mattison, J.A., Ingram, D.K., Miller, R.A., and Roth, G.S. (2001). Extending the lifespan of long-lived mice. Nature *414*, 412.

Baur, J.A., and Sinclair, D.A. (2006). Therapeutic potential of resveratrol: The in vivo evidence. Nat. Rev. Drug Discov. *5*, 493–506.

Baur, J.A., Pearson, K.J., Price, N.L., Jamieson, H.A., Lerin, C., Kalra, A., Prabhu, V. V, Allard, J.S., Lopez-Lluch, G., Lewis, K., et al. (2006). Resveratrol improves health and survival of mice on a high-calorie diet. Nature *444*, 337–342.

Baze, M.M., Schlauch, K., and Hayes, J.P. (2010a). Gene expression of the liver in response to chronic hypoxia. Physiol Genomics *41*, 275–288.

Baze, M.M., Schlauch, K., and Hayes, J.P. (2010b). Gene expression of the liver in response to chronic hypoxia. 275–288.

Bejerano, G., Pheasant, M., Makunin, I., Stephen, S., Kent, W.J., Mattick, J.S., and Haussler, D. (2004). Ultraconserved elements in the human genome. Science *304*, 1321–1325.

Benedusi, V., Meda, C., Della Torre, S., Monteleone, G., Vegeto, E., and Maggi, A. (2012). A lack of ovarian function increases neuroinflammation in aged mice. Endocrinology *153*, 2777–2788.

Benjamini, Y., and Hochberg, Y. (1995). Controlling the False Discovery Rate: A Practical and Powerful Approach to Multiple Testing. J. R. Stat. Soc. Ser. B *57*, 289–300.

Berdichevsky, A., Viswanathan, M., Horvitz, H.R., and Guarente, L. (2006). *C. elegans* SIR-2.1 Interacts with 14-3-3 Proteins to Activate DAF-16 and Extend Life Span. Cell *125*, 1165–1177.

Bird, A.P. (1980). DNA methylation and the frequency of CpG in animal DNA. Nucleic Acids Res. *8*, 1499–1504.

Bjedov, I., Toivonen, J.M., Kerr, F., Slack, C., Jacobson, J., Foley, A., and Partridge, L. (2010). Mechanisms of Life Span Extension by Rapamycin in the Fruit Fly Drosophila melanogaster. Cell Metab. *11*, 35–46.

Bonafè, M., Barbieri, M., Marchegiani, F., Olivieri, F., Ragno, E., Giampieri, C., Mugianesi, E., Centurelli, M., Franceschi, C., and Paolisso, G. (2003). Polymorphic variants of insulin-like growth factor I (IGF-I) receptor and phosphoinositide 3-kinase genes affect IGF-I plasma levels and human longevity: Cues for an evolutionarily conserved mechanism of life span control. J. Clin. Endocrinol. Metab. *88*, 3299–3304.

Bordone, L., and Guarente, L. (2005). Calorie restriction, SIRT1 and metabolism: understanding longevity. Nat. Rev. Mol. Cell Biol. *6*, 298–305.

Bozek, K., Khrameeva, E.E., Reznick, J., Omerbašić, D., Bennett, N.C., Lewin, G.R., Azpurua, J., Gorbunova, V., Seluanov, A., Regnard, P., et al. (2017). Lipidome determinants of maximal lifespan in mammals. Sci. Rep. *7*, 1–10.

Brown-Borg, H.M., Borg, K.E., Meliska, C.J., and Bartke, A. (1996). Dwarf mice and the ageing process. Nature *384*, 33.

Brown-Borg, H.M., Rakoczy, S.G., and Uthus, E.O. (2005). Growth hormone alters methionine and glutathione metabolism in Ames dwarf mice. Mech. Ageing Dev. *126*, 389–398.

Buckley, D.B., and Klaassen, C.D. (2009). Mechanism of Gender-Divergent UDP-Glucuronosyltransferase mRNA Expression in Mouse Liver and Kidney. *37*, 834–840.

Buffenstein, R. (2005). The naked mole-rat: a new long-living model for human aging

research. J Gerontol A Biol Sci Med Sci *60*, 1369–1377.

Buffenstein, R. (2008). Negligible senescence in the longest living rodent, the naked mole-rat: insights from a successfully aging species. J Comp Physiol B *178*, 439–445.

Buffenstein, R., and Yahav, S. (1991). Is the naked mole-rat Hererocephalus glaber an endothermic yet poikilothermic mammal? J. Therm. Biol. *16*, 227–232.

Calin, G.A., Liu, C., Ferracin, M., Hyslop, T., Spizzo, R., Sevignani, C., Fabbri, M., Cimmino, A., Lee, E.J., Wojcik, S.E., et al. (2007). Ultraconserved regions encoding ncRNAs are altered in human leukemias and carcinomas. Cancer Cell *12*, 215–229.

Campisi, J. (2005). Senescent cells, tumor suppression, and organismal aging: Good citizens, bad neighbors. Cell *120*, 513–522.

Cao, L., Li, W., Kim, S., Brodie, S.G., and Deng, C.X. (2003). Senescence, aging, and malignant transformation mediated by p53 in mice lacking the brca1 full-length isoform. Genes Dev. *17*, 201–213.

Carlson, M.E., Silva, H.S., and Conboy, I.M. (2008). Aging of signal transduction pathways, and pathology. Exp. Cell Res. *314*, 1951–1961.

Caulin, A.F., Graham, T.A., Wang, L.S., and Maley, C.C. (2015). Solutions to Peto's paradox revealed by mathematical modelling and cross-species cancer gene analysis. Philos. Trans. R. Soc. B Biol. Sci. *370*.

Cavalcante, R.G., and Sartor, M.A. (2017). annotatr: Genomic regions in context. Bioinformatics.

Chen, D., Thomas, E.L., and Kapahi, P. (2009). HIF-1 modulates dietary restriction-mediated lifespan extension via IRE-1 in *Caenorhabditis elegans*. PLoS Genet. *5*.

Childs, B.G., Baker, D.J., Kirkland, J.L., Campisi, J., and van Deursen, J.M. (2014). Senescence and apoptosis: dueling or complementary cell fates? EMBO Rep. *15*, 1139–1153.

Childs, B.G., Baker, D.J., Wijshake, T., Conover, C.A., Campisi, J., and van Deursen, J.M. (2016). Senescent intimal foam cells are deleterious at all stages of atherosclerosis. Science (80-.). *354*, 472–477.

Cole, J.J., Robertson, N.A., Rather, M.I., Thomson, J.P., McBryan, T., Sproul, D., Wang, T., Brock, C., Clark, W., Ideker, T., et al. (2017). Diverse interventions that extend mouse lifespan suppress shared age-associated epigenetic changes at critical gene regulatory regions. Genome Biol. *18*, 58.

Collado, M., Gil, J., Efeyan, A., Guerra, C., Schuhmacher, A.J., Barradas, M., Benguría, A., Zaballos, A., Flores, J.M., Barbacid, M., et al. (2005). Tumour biology: Senescence in premalignant tumours. Nature *436*, 642.

Coppé, J.-P., Desprez, P.-Y., Krtolica, A., and Campisi, J. (2010a). The Senescence-Associated Secretory Phenotype: The Dark Side of Tumor Suppression. Annu. Rev. Pathol. Mech. Dis. *5*, 99–118.

Coppé, J.P., Patil, C.K., Rodier, F., Sun, Y., Muñoz, D.P., Goldstein, J., Nelson, P.S., Desprez, P.Y., and Campisi, J. (2008). Senescence-associated secretory phenotypes reveal cell-nonautonomous functions of oncogenic RAS and the p53 tumor suppressor. PLoS

Biol. *6*.

Coppé, J.P., Patil, C.K., Rodier, F., Krtolica, A., Beauséjour, C.M., Parrinello, S., Hodgson, J.G., Chin, K., Desprez, P.Y., and Campisi, J. (2010b). A human-like senescence-associated secretory phenotype is conserved in mouse cells dependent on physiological oxygen. PLoS One *5*.

Coschigano, K.T., Holland, A.N., Riders, M.E., List, E.O., Flyvbjerg, A., and Kopchick, J.J. (2003). Deletion, but not antagonism, of the mouse growth hormone receptor results in severely decreased body weights, insulin, and insulin-like growth factor I levels and increased life span. Endocrinology *144*, 3799–3810.

Czarny, P., Pawlowska, E., Bialkowska-Warzecha, J., Kaarniranta, K., and Blasiak, J. (2015). Autophagy in DNA damage response. Int. J. Mol. Sci. *16*, 2641–2662.

D'Adda Di Fagagna, F. (2008). Living on a break: Cellular senescence as a DNA-damage response. Nat. Rev. Cancer *8*, 512–522.

Dhahbi, J.M., Mote, P.L., Fahy, G.M., and Spindler, S.R. (2005). Identification of potential caloric restriction mimetics by microarray profiling. Am. Physiol. Soc. *23*, 343–350.

Dobin, A., Davis, C.A., Schlesinger, F., Drenkow, J., Zaleski, C., Jha, S., Batut, P., Chaisson, M., and Gingeras, T.R. (2013). STAR: Ultrafast universal RNA-seq aligner. Bioinformatics *29*, 15–21.

Drori, D., and Folman, Y. (1976). Environmental effects on longevity in the male rat: Exercise, mating, castration and restricted feeding. Exp. Gerontol. *11*, 25–32.

Estep, P.W., Warner, J.B., and Bulyk, M.L. (2009). Short-term calorie restriction in male mice feminizes gene expression and alters key regulators of conserved aging regulatory pathways. PLoS One *4*.

Florath, I., Butterbach, K., Muller, H., Bewerunge-Hudler, M., and Brenner, H. (2014). Cross-sectional and longitudinal changes in DNA methylation with age: an epigenome-wide analysis revealing over 60 novel age-associated CpG sites. Hum. Mol. Genet. *23*, 1186–1201.

Flurkey, K., Papaconstantinou, J., Miller, R.A., and Harrison, D.E. (2001). Lifespan extension and delayed immune and collagen aging in mutant mice with defects in growth hormone production. Proc. Natl. Acad. Sci. *98*, 6736–6741.

Fok, W.C., Bokov, A., Gelfond, J., Yu, Z., Zhang, Y., Doderer, M., Chen, Y., Javors, M., Wood, W.H., Zhang, Y., et al. (2014). Combined treatment of rapamycin and dietary restriction has a larger effect on the transcriptome and metabolome of liver. Aging Cell *13*, 311–319.

Fontana, L., Partridge, L., and Longo, V.D. (2010). Extending Healthy Life Span—From Yeast to Humans. Science (80-.). *328*, 321–326.

Fontana, L., Villareal, D.T., Das, S.K., Smith, S.R., Meydani, S.N., Pittas, A.G., Klein, S., Bhapkar, M., Rochon, J., Ravussin, E., et al. (2016). Effects of 2-year calorie restriction on circulating levels of IGF-1, IGF-binding proteins and cortisol in nonobese men and women: A randomized clinical trial. Aging Cell *15*, 22–27.

Foukas, L.C., Bilanges, B., Bettedi, L., Pearce, W., Ali, K., Sancho, S., Withers, D.J., and

Vanhaesebroeck, B. (2013). Long-term p110α PI3K inactivation exerts a beneficial effect on metabolism. EMBO Mol. Med. *5*, 563–571.

Fu, Z.D., and Klaassen, C.D. (2014). Short-term calorie restriction feminizes the mRNA profiles of drug metabolizing enzymes and transporters in livers of mice. Toxicol. Appl. Pharmacol. *274*, 137–146.

Fushan, A.A., Turanov, A.A., Lee, S.G., Kim, E.B., Lobanov, A. V., Yim, S.H., Buffenstein, R., Lee, S.R., Chang, K.T., Rhee, H., et al. (2015). Gene expression defines natural changes in mammalian lifespan. Aging Cell *14*, 352–365.

Gadó, K., Domján, G., Hegyesi, H., and Falus, A. (2000). Role of interleukin-6 in the pathogenesis of multiple myeloma. Cell Biol. Int. *24*, 195–209.

Galluzzi, L., Pietrocola, F., Levine, B., and Kroemer, G. (2014). Metabolic control of autophagy. Cell *159*, 1263–1276.

Garinis, G.A., van der Horst, G.T.J., Vijg, J., and Hoeijmakers, J.H.J. (2008). DNA damage and ageing: New-age ideas for an age-old problem. Nat. Cell Biol. *10*, 1241–1247.

Garratt, M., Nakagawa, S., and Simons, M.J.P. (2016). Comparative idiosyncrasies in life extension by reduced mTOR signalling and its distinctiveness from dietary restriction. Aging Cell *15*, 737–743.

Gatza, C., Moore, L., Dumble, M., and Donehower, L.A. (2007). Tumor suppressor dosage regulates stem cell dynamics during aging. Cell Cycle *6*, 52–55.

Gautier, H. (1996). Interactions and control among metabolic of breathing rate, hypoxia,

and control of breathing. 521–527.

Gaztelumendi, N., and Nogués, C. (2014). Chromosome Instability in mouse Embryonic Stem Cells. Sci. Rep. *4*, 1–8.

George, J.C., and Bockstoce, J.R. (2008). Two historical weapon fragments as an aid to estimating the longevity and movements of bowhead whales. Polar Biol. *31*, 751–754.

Gertz, M., Nguyen, G.T.T., Fischer, F., Suenkel, B., Schlicker, C., Fränzel, B., Tomaschewski, J., Aladini, F., Becker, C., Wolters, D., et al. (2012). A Molecular Mechanism for Direct Sirtuin Activation by Resveratrol. PLoS One *7*, 1–12.

Gladyshev, V.N. (2016). Aging: progressive decline in fitness due to the rising deleteriome adjusted by genetic, environmental, and stochastic processes. Aging Cell *15*, 594–602.

Gompertz, B. (1825). On the nature of the function expressive of the law of human mortality and on a new model of determining life contingencies. Philos. Trans. R. Soc. *115*, 513–585.

Gonzalez-Covarrubias, V., Beekman, M., Uh, H.W., Dane, A., Troost, J., Paliukhovich, I., van der Kloet, F.M., Houwing-Duistermaat, J., Vreeken, R.J., Hankemeier, T., et al. (2013). Lipidomics of familial longevity. Aging Cell *12*, 426–434.

Gonzalgo, M.L., and Jones, P.A. (1997). Mutagenic and epigenetic effects of DNA methylation. Mutat. Res. *386*, 107–118.

van der Goot, A.T., Zhu, W., Vazquez-Manrique, R.P., Seinstra, R.I., Dettmer, K., Michels, H., Farina, F., Krijnen, J., Melki, R., Buijsman, R.C., et al. (2012). Delaying aging and the

aging-associated decline in protein homeostasis by inhibition of tryptophan degradation. Proc. Natl. Acad. Sci. *109*, 14912–14917.

Gorrini, C., Baniasadi, P.S., Harris, I.S., Silvester, J., Inoue, S., Snow, B., Joshi, P.A., Wakeham, A., Molyneux, S.D., Martin, B., et al. (2013). BRCA1 interacts with Nrf2 to regulate antioxidant signaling and cell survival. J. Exp. Med. *210*, 1529–1544.

Grandison, R.C., Piper, M.D.W., and Partridge, L. (2009). Amino acid imbalance explains extension of lifespan by dietary restriction in Drosophila. Nature *462*, 1061–1064.

De Haes, W., Frooninckx, L., Van Assche, R., Smolders, A., Depuydt, G., Billen, J., Braeckman, B.P., Schoofs, L., and Temmerman, L. (2014). Metformin promotes lifespan through mitohormesis via the peroxiredoxin PRDX-2. Proc. Natl. Acad. Sci. *111*, E2501–E2509.

Hahn, O., Gronke, S., Stubbs, T.M., Ficz, G., Hendrich, O., Krueger, F., Andrews, S., Zhang, Q., Wakelam, M.J., Beyer, A., et al. (2017). Dietary restriction protects from age-associated DNA methylation and induces epigenetic reprogramming of lipid metabolism. Genome Biol. *18*, 56.

Hannum, G., Guinney, J., Zhao, L., Zhang, L., Hughes, G., Sadda, S.V., Klotzle, B., Bibikova, M., Fan, J.B., Gao, Y., et al. (2013). Genome-wide Methylation Profiles Reveal Quantitative Views of Human Aging Rates. Mol. Cell *49*, 359–367.

Harrison, D.E., Strong, R., Sharp, Z.D., Nelson, J.F., Astle, C.M., Flurkey, K., Nadon, N.L., Wilkinson, J.E., Frenkel, K., Carter, C.S., et al. (2009). Rapamycin fed late in life extends lifespan in genetically heterogeneous mice. Nature *460*, 392–395.

Harrison, D.E., Strong, R., Allison, D.B., Ames, B.N., Astle, C.M., Atamna, H., Fernandez, E., Flurkey, K., Javors, M.A., Nadon, N.L., et al. (2014). Acarbose, 17-α-estradiol, and nordihydroguaiaretic acid extend mouse lifespan preferentially in males. Aging Cell *13*, 273–282.

Hart, R.W., and Setlow, R.B. (1974). Correlation between deoxyribonucleic acid excision-repair and life-span in a number of mammalian species. Proc. Natl. Acad. Sci. USA *71*, 2169–2173.

van Heemst, D. (2010). Insulin, IGF-1 and longevity. Aging Dis. *1*, 147–157.

Heilbronn, L.K., and Ravussin, E. (2003). Calorie restriction and aging: review of the literature and implications for studies in humans. Am. J. Clin. Nutr. *78*, 361–369.

Hine, C., Harputlugil, E., Zhang, Y., Ruckenstuhl, C., Lee, B.C., Brace, L., Longchamp, A., Treviño-Villarreal, J.H., Mejia, P., Ozaki, C.K., et al. (2015). Endogenous hydrogen sulfide production is essential for dietary restriction benefits. Cell *160*, 132–144.

Hinrichs, A.S., Karolchik, D., Baertsch, R., Barber, G.P., Bejerano, G., Clawson, H., Diekhans, M., Furey, T.S., Harte, R.A., Hsu, F., et al. (2006). The UCSC Genome Browser Database: update 2006. Nucleic Acids Res. *34*, D590-8.

Hofmann, J.W., Zhao, X., De Cecco, M., Peterson, A.L., Pagliaroli, L., Manivannan, J., Hubbard, G.B., Ikeno, Y., Zhang, Y., Feng, B., et al. (2015). Reduced expression of MYC increases longevity and enhances healthspan. Cell *160*, 477–488.

Honda, Y., and Honda, S. (2002). Oxidative Stress and Life Span Determination in the Nematode *Caenorhabditis elegans*. Ann. New York Acad. Sci. *959*, 466–474.

Horvath, S. (2013). DNA methylation age of human tissues and cell types. Genome Biol *14*, R115.

Horvath, S., Zhang, Y., Langfelder, P., Kahn, R.S., Boks, M.P.M., van Eijk, K., van den Berg, L.H., and Ophoff, R.A. (2012). Aging effects on DNA methylation modules in human brain and blood tissue. Genome Biol. *13*, R97.

Houseman, E.A., Kile, M.L., Christiani, D.C., Ince, T.A., Kelsey, K.T., and Marsit, C.J. (2016). Reference-free deconvolution of DNA methylation data and mediation by cell composition effects. BMC Bioinformatics *17*.

Huang, D.W., Sherman, B.T., and Lempicki, R.A. (2009a). Bioinformatics enrichment tools: Paths toward the comprehensive functional analysis of large gene lists. Nucleic Acids Res. *37*, 1–13.

Huang, D.W., Lempicki, R. a, and Sherman, B.T. (2009b). Systematic and integrative analysis of large gene lists using DAVID bioinformatics resources. Nat. Protoc. *4*, 44–57.

Hulbert, A.J. (2008). Explaining longevity of different animals: Is membrane fatty acid composition the missing link? Age (Omaha). *30*, 89–97.

Hulbert, A.J., Kelly, M.A., and Abbott, S.K. (2014). Polyunsaturated fats, membrane lipids and animal longevity. J. Comp. Physiol. B Biochem. Syst. Environ. Physiol. *184*, 149–166.

Jain, I.H., Zazzeron, L., Goli, R., Alexa, K., Schatzman-Bone, S., Dhillon, H., Goldberger, O., Peng, J., Shalem, O., Sanjana, N.E., et al. (2016). Hypoxia as a therapy for mitochondrial disease. Science (80-.). *352*, 54–61.

Jeon, O.H., Kim, C., Laberge, R.M., Demaria, M., Rathod, S., Vasserot, A.P., Chung, J.W., Kim, D.H., Poon, Y., David, N., et al. (2017). Local clearance of senescent cells attenuates the development of post-traumatic osteoarthritis and creates a pro-regenerative environment. Nat. Med. *23*, 775–781.

Johansson, A., Enroth, S., and Gyllensten, U. (2013). Continuous Aging of the Human DNA Methylome Throughout the Human Lifespan. PLoS One *8*, e67378.

Johnson, F.B., Sinclair, D.A., and Guarente, L. (1999). Molecular biology of aging. Cell *96*, 291–302.

Johnson, S.C., Rabinovitch, P.S., and Kaeberlein, M. (2013). mTOR is a key modulator of ageing and age-related disease Simon. Nature *493*, 338–345.

Jones, M.J., Goodman, S.J., and Kobor, M.S. (2015). DNA methylation and healthy human aging. Aging Cell *14*, 924–932.

Jones, O.R., Scheuerlein, A., Salguero-Gómez, R., Camarda, C.G., Schaible, R., Casper, B.B., Dahlgren, J.P., Ehrlén, J., García, M.B., Menges, E.S., et al. (2014). Diversity of ageing across the tree of life. Nature *505*, 169–173.

Kabil, O., Vitvitsky, V., Xie, P., and Banerjee, R. (2011). The quantitative significance of the transsulfuration enzymes for H2S production in murine tissues. Antioxid. Redox Signal. *15*, 363–372.

Kaeberlein, M. (2012). Response to Nutrients Regulation of Yeast Replicative Life Span by TOR and Sch9 in Response to Nutrients. Science (80-.). *1193*, 1193–1197.

Kaeberlein, M., and Kennedy, B.K. (2008). Protein translation, 2008. Aging Cell *7*, 777–782.

Kaeberlein, M., McVey, M., and Guarente, L. (1999). The *SIR2/3/4* complex and *SIR2* alone promote longevity in Saccharomyces cerevisiae by two different mechanisms. Genes Dev. *13*, 2570–2580.

Kanfi, Y., Naiman, S., Amir, G., Peshti, V., Zinman, G., Nahum, L., Bar-Joseph, Z., and Cohen, H.Y. (2012). The sirtuin SIRT6 regulates lifespan in male mice. Nature *483*, 218–221.

Karolchik, D., Hinrichs, A.S., Furey, T.S., Roskin, K.M., Sugnet, C.W., Haussler, D., and Kent, W.J. (2004). The UCSC Table Browser data retrieval tool. Nucleic Acids Res. *32*, D493-6.

Kautz, L., Meynard, D., Monnier, A., Darnaud, V., Bouvet, R., Wang, R.H., Deng, C., Vaulont, S., Mosser, J., Coppin, H., et al. (2008). Iron regulates phosphorylation of Smad1/5/8 and gene expression of Bmp6, Smad7, Id1, and Atoh8 in the mouse liver. Blood *112*, 1503–1509.

Kealy, R.D., Lawler, D.F., Ballam, J.M., Mantz, S.L., Biery, D.N., Greeley, E.H., Lust, G., Segre, M., Smith, G.K., and Stowe, H.D. (2002). Effects of diet restriction on life span and age-related changes in dogs. J. Am. Vet. Med. Assoc. *220*, 1315–1320.

Keane, M., Semeiks, J., Webb, A.E., Li, Y.I., Quesada, V., Craig, T., Madsen, L.B., van Dam, S., Brawand, D., Marques, P.I., et al. (2015). Insights into the evolution of longevity from the bowhead whale genome. Cell Rep. *10*, 112–122.

Khan, A., and Zhang, X. (2016). dbSUPER: a database of super-enhancers in mouse and human genome. Nucleic Acids Res. *44*, D164-71.

Kim, E.B., Fang, X., Fushan, A.A., Huang, Z., Lobanov, A. V., Han, L., Marino, S.M., Sun, X., Turanov, A.A., Yang, P., et al. (2011). Genome sequencing reveals insights into physiology and longevity of the naked mole rat. Nature *479*, 223–227.

Kobayashi, T., Shimabukuro-Demoto, S., Yoshida-Sugitani, R., Furuyama-Tanaka, K., Karyu, H., Sugiura, Y., Shimizu, Y., Hosaka, T., Goto, M., Kato, N., et al. (2014). The histidine transporter SLC15A4 coordinates mTOR-dependent inflammatory responses and pathogenic antibody production. Immunity *41*, 375–388.

Kozomara, A., and Griffiths-Jones, S. (2014). miRBase: annotating high confidence microRNAs using deep sequencing data. Nucleic Acids Res. *42*, D68-73.

Kristiansen, O.P., and Mandrup-Poulsen, T. (2005). Interleukin-6 and Diabetes. Diabetes *54*, S114 LP-S124.

Kryukov, G. V., and Castellano, S. (2003). Characterization of Mammalian Selenoproteomes. Science (80-.). *300*, 1439–1443.

Laberge, R.M., Sun, Y., Orjalo, A. V., Patil, C.K., Freund, A., Zhou, L., Curran, S.C., Davalos, A.R., Wilson-Edell, K.A., Liu, S., et al. (2015). MTOR regulates the pro-tumorigenic senescence-associated secretory phenotype by promoting IL1A translation. Nat. Cell Biol. *17*, 1049–1061.

Lakowski, B., and Hekimi, S. (1998). The genetics of caloric restriction in *Caenorhabditis elegans*. Proc. Natl. Acad. Sci. *95*, 13091–13096.

Lamb, J., Crawford, E.D., Peck, D., Modell, J.W., Blat, I.C., Wrobel, M.J., Lerner, J., Brunet, J., Subramanian, A., Ross, K.N., et al. (2006). The Connectivity Map : Using Gene-Expression Signatures to Connect Small Molecules, Genes, and Disease. Science (80-.). *313*, 1929–1935.

Lee, S.G., Mikhalchenko, A.E., Yim, S.H., Lobanov, A. V., Park, J.K., Choi, K.H., Bronson, R.T., Lee, C.K., Park, T.J., and Gladyshev, V.N. (2017). Naked Mole Rat Induced Pluripotent Stem Cells and Their Contribution to Interspecific Chimera. Stem Cell Reports *9*, 1706–1720.

Leiser, S.F., and Miller, R.A. (2010). Nrf2 Signaling, a Mechanism for Cellular Stress Resistance in Long-Lived Mice. Mol. Cell. Biol. *30*, 871–884.

Leontieva, O. V., Demidenko, Z.N., and Blagosklonny, M. V. (2014). Contact inhibition and high cell density deactivate the mammalian target of rapamycin pathway, thus suppressing the senescence program. Proc. Natl. Acad. Sci. *111*, 8832–8837.

Li, X., Bartke, A., Berryman, D.E., Funk, K., Kopchick, J.J., List, E.O., Sun, L., and Miller, R.A. (2013). Direct and indirect effects of growth hormone receptor ablation on liver expression of xenobiotic metabolizing genes. AJP Endocrinol. Metab. *305*, E942–E950.

Liao, Y., Smyth, G.K., and Shi, W. (2014). FeatureCounts: An efficient general purpose program for assigning sequence reads to genomic features. Bioinformatics *30*, 923–930.

Lin, A.S., Defossez, P., Guarente, L., Lin, S., Defossez, P., and Guarentet, L. (2000). Requirement of NAD and SIR2 for Life-Span Extension by Calorie Restriction in *Saccharomyces cerevisiae*. Science (80-.). *289*, 2126–2128.

Lomonaco, V., Martoglia, R., Mandreoli, F., Anderlucci, L., Emmett, W., Bicciato, S., and Taccioli, C. (2014). UCbase 2.0: ultraconserved sequences database (2014 update). Database (Oxford). *2014*.

Loots, G., and Ovcharenko, I. (2007). ECRbase: database of evolutionary conserved regions, promoters, and transcription factor binding sites in vertebrate genomes. Bioinformatics *23*, 122–124.

Lopez-Otin, C., Blasco, M.A., Partridge, L., Serrano, M., and Kroemer, G. (2013). The hallmarks of aging. Cell *153*.

Lujambio, A., and Esteller, M. (2009). How epigenetics can explain human metastasis: a new role for microRNAs. Cell Cycle *8*, 377–382.

Lujambio, A., Portela, A., Liz, J., Melo, S.A., Rossi, S., Spizzo, R., Croce, C.M., Calin, G.A., and Esteller, M. (2010). CpG island hypermethylation-associated silencing of non-coding RNAs transcribed from ultraconserved regions in human cancer. Oncogene *29*, 6390–6401.

Ma, S., and Gladyshev, V.N. (2017). Molecular signatures of longevity: Insights from cross-species comparative studies. Semin. Cell Dev. Biol. *70*, 190–203.

Ma, S., Yim, S.H., Lee, S.-G., Kim, E.B., Lee, S.-R., Chang, K.-T., Buffenstein, R., Lewis, K.N., Park, T.J., Miller, R.A., et al. (2015a). Organization of the Mammalian Metabolome according to Organ Function, Lineage Specialization, and Longevity. Cell Metab. *22*, 332–343.

Ma, S., Lee, S.G., Kim, E.B., Park, T.J., Seluanov, A., Gorbunova, V., Buffenstein, R.,

Seravalli, J., and Gladyshev, V.N. (2015b). Organization of the Mammalian Ionome According to Organ Origin, Lineage Specialization, and Longevity. Cell Rep. *13*, 1319–1326.

Ma, S., Upneja, A., Galecki, A., Tsai, Y.M., Burant, C.F., Raskind, S., Zhang, Q., Zhang, Z.D., Seluanov, A., Gorbunova, V., et al. (2016). Cell culture-based profiling across mammals reveals DNA repair and metabolism as determinants of species longevity. Elife *5*, 1–25.

MacRae, S.L., Croken, M.M.K., Calder, R.B., Aliper, A., Milholland, B., White, R.R., Zhavoronkov, A., Gladyshev, V.N., Seluanov, A., Gorbunova, V., et al. (2015). DNA repair in species with extreme lifespan differences. Aging (Albany. NY). *7*, 1171–1184.

Madeo, F., Zimmermann, A., Maiuri, M.C., Kroemer, G., Metabolomics, F., Platforms, C.B., Roussy, I.G., Université, F., Descartes, P., Cité, S.P., et al. (2015). Essential role for autophagy in life span extension. *125*, 85–93.

Maegawa, S., Hinkal, G., Kim, H.S., Shen, L., Zhang, L., Zhang, J., Zhang, N., Liang, S., Donehower, L.A., and Issa, J.-P.J. (2010). Widespread and tissue specific age-related DNA methylation changes in mice. Genome Res. *20*, 332–340.

Maegawa, S., Lu, Y., Tahara, T., Lee, J.T., Madzo, J., Liang, S., Jelinek, J., Colman, R.J., and Issa, J.-P.J. (2017). Caloric restriction delays age-related methylation drift. Nat. Commun. *8*, 539.

de Magalhães, J.P., Costa, J., and Toussaint, O. (2005). HAGR: The Human Ageing Genomic Resources. Nucleic Acids Res. *33*, 537–543.

Mair, W., Goymer, P., Pletcher, S.D., Partridge, L., Mair, W., and Partridget, L. (2003). Demography of Dietawy Restriction and Death in Drosophita. Science (80-.). *301*, 1731–1733.

Mann, V., Huber, C., Kogianni, G., Collins, F., and Noble, B. (2007). The antioxidant effect of estrogen and Selective Estrogen Receptor Modulators in the inhibition of osteocyte apoptosis in vitro. Bone *40*, 674–684.

Marioni, R.E., Shah, S., McRae, A.F., Chen, B.H., Colicino, E., Harris, S.E., Gibson, J., Henders, A.K., Redmond, P., Cox, S.R., et al. (2015). DNA methylation age of blood predicts all-cause mortality in later life. Genome Biol. *16*, 1–12.

Martin-Montalvo, A., Mercken, E.M., Mitchell, S.J., Palacios, H.H., Mote, P.L., Scheibye-Knudsen, M., Gomes, A.P., Ward, T.M., Minor, R.K., Blouin, M.-J., et al. (2013). Metformin improves healthspan and lifespan in mice. Nat Commun. *4*, 2192.

Mattison, J.A., Colman, R.J., Beasley, T.M., Allison, D.B., Kemnitz, J.W., Roth, G.S., Ingram, D.K., Weindruch, R., De Cabo, R., and Anderson, R.M. (2017). Caloric restriction improves health and survival of rhesus monkeys. Nat. Commun. *8*, 1–12.

Matys, V. (2006). TRANSFAC(R) and its module TRANSCompel(R): transcriptional gene regulation in eukaryotes. Nucleic Acids Res. *34*, D108–D110.

McClay, J.L., Aberg, K.A., Clark, S.L., Nerella, S., Kumar, G., Xie, L.Y., Hudson, A.D., Harada, A., Hultman, C.M., Magnusson, P.K.E., et al. (2014). A methylome-wide study of aging using massively parallel sequencing of the methyl-CpG-enriched genomic fraction from blood in over 700 subjects. Hum. Mol. Genet. *23*, 1175–1185.

Mehta, R., Steinkraus, K.A., Sutphin, G.L., Ramos, F.J., S, L., Huh, A., Davis, C., Chandler-brown, D., and Kaeberlein, M. (2009). Proteasomal Regulation of the Hypoxic Response Modulates Aging in *C.elegans*. Science (80-.). *324*, 1196–1198.

Mercken, E.M., Hu, J., Krzysik-Walker, S., Wei, M., Li, Y., Mcburney, M.W., de Cabo, R., and Longo, V.D. (2014). SIRT1 but not its increased expression is essential for lifespan extension in caloric-restricted mice. Aging Cell *13*, 193–196.

Miller, R.A., Harrison, D.E., Astle, C.M., Floyd, R.A., Flurkey, K., Hensley, K.L., Javors, M.A., Leeuwenburgh, C., Nelson, J.F., Ongini, E., et al. (2007). An aging Interventions Testing Program: Study design and interim report. Aging Cell *6*, 565–575.

Miller, R.A., Harrison, D.E., Astle, C.M., Baur, J.A., Boyd, A.R., De Cabo, R., Fernandez, E., Flurkey, K., Javors, M.A., Nelson, J.F., et al. (2011). Rapamycin, but not resveratrol or simvastatin, extends life span of genetically heterogeneous mice. Journals Gerontol. - Ser. A Biol. Sci. Med. Sci. *66 A*, 191–201.

Miller, R.A., Harrison, D.E., Astle, C.M., Fernandez, E., Flurkey, K., Han, M., Javors, M.A., Li, X., Nadon, N.L., Nelson, J.F., et al. (2014). Rapamycin-mediated lifespan increase in mice is dose and sex dependent and metabolically distinct from dietary restriction. Aging Cell *13*, 468–477.

Mitchell, S.J., Madrigal-Matute, J., Scheibye-Knudsen, M., Fang, E., Aon, M., Gonzalez-Reyes, J.A., Cortassa, S., Kaushik, S., Gonzalez-Freire, M., Patel, B., et al. (2016). Effects of Sex, Strain, and Energy Intake on Hallmarks of Aging in Mice. Cell Metab. *23*, 1093–1112.

Miyawaki, S., Kawamura, Y., Hachiya, T., Shimizu, A., and Miura, K. (2015). Molecular cloning and characterization of the INK4a and ARF genes in naked mole-rat. Inflamm. Regen. *35*, 42–50.

Miyawaki, S., Kawamura, Y., Oiwa, Y., Shimizu, A., Hachiya, T., Bono, H., Koya, I., Okada, Y., Kimura, T., Tsuchiya, Y., et al. (2016). Tumour resistance in induced pluripotent stem cells derived from naked mole-rats. Nat. Commun. *7*, 1–9.

Moorad, J.A., Promislow, D.E.L., Nate, F., and Miller Richard A. (2012). A comparative assessment of univariate longevity measures using zoological animal records. Aging Cell *11*, 940–948.

Muñoz-Espín, D., Cañamero, M., Maraver, A., Gómez-López, G., Contreras, J., Murillo-Cuesta, S., Rodríguez-Baeza, A., Varela-Nieto, I., Ruberte, J., Collado, M., et al. (2013). XProgrammed cell senescence during mammalian embryonic development. Cell *155*.

Mutter, F.E., Park, B.K., and Copple, I.M. (2015). Value of monitoring Nrf2 activity for the detection of chemical and oxidative stress. Biochem. Soc. Trans. *43*, 657–662.

Nakamura, N., Lill, J.R., Phung, Q., Jiang, Z., Bakalarski, C., De Mazière, A., Klumperman, J., Schlatter, M., Delamarre, L., and Mellman, I. (2014). Endosomes are specialized platforms for bacterial sensing and NOD2 signalling. Nature *509*, 240–244.

Narod, S.A., and Foulkes, W.D. (2004). BRCA1 and BRCA2: 1994 and beyond. Nat. Rev. Cancer *4*, 665–676.

Newman, J.C., Covarrubias, A.J., Zhao, M., Yu, X., Gut, P., Ng, C.P., Huang, Y., Haldar, S., and Verdin, E. (2017). Ketogenic Diet Reduces Midlife Mortality and Improves

Memory in Aging Mice. Cell Metab. *26*, 547–557.e8.

Nojima, A., Yamashita, M., Yoshida, Y., Shimizu, I., Ichimiya, H., Kamimura, N., Kobayashi, Y., Ohta, S., Ishii, N., and Minamino, T. (2013). Haploinsufficiency of Akt1 Prolongs the Lifespan of Mice. PLoS One *8*, 1–10.

O'Connor, T.P., Lee, A., Jarvis, J.U.M., and Buffenstein, R. (2002). Prolonged longevity in naked mole-rats: Age-related changes in metabolism, body composition and gastrointestinal function. Comp. Biochem. Physiol. - A Mol. Integr. Physiol. *133*, 835–842.

Osburn, W.O., Yates, M.S., Dolan, P.D., Chen, S., Liby, K.T., Sporn, M.B., Taguchi, K., Yamamoto, M., and Kensler, T.W. (2008). Genetic or pharmacologic amplification of Nrf2 signaling inhibits acute inflammatory liver injury in mice. Toxicol. Sci. *104*, 218–227.

Ott, C., and Grune, T. (2014). Protein oxidation and proteolytic signalling in aging. Curr. Pharm. Des. *20*, 3040–3051.

Oxenkrug, G.F. (2010). The extended life span of *Drosophila melanogaster* eye-color (white and vermilion) mutants with impaired formation of kynurenine. J. Neural Transm. *117*, 23–26.

Ozerov, I. V., Lezhnina, K. V., Izumchenko, E., Artemov, A. V., Medintsev, S., Vanhaelen, Q., Aliper, A., Vijg, J., Osipov, A.N., Labat, I., et al. (2016). In silico Pathway Activation Network Decomposition Analysis (iPANDA) as a method for biomarker development. Nat. Commun. *7*, 1–11.

Park, T.J., Reznick, J., Peterson, B.L., Blass, G., Omerbašić, D., Bennett, N.C., Kuich,

P.H.J.L., Zasada, C., Browe, B.M., Hamann, W., et al. (2017). Fructose-driven glycolysis supports anoxia resistance in the naked mole-rat. Science (80-.). *356*, 307–311.

Pawlikowska, L., Hu, D., Huntsman, S., Sung, A., Chu, C., Chen, J., Joyner, A.H., Schork, N.J., Hsueh, W.C., Reiner, A.P., et al. (2009). Association of common genetic variation in the insulin/IGF1 signaling pathway with human longevity. Aging Cell *8*, 460–472.

Pearson, K.J., Baur, J.A., Lewis, K.N., Peshkin, L., Price, N.L., Labinskyy, N., Swindell, W.R., Kamara, D., Minor, R.K., Perez, E., et al. (2008a). Resveratrol Delays Age-Related Deterioration and Mimics Transcriptional Aspects of Dietary Restriction without Extending Life Span. Cell Metab. *8*, 157–168.

Pearson, K.J., Lewis, K.N., Price, N.L., Chang, J.W., Perez, E., Cascajo, M. V., Tamashiro, K.L., Poosala, S., Csiszar, A., Ungvari, Z., et al. (2008b). Nrf2 mediates cancer protection but not prolongevity induced by caloric restriction. Proc. Natl. Acad. Sci. *105*, 2325–2330.

Perez, V.I., Buffenstein, R., Masamsetti, V., Leonard, S., Salmon, A.B., Mele, J., Andziak, B., Yang, T., Edrey, Y., Friguet, B., et al. (2009). Protein stability and resistance to oxidative stress are determinants of longevity in the longest-living rodent, the naked mole-rat. Proc. Natl. Acad. Sci. *106*, 3059–3064.

Petkovich, D.A., Podolskiy, D.I., Lobanov, A. V, Lee, S., Miller, R.A., and Gladyshev, V.N. (2017). Using DNA Methylation Profiling to Evaluate Biological Age and Longevity Interventions. Cell Metab. *25*, 954–960.e6.

Peto, H., Roe, F.J.C., Lee, P.N., Levy, L., and Clack, J. (1975). Cancer and ageing in mice and men. Br. J. Cancer *32*, 411–426.

Pifferi, F., Terrien, J., Marchal, J., Dal-Pan, A., Djelti, F., Hardy, I., Chahory, S., Cordonnier, N., Desquilbet, L., Hurion, M., et al. (2018). Caloric restriction increases lifespan but affects brain integrity in grey mouse lemur primates. Commun. Biol. *1*, 30.

Plank, M., Wuttke, D., van Dam, S., Clarke, S.A., and de Magalhães, J.P. (2012). A meta-analysis of caloric restriction gene expression profiles to infer common signatures and regulatory mechanisms. Mol. Biosyst. *8*, 1339.

Podolskiy, D.I., Lobanov, A. V., Kryukov, G. V., and Gladyshev, V.N. (2016). Analysis of cancer genomes reveals basic features of human aging and its role in cancer development. Nat. Commun. *7*, 1–12.

Proteggente, A.R., England, T.G., Rehman, A., Rice-Evans, C.A., and Halliwell, B. (2002). Gender differences in steady-state levels of oxidative damage to DNA in healthy individuals. Free Radic. Res. *36*, 157–162.

Pyo, J.O., Yoo, S.M., Ahn, H.H., Nah, J., Hong, S.H., Kam, T.I., Jung, S., and Jung, Y.K. (2013). Overexpression of Atg5 in mice activates autophagy and extends lifespan. Nat. Commun. *4*, 1–9.

Quach, A., Levine, M.E., Tanaka, T., Lu, A.T., Chen, B.H., Ferrucci, L., Ritz, B., Bandinelli, S., Neuhouser, M.L., Beasley, J.M., et al. (2017). Epigenetic clock analysis of diet, exercise, education, and lifestyle factors. Aging (Albany. NY). *9*, 419–446.

Rakyan, V.K., Down, T.A., Maslau, S., Andrew, T., Yang, T.-P., Beyan, H., Whittaker, P., McCann, O.T., Finer, S., Valdes, A.M., et al. (2010). Human aging-associated DNA hypermethylation occurs preferentially at bivalent chromatin domains. Genome Res. *20*,

434–439.

Ramadoss, P., Chiappini, F., Bilban, M., and Hollenberg, A.N. (2010). Regulation of hepatic six transmembrane epithelial antigen of prostate 4 (STEAP4) expression by STAT3 and CCAAT/enhancer-binding protein α. J. Biol. Chem. *285*, 16453–16466.

Ray, D., Wu, A., Wilkinson, J.E., Murphy, H.S., Lu, Q., Kluve-Beckerman, B., Liepnieks, J.J., Benson, M., Yung, R., and Richardson, B. (2006). Aging in heterozygous Dnmt1-deficient mice: effects on survival, the DNA methylation genes, and the development of amyloidosis. J. Gerontol. A. Biol. Sci. Med. Sci. *61*, 115–124.

Richardson, B. (2003). Impact of aging on DNA methylation. Ageing Res. Rev. *2*, 245–261.

Richie, J.P., Leutzinger, Y., Parthasarathy, S., Malloy, V., Orentreich, N., and Zimmerman, J. a (1994). Methionine restriction increases blood glutathione and longevity in F344 rats. FASEB J. *8*, 1302–1307.

Ritchie, M.E., Phipson, B., Wu, D., Hu, Y., Law, C.W., Shi, W., and Smyth, G.K. (2015). Limma powers differential expression analyses for RNA-sequencing and microarray studies. Nucleic Acids Res. *43*, e47.

Roberts, M.N., Wallace, M.A., Tomilov, A.A., Zhou, Z., Marcotte, G.R., Tran, D., Perez, G., Gutierrez-Casado, E., Koike, S., Knotts, T.A., et al. (2017). A Ketogenic Diet Extends Longevity and Healthspan in Adult Mice. Cell Metab. *26*, 539–546.e5.

Robertson, K.D., and Wolffe, A.P. (2000). DNA methylation in health and disease. Nat. Rev. Genet. *1*, 11–19.

Robida-Stubbs, S., Glover-Cutter, K., Lamming, D.W., Mizunuma, M., Narasimhan, S.D., Neumann-Haefelin, E., Sabatini, D.M., and Blackwell, T.K. (2012). TOR signaling and rapamycin influence longevity by regulating SKN-1/Nrf and DAF-16/FoxO. Cell Metab. *15*, 713–724.

Robins, C., McRae, A.F., Powell, J.E., Wiener, H.W., Aslibekyan, S., Kennedy, E.M., Absher, D.M., Arnett, D.K., Montgomery, G.W., Visscher, P.M., et al. (2017). Testing Two Evolutionary Theories of Human Aging with DNA Methylation Data. Genetics.

Robinson, M.D., McCarthy, D.J., and Smyth, G.K. (2009). edgeR: A Bioconductor package for differential expression analysis of digital gene expression data. Bioinformatics *26*, 139–140.

Rochette, P.J., and Brash, D.E. (2008). Progressive apoptosis resistance prior to senescence and control by the anti-apoptotic protein BCL-xL. Mech. Ageing Dev. *129*, 207–214.

Rosenbloom, K.R., Armstrong, J., Barber, G.P., Casper, J., Clawson, H., Diekhans, M., Dreszer, T.R., Fujita, P.A., Guruvadoo, L., Haeussler, M., et al. (2015). The UCSC Genome Browser database: 2015 update. Nucleic Acids Res. *43*, D670-81.

Ruby, J.G., Smith, M., and Buffenstein, R. (2018). Naked mole-rat mortality rates defy gompertzian laws by not increasing with age. Elife *7*, 1–18.

Sacher, G.A. (1959). Relation of lifespan to brain weight and body weight in mammals. G.E.W. Wolstenholme, M. O'Conner (Eds.), Ciba Found. Symp. – Lifesp. Anim. (Colloquia Ageing), John Wiley Sons, Ltd, Chichester 115–141.

Saxonov, S., Berg, P., and Brutlag, D.L. (2006). A genome-wide analysis of CpG

dinucleotides in the human genome distinguishes two distinct classes of promoters. Proc. Natl. Acad. Sci. U. S. A. *103*, 1412–1417.

Schumacher, B., Van Der Pluijm, I., Moorhouse, M.J., Kosteas, T., Robinson, A.R., Suh, Y., Breit, T.M., Van Steeg, H., Niedernhofer, L.J., Van Ijcken, W., et al. (2008). Delayed and accelerated aging share common longevity assurance mechanisms. PLoS Genet. *4*.

Seim, I., Fang, X., Xiong, Z., Lobanov, A. V., Huang, Z., Ma, S., Feng, Y., Turanov, A.A., Zhu, Y., Lenz, T.L., et al. (2013). Genome analysis reveals insights into physiology and longevity of the Brandt's bat Myotis brandtii. Nat. Commun. *4*, 1–8.

Selman, C., Tullet, J.M.A., Wieser, D., Irvine, E., Lingard, S.J., Choudhury, A.I., Claret, M., Al-qassab, H., Carmignac, D., Ramadani, F., et al. (2009). Ribosomal Protein S6 Kinase 1 Signaling Regulates Mammalian Life Span. Science (80-.). *326*, 140–144.

Seluanov, A., Chen, Z., Hine, C., Sasahara, T.H.C., Ribeiro, A.A.C.M., Catania, K.C., Presgraves, D.C., and Gorbunova, V. (2007). Telomerase activity coevolves with body mass not lifespan. Aging Cell *6*, 45–52.

Seluanov, A., Hine, C., Bozzella, M., Hall, A., Sasahara, T.H.C., Ribeiro, A.A.C.M., Catania, K.C., Presgraves, D.C., and Gorbunova, V. (2008). Distinct tumor suppressor mechanisms evolve in rodent species that differ in size and lifespan. Aging Cell *7*, 813–823.

Seluanov, A., Hine, C., Azpurua, J., Feigenson, M., Bozzella, M., Mao, Z., Catania, K.C., and Gorbunova, V. (2009). Hypersensitivity to contact inhibition provides a clue to cancer resistance of naked mole-rat. Proc. Natl. Acad. Sci. *106*, 19352–19357.

Senn, J.J., Klover, P.J., Nowak, I.A., and Mooney, R.A. (2002). Interleukin-6 induces cellular insulin resistance in hepatocytes. Diabetes *51*, 3391–3399.

Shannon, P., Markiel, A., Owen Ozier, 2, Baliga, N.S., Wang, J.T., Ramage, D., Amin, N., Schwikowski, B., and Ideker, T. (2003). Cytoscape: a software environment for integrated models of biomolecular interaction networks. Genome Res. 2498–2504.

Shirakawa, K., Moan, N. Le, Grueter, C.A., Lim, H., Saunders, L.R., Stevens, R.D., Newgard, C.B., Jr, R.V.F., Cabo, R. De, Ulrich, S., et al. (2013). Suppression of Oxidative Stress by b-Hydroxybutyrate, an Endogenous Histone Deacetylase Inhibitor. Science (80-.). *339*, 211–214.

Simons, M.J.P., Koch, W., and Verhulst, S. (2013). Dietary restriction of rodents decreases aging rate without affecting initial mortality rate -- a meta-analysis. Aging Cell *12*, 410–414.

Steinbaugh, M.J., Sun, L.Y., Bartke, A., and Miller, R.A. (2012). Activation of genes involved in xenobiotic metabolism is a shared signature of mouse models with extended lifespan. Am. J. Physiol. Endocrinol. Metab. *303*, E488-95.

Steiner, A.A., and Branco, L.G.S. (2002). Hypoxia-Induced Anapyrexia: Implications and Putative Mediators. Annu. Rev. Physiol. *64*, 263–288.

Streeper, R.S., Grueter, C.A., Salomonis, N., Cases, S., Levin, M.C., Koliwad, S.K., Zhou, P., Hirschey, M.D., Verdin, E., and Farese, R. V. (2012). Deficiency of the lipid synthesis enzyme, DGAT1, extends longevity in mice. Aging (Albany. NY). *4*, 13–27.

Strong, R., Miller, R.A., Astle, C.M., Floyd, R.A., Flurkey, K., Hensley, K.L., Javors,

M.A., Leeuwenburgh, C., Nelson, J.F., Ongini, E., et al. (2008). Nordihydroguaiaretic acid and aspirin increase lifespan of genetically heterogeneous male mice. Aging Cell *7*, 641–650.

Strong, R., Miller, R.A., Astle, C.M., Baur, J.A., De Cabo, R., Fernandez, E., Guo, W., Javors, M., Kirkland, J.L., Nelson, J.F., et al. (2013). Evaluation of resveratrol, green tea extract, curcumin, oxaloacetic acid, and medium-chain triglyceride oil on life span of genetically heterogeneous mice. Journals Gerontol. - Ser. A Biol. Sci. Med. Sci. *68*, 6–16.

Strong, R., Miller, R.A., Antebi, A., Astle, C.M., Bogue, M., Denzel, M.S., Fernandez, E., Flurkey, K., Hamilton, K.L., Lamming, D.W., et al. (2016). Longer lifespan in male mice treated with a weakly estrogenic agonist, an antioxidant, an α-glucosidase inhibitor or a Nrf2-inducer. Aging Cell *15*, 872–884.

Stubbs, T.M., Bonder, M.J., Stark, A.K., Krueger, F., von Meyenn, F., Stegle, O., Reik, W., Bolland, D., Butcher, G., Chandra, T., et al. (2017). Multi-tissue DNA methylation age predictor in mouse. Genome Biol. *18*, 1–14.

Subramanian, A., Tamayo, P., Mootha, V.K., Mukherjee, S., Ebert, B.L., Gillette, M. a, Paulovich, A., Pomeroy, S.L., Golub, T.R., Lander, E.S., et al. (2005). Gene set enrichment analysis: a knowledge-based approach for interpreting genome-wide expression profiles. Proc. Natl. Acad. Sci. U. S. A. *102*, 15545–15550.

Suh, Y., Atzmon, G., Cho, M.-O., Hwang, D., Liu, B., Leahy, D.J., Barzilai, N., and Cohen, P. (2008). Functionally significant insulin-like growth factor I receptor mutations in centenarians. Proc. Natl. Acad. Sci. U. S. A. *105*, 3438–3442.

Sun, L.Y., Spong, A., Swindell, W.R., Fang, Y., Hill, C., Huber, J.A., Boehm, J.D., Westbrook, R., Salvatori, R., and Bartke, A. (2013). Growth hormone-releasing hormone disruption extends lifespan and regulates response to caloric restriction in mice. Elife *2*, e01098.

Sun, Y. V, Turner, S.T., Smith, J.A., Hammond, P.I., Lazarus, A., Van De Rostyne, J.L., Cunningham, J.M., and Kardia, S.L.R. (2010). Comparison of the DNA methylation profiles of human peripheral blood cells and transformed B-lymphocytes. Hum. Genet. *127*, 651–658.

Swardfager, W., Lanctt, K., Rothenburg, L., Wong, A., Cappell, J., and Herrmann, N. (2010). A meta-analysis of cytokines in Alzheimer's disease. Biol. Psychiatry *68*, 930–941.

Swindell, W.R. (2008). Comparative analysis of microarray data identifies common responses to caloric restriction among mouse tissues. Mech. Ageing Dev. *129*, 138–153.

Sykiotis, G.P., and Bohmann, D. (2008). Keap1/Nrf2 Signaling Regulates Oxidative Stress Tolerance and Lifespan in Drosophila. Dev. Cell *14*, 76–85.

Tacutu, R., Budovsky, A., Yanai, H., and Fraifeld, V.E. (2011). Molecular links between cellular senescence, longevity and agerelated diseases - A systems biology perspective. Aging (Albany. NY). *3*, 1178–1191.

Taylor, K.R., Milone, N.A., and Rodriguez, C.E. (2017). Four cases of spontaneous neoplasia in the naked mole-rat (*Heterocephalus glaber*), a putative cancer-resistant species. Journals Gerontol. - Ser. A Biol. Sci. Med. Sci. *72*, 38–43.

Tian, X., Azpurua, J., Hine, C., Vaidya, A., Myakishev-Rempel, M., Ablaeva, J., Mao, Z., Nevo, E., Gorbunova, V., and Seluanov, A. (2013). High-molecular-mass hyaluronan mediates the cancer resistance of the naked mole rat. Nature *499*, 346–349.

Tian, X., Azpurua, J., Ke, Z., Augereau, A., Zhang, Z.D., Vijg, J., Gladyshev, V.N., Gorbunova, V., and Seluanov, A. (2015). *INK4* locus of the tumor-resistant rodent, the naked mole rat, expresses a functional p15/p16 hybrid isoform. Proc. Natl. Acad. Sci. *112*, 1053–1058.

Tsuchiya, T., Dhahbi, J.M., Cui, X., Mote, P.L., Bartke, A., and Spindler, S.R. (2004). Additive regulation of hepatic gene expression by dwarfism and caloric restriction. Physiol. Genomics *17*, 307–315.

Tullet, J.M.A., Hertweck, M., An, J.H., Baker, J., Hwang, J.Y., Liu, S., Oliveira, R.P., Baumeister, R., and Blackwell, T.K. (2008). Direct Inhibition of the Longevity-Promoting Factor SKN-1 by Insulin-like Signaling in *C. elegans*. Cell *132*, 1025–1038.

Tyner, S.D., Venkatachalam, S., Choi, J., Jones, S., Ghebranious, N., Igelmann, H., Lu, X., Soron, G., Cooper, B., Brayton, C., et al. (2002). P53 mutant mice that display early ageing-associated phenotypes. Nature *415*, 45–53.

Ubagai, T., Lei, K.J., Huang, S., Mudd, S.H., Levy, H.L., and Chou, J.Y. (1995). Molecular mechanisms of an inborn error of methionine pathway. Methionine adenosyltransferase deficiency. J. Clin. Invest. *96*, 1943–1947.

Uthus, E.O., and Brown-Borg, H.M. (2003). Altered methionine metabolism in long living Ames dwarf mice. Exp. Gerontol. *38*, 491–498.

Valenzano, D.R., Terzibasi, E., Genade, T., Cattaneo, A., Domenici, L., and Cellerino, A. (2006). Resveratrol prolongs lifespan and retards the onset of age-related markers in a short-lived vertebrate. Curr. Biol. *16*, 296–300.

Viechtbauer, W. (2010). Conducting Meta-Analyses in R with the metafor Package. J. Stat. Softw. *36*, 1–48.

Viña, J., Borrás, C., Gambini, J., Sastre, J., and Pallardó, F. V. (2005). Why females live longer than males? Importance of the upregulation of longevity-associated genes by oestrogenic compounds. FEBS Lett. *579*, 2541–2545.

Viswanathan, M., Kim, S.K., Berdichevsky, A., and Guarente, L. (2005). A role for SIR-2.1 regulation of ER stress response genes in determining *C. elegans* life span. Dev. Cell *9*, 605–615.

Wang, T., Tsui, B., Kreisberg, J.F., Robertson, N.A., Gross, A.M., Yu, M.K., Carter, H., Brown-Borg, H.M., Adams, P.D., and Ideker, T. (2017). Epigenetic aging signatures in mice livers are slowed by dwarfism, calorie restriction and rapamycin treatment. Genome Biol. *18*, 57.

Wang, Y., Zhang, N., Zhang, L., Li, R., Fu, W., Ma, K., Li, X., Wang, L., Wang, J., Zhang, H., et al. (2016). Autophagy Regulates Chromatin Ubiquitination in DNA Damage Response through Elimination of SQSTM1/p62. Mol. Cell *63*, 34–48.

Waxman, D.J., and Holloway, M.G. (2009). Sex Differences in the Expression of Hepatic Drug Metabolizing Enzymes. Mol Pharmacol *76*, 215–228.

Wei, Y., Zhang, S., Shang, S., Zhang, B., Li, S., Wang, X., Wang, F., Su, J., Wu, Q., Liu,

H., et al. (2016). SEA: a super-enhancer archive. Nucleic Acids Res. *44*, D172-9.

Weidner, C.I., Lin, Q., Koch, C.M., Eisele, L., Beier, F., Ziegler, P., Bauerschlag, D.O., Jöckel, K.H., Erbel, R., Mühleisen, T.W., et al. (2014). Aging of blood can be tracked by DNA methylation changes at just three CpG sites. Genome Biol. *15*.

Wen, Y., Li, W., Poteet, E.C., Xie, L., Tan, C., Yan, L.J., Ju, X., Liu, R., Qian, H., Marvin, M.A., et al. (2011). Alternative mitochondrial electron transfer as a novel strategy for neuroprotection. J. Biol. Chem. *286*, 16504–16515.

Western, D. (1979). Size, life history and ecology in mammals. Afr. J. Ecol. *17*, 185–204.

Wood, J.G., Regina, B., Lavu, S., Hewitz, K., Helfand, S.L., Tatar, M., and Sinclair, D. (2004). Sirtuin activators mimic caloric restriction and delay ageing in metazoans. Nature *430*, 686–689.

Xie, K., Neff, F., Markert, A., Rozman, J., Aguilar-Pimentel, J.A., Amarie, O.V., Becker, L., Brommage, R., Garrett, L., Henzel, K.S., et al. (2017). Every-other-day feeding extends lifespan but fails to delay many symptoms of aging in mice. Nat. Commun. *8*.

Xue, W., Zender, L., Miething, C., Dickins, R.A., Hernando, E., Krizhanovsky, V., Cordon-cardo, C., and Lowe, S.W. (2007). Senescence and tumour clearance is triggered by p53 restoration in murine liver carcinomas. Nature *445*, 656–660.

Yanai, H., and Fraifeld, V.E. (2018). The role of cellular senescence in aging through the prism of Koch-like criteria. Ageing Res. Rev. *41*, 18–33.

Yilmaz, O.H., Katajisto, P., Lamming, D.W., and Sabitini, D.M. (2012). mTORC1 in the

Paneth cell niche couples ISC function to calorie intake. Nature *486*, 490–495.

Yoder, J.A., Walsh, C.P., and Bestor, T.H. (1997). Cytosine methylation and the ecology of intragenomic parasites. Trends Genet. *13*, 335–340.

Yuan, R., Tsaih, S., Petkova, S.B., Evsikova, C.M. De, Marion, M.A., Bogue, M.A., Mills, K.D., Peters, L.L., Bult, C.J., Rosen, C.J., et al. (2009). Aging in inbred strains of mice: Study design and interim report on median lifespan and circulating IGF1 levels. Aging Cell *8*, 277–287.

Yue, F., Cheng, Y., Breschi, A., Vierstra, J., Wu, W., Ryba, T., Sandstrom, R., Ma, Z., Davis, C., Pope, B.D., et al. (2014). A comparative encyclopedia of DNA elements in the mouse genome. Nature *515*, 355–364.

Zhang, B., Xiao, R., Ronan, E.A., He, Y., Hsu, A.L., Liu, J., and Xu, X.Z.S. (2015). Environmental Temperature Differentially Modulates *C. elegans* Longevity through a Thermosensitive TRP Channel. Cell Rep. *11*, 1414–1424.

Zhang, G., Cowled, C., Shi, Z., Huang, Z., Bishop-Lilly, K. a, Fang, X., Wynne, J.W., Xiong, Z., Baker, M.L., Zhao, W., et al. (2013). Comparative Analysis of Bat Genomes. Science (80-.). *339*, 456–460.

Zhang, L., Ebenezer, P.J., Dasuri, K., Fernandez-Kim, S.O., Francis, J., Mariappan, N., Gao, Z., Ye, J., Bruce-Keller, A.J., and Keller, J.N. (2011). Aging is associated with hypoxia and oxidative stress in adipose tissue: implications for adipose function. Am. J. Physiol. Endocrinol. Metab. *301*, E599-607.

Zhang, Y., Xie, Y., Berglund, E.D., Colbert Coate, K., He, T.T., Katafuchi, T., Xiao, G.,

Potthoff, M.J., Wei, W., Wan, Y., et al. (2012). The starvation hormone, fibroblast growth factor-21, extends lifespan in mice. Elife *2012*, 1–14.

Zhao, S., Lin, L., Kan, G., Xu, C., Tang, Q., Yu, C., Sun, W., Cai, L., Xu, C., and Cui, S. (2014). High autophagy in the naked mole rat may play a significant role in maintaining good health. Cell. Physiol. Biochem. *33*, 321–332.

Zhou, Y., Xu, B.C., Maheshwari, H.G., He, L., Reed, M., Lozykowski, M., Okada, S., Cataldo, L., Coschigamo, K., Wagner, T.E., et al. (1997). A mammalian model for Laron syndrome produced by targeted disruption of the mouse growth hormone receptor/binding protein gene (the Laron mouse). Proc. Natl. Acad. Sci. U. S. A. *94*, 13215–13220.

Zid, B.M., Rogers, A.N., Katewa, S.D., Vargas, M.A., Kolipinski, M.C., Lu, T.A., Benzer, S., and Kapahi, P. (2009). 4E-BP Extends Lifespan upon Dietary Restriction by Enhancing Mitochondrial Activity in Drosophila. Cell *139*, 149–160.

(2013). Breakthrough of the year 2013. Notable developments. Science (80-.). *342*, 1435–1441.